**The Dissertation Committee for Kate Frances Monzo Certifies that this is the approved version of the following dissertation:**

# The role of Fragile X mental retardation protein in *Drosophila* cleavage furrow formation

**Committee:**

John Sisson, Supervisor

Paul Macdonald, Co-Supervisor

Janice Fischer

Arlen Johnson

John Wallingford

# The role of Fragile X mental retardation protein in *Drosophila* cleavage furrow formation

**by**

**Kate Frances Monzo, B.S.**

**Dissertation**

Presented to the Faculty of the Graduate School of

The University of Texas at Austin

in Partial Fulfillment

of the Requirements

for the Degree of

**Doctor of Philosophy**

**The University of Texas at Austin**

**December, 2009**

## Dedication

To my most dear and trusted friend, Paul Paukstelis.

With Paul, the road always seems to rise to meet my feet,

the wind is at my back, and the sun shines bright on my face.

## Acknowledgements

I would like to thank John Sisson for sharing his passion for science and his unmatched determination for trying to understand the unknown. My time as John's student has taught me the worth of a well-designed experiment, the importance of thoughtful and critical analysis of data, and the value of a fruitful collaboration. I will always try to apply all that I have learned from John to my future work, and I hope to make him proud.

I would also like to thank my committee members for their support and encouragement, especially Janice Fischer and John Wallingford for treating me as one of their own. I owe a lot to all of the present and past Sisson lab members. Most of all, I thank Ophelia Papoulas for being an invaluable mentor, colleague, and friend. I also thank Howard Wang and Young Hee Ryu for being such considerate and caring lab mates. I thank our excellent collaborators: John Minden, Susan Dowd, and Anupam Goyal at Carnegie Mellon University and John Yates, Lujian Liao, Greg Cantin, and Cristian Ruse at the Scripps Research Institute.

I am grateful for all of the students, faculty and especially the fly community at the University of Texas at Austin for their advice and support. I am so happy that I had such a great group of thoughtful students around me to share beers and argue with. Special thanks to Ryan Gray for starting the MCDB journal club with me and to the

MCDB department for giving us the opportunity to invite and host seminar speakers. I hope this is a tradition that will continue.

I also thank all of my family and friends. My mother always nutured my curiosity and love for exploration. She also has a fierce tenacity for sticking to her guns, and I am forever grateful to her for giving me the strength to never back down (even though sometimes it gets me into trouble). I thank my dad for making me laugh even when I feel like crying. I consider myself very lucky to have such incredible siblings who are so often a needed voice of reason and comfort. My friends in Austin have become a second family for me, and I don't know what I would do without them. Finally, I don't have the words to describe how much I appreciate my husband Paul for all of his encouragement and advice and will also be forever grateful that he has shared his awesome family with me.

# The role of Fragile X mental retardation protein in *Drosophila* cleavage furrow formation

Publication No._____

Kate Frances Monzo, Ph.D.

The University of Texas at Austin, 2009

Supervisors: John Sisson and Paul Macdonald

Reduced activity of Fragile X mental retardation protein (FMRP) in brain neurons results in the most common form of heritable mental retardation in humans, Fragile X Syndrome (FXS). FMRP is a selective RNA-binding protein that is implicated in the translational regulation of specific mRNAs in neurons. Although very few direct targets of FMRP have been identified and verified *in vivo*, FXS is thought to result from the aberrant regulation of potentially hundreds of mRNAs causing defects in neuron morphology and synapse function. Identifying additional targets will be important for elucidating the mechanism of FMRP regulation as well as the etiology of FXS.

*Drosophila melanogaster* offers a unique and powerful system for studying the function of FMRP. Flies with loss of FMRP activity have neuronal and behavioral defects similar to those observed in humans with FXS. Importantly, FMRP regulates common target mRNAs in neurons in both mice and flies. Here, I will describe our discovery of a previously unknown requirement for *Drosophila* FMRP (dFMRP) during the cleavage stage of early embryonic development. First, we identified a requirement

for dFMRP for proper cleavage furrow formation and found that dFMRP functions to regulate the expression of specific target mRNAs during the cleavage stage. Among these is *trailer hitch (tral)* mRNA, which encodes a translational regulator as well, and represents a new *in vivo* target of dFMRP translational regulation. In addition, I have identified twenty-eight proteins that change in expression in the absence of dFMRP using a comparative proteomics based screen for dFMRP targets. One of these is the Chaperonin containing tcp-1 complex (CCT), a previously unidentified target, which I found is itself also required for cleavage furrow formation. Finally, we have identified a new dFMRP protein-binding partner, Caprin, and found that together dFMRP and Caprin are required for the proper timing of the MBT. This set of work has led to a better understanding of the mechanism of dFMRP-dependent regulation of cellular morphogenesis in early embryos and has the potential to lead to a better understanding of the etiology of FXS.

# Table of Contents

# List of Tables

# List of Figures

# Chapter 1: General Introduction

## 1.1 FRAGILE X MENTAL RETARDATION PROTEIN

Mental retardation is a prevalent intellectual and developmental disability affecting as many as 3% of children and their families in the United States (Inlow and Restifo 2004). Fragile X Syndrome (FXS) is the most common form of heritable mental retardation as well as a leading known cause of autism. FXS results from the reduced activity of the Fragile X Mental Retardation Protein (FMRP) as a consequence of either the transcriptional silencing of or mutations within the *FMR1* gene. Common symptoms of FXS include learning and behavioral disabilities, sleep disorders, delayed speech, facial dismorphia, and macroorchidism (O'donnell and Warren 2002). Although some progress has been made in understanding the effects of loss of FMRP activity, there is still much to learn about the mechanism of FMRP action.

### 1.1.1 FMRP and target mRNAs

In addition to the symptoms mentioned above, FXS has been associated with more specific cellular phenotypes. FXS patients have been reported to have an elongated dendritic spine morphology in brain neurons, which is often associated with mental retardation (Hinton *et al*. 1991). A similar phenotype has been reported in *FMR1* knock-out mice, suggesting that reduced activity of FMRP in brain neurons is responsible for the neuronal defects (Penagarikano *et al*. 2007). Dendritic spines are dynamic structures that are found along the entire length of a dendrite and are responsible for receiving signals from the axon terminals of other signal-sending neurons. These structures are home to the postsynaptic density (PSD), which is a multiprotein complex that is required for the targeting of neurotransmitter receptors to their sites of function at the synapse

(Sheng 2001). The initial development and maintenance of dendritic spines requires appropriate local translation of specific 'target' messenger RNAs (mRNAs) for their proper function. Important known regulators of synaptic development and remodeling include effectors of the actin and microtubule (MT) cytoskeletons and membrane trafficking (Kennedy and Ehlers 2006).

FMRP is a selective RNA-binding protein that is implicated in the translational regulation of specific mRNAs in neurons. It contains two types of RNA-binding domains: two K homology (KH) domains and an arginine glycine rich motif, also referred to as an RGG box (Figure 1.1; Siomi *et al*. 1993). The KH2 domain has been implicated in binding to a complex tertiary RNA structure referred to as a kissing complex, which is hypothesized to mediate binding between FMRP and polyribosomes (Darnell *et al*. 2005). The RGG box of FMRP has high affinity for G-quartet RNA motifs as shown by *in vitro* selection with human FMRP and microarray analysis using murine brain tissue (Brown *et al*. 2001; Darnell *et al*. 2001). Although few direct targets of FMRP-dependent regulation have been identified, efforts have been made to identify target mRNAs using a variety of approaches including bioinformatics, immunoprecipitation and microarray analysis, antibody-positioned RNA amplification, and proteome analysis (Brown *et al*. 2001; Darnell *et al*. 2001; Schaeffer *et al*. 2001; Miyashiro *et al*. 2003; Todd *et al*. 2003; Liao *et al*. 2008). These approaches have been successful in producing long lists of candidate RNAs although, few direct targets have been shown to be physiologically relevant *in vivo* targets underscoring the importance of validation studies.

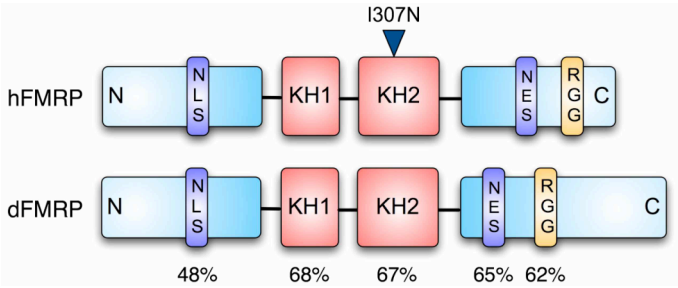


**Figure 1.1 Human FMRP and *Drosophila* FMRP protein domains**

Percent identity between hFMRP and dFMRP are shown below protein schematic. K homology domains (KH) and RGG box indicate RNA binding domains. I3047N indicates a missense mutation that causes severe FXS phenotype. Amino terminus (N), carboxy terminus (C), nuclear localization signal (NLS), and nuclear export signal (NES) are located as indicated. Figure is adapted from Zhang *et al*. 2001.

### 1.1.2 FMRP and translational regulation

Although very few direct targets of FMRP have been verified *in vivo*, FXS is thought to result from the aberrant translational regulation of potentially hundreds of mRNAs causing defects in neuron morphology and synapse function (Brown *et al*. 2001). Although FMRP is generally thought to function as a repressor of translation and can repress translation of reporter mRNAs in translation assays, there is also evidence that it can also function to activate translation (Brown *et al*. 2001; Darnell *et al*. 2001; Laggerbauer *et al*. 2001; Schaeffer *et al*. 2001; Miyashiro *et al*. 2003; Todd *et al*. 2003; Liao *et al*. 2008). mRNA translation can be inhibited at various steps through the process, including inititation, elongation, and termination. While global regulation is generally regulated at the level of initiation, there are thought to be more diverse mechanisms that control mRNA-specific regulation that affect elongation and termination (Gebauer and Hentze 2004). Although the mechanism of regulation is not well understood, some studies suggest that FMRP affects translation elongation or termination

on polyribosomes, whereas others suggest it is excluded from polyribosomes and affects translation initiation (Zalfa *et al*. 2006). FMRP has been shown to directly interact with the 60S ribosomal subunit (Khandjian *et al*. 1996; Siomi *et al*. 1996), which could support either model. Nevertheless, FMRP has been reported to be associated with polyadenylated mRNAs on actively translating polyribosomes, and a missense mutation causing a severe form of FXS (I304N) abolishes this association in human cell culture (Corbin *et al*. 1997; Feng *et al*. 1997), consistent with an effect on elongation or termination. FMRP has also been shown to localize to RNA granules, which are dynamic sites of translational repression, storage, transport and degradation of mRNAs (Mazroui *et al*. 2002; Costa *et al*. 2005; Barbee *et al*. 2006). Many different types of RNA granules have been described, each containing a unique and sometimes overlapping constellation of proteins and RNAs: somatic processing bodies (GW/P bodies), stress granules, neuronal granules, and germ cell (polar) granules (Anderson and Kedersha 2006). GW/P bodies are generally sites of mRNA decay and contain components of the mRNA decay and silencing machinery, while stress granules are generally structures that house stalled preinitiation complexes during times of stress (Anderson and Kedersha 2006). Neuronal granules contain translationally repressed mRNAs that are to be transported to dendritic spines where the mRNAs are released for translation in response to external cues. Finally, germ cell granules contain maternal mRNA that is required for germ cell specification. Although FMRP seems to localize to different types of granules (neuronal and stress granules in mammalian cells and neuronal and P body-like granules in *Drosophila*), it seems clear that it is present in structures that are translationally quiescent. These observations are consistent with FMRP functioning to inhibit initiation of translation, possibly by sequestering mRNAs away from the translation machinery or by affecting the translational competency of mRNAs. Interestingly, mammalian FMRP

has been shown to associate with Dicer and Argonaute 1 (AGO1), components of the RNA silencing machinery, *in vitro* (Jin *et al*. 2004). *Drosophila* FMRP has also been shown to physically interact with Argonaute 2 (AGO2) in cell culture and genetically interact with AGO1 (Caudy *et al*. 2002; Jin *et al*. 2004). It is still unclear how FMRP may be interacting with the RNA silencing machinery *in vivo*. Taken together it is clear that FMRP is a translational regulator, but its method of action may be dynamic and varies with cellular context.

### 1.1.3 *Drosophila* FMRP

*Drosophila* has a single *FMR1* ortholog called *dfmr1*, and the fly and human protein sequences share a high degree of similarity in the known functional domains (Figure 1.1). The *dfmr1* mRNA and protein product (dFMRP) are expressed throughout the developing embryo with elevated expression in the mesoderm and central nervous system (CNS) (Wan *et al*. 2000). *dfmr1* mutants are viable and display defects in circadian rhythm and courtship activity (Dockendorff *et al*. 2002). These abnormal behaviors are likely the result of abnormal arborization of dendrites as seen in the neocortex of human FXS patients and mutant mice (Gao 2002; Penagarikano *et al*. 2007). *dfmr1* mutants also have defects in synapse morphology and function in the neuromuscular junction (NMJ) (Zhang *et al*. 2001). Because of the similar behavioral and cell morphological phenotypes seen in *dfmr1* mutant *Drosophila*, *FMR1* knock-out mice, and FXS patients, *Drosophila* is a useful model system for studying FMRP function.

Roles for dFMRP outside of the nervous system have been identified during oogenesis (Costa *et al*. 2005), pole cell formation (Deshpande *et al*. 2006), and spermatogenesis (Zhang *et al*. 2004). In the ovary, dFMRP is required for the down regulation of the Orb (oo18 RNA binding) pathway which is required for the

establishment of the anterior–posterior and dorsal–ventral axes of the developing egg (Costa *et al*. 2005). Loss of *dfmr1* causes defects in cyst formation and oocyte specification, a likely consequence of the misregulation of the Orb pathway. In embryos laid by *dfmr1* mutant females mated to *dfmr1* mutant males, initial pole bud formation is perturbed and pole cells are not properly separated from the underlying syncytial layer (Deshpande *et al*. 2006). Orb levels appear normal in these embryos, so the pole cell defect is suggested to be a result of the misregulation of the actomyosin cytoskeleton. Finally, dFMRP is required during spermatogenesis for the structural integrity of the sperm tail axoneme (Zhang *et al*. 2004). Although it is still unclear how dFMRP affects axoneme development, it has been suggested that dFMRP may be required for the stabilization of the central pair of microtubules through the translational regulation of MT stability factors (Zhang *et al*. 2004). Interestingly, the axoneme phenotype was also observed in mouse *FMR1* knockout mice, suggesting that this role for FMRP is evolutionarily conserved (Zhang *et al*. 2004). Despite these studies, the specific molecular function of dFMRP remains elusive. Identification and validation of new direct targets and investigation of FMRP in developmental systems outside of the nervous system may be important for fully understanding how FMRP functions.

### 1.1.4 dFMRP and target mRNAs

A handful of direct targets of dFMRP regulation has been identified and verified in neurons including *futsch, Rac1*, *pickpocket (ppk1)*, and *chickadee* (*chic*, Profilin) (Zhang *et al*. 2001; Lee *et al*. 2003; Xu *et al*. 2004; Reeve *et al*. 2005). Futsch is the homolog of mammalian MAP1B, a MT-associated protein that regulates the MT cytoskeleton in neurons (Zhang *et al*. 2001) that has also been found to be a target of FMRP regulation in mice (Lu *et al*. 2004). dFMRP is normally required for the translational repression of *futsch (Zhang et al. 2001)*. The upregulation of Futsch in

*dfmr1* mutants seems to account for the defects observed in the NMJ but not in other types of neurons because loss of *futsch* in a *dfmr*1 mutant specifically rescues the NMJ neuronal phenotype (Zhang *et al*. 2001). *Rac1*, a regulator of the actin cytoskeleton, has been identified as a target of FMRP regulation in *Drosophila* and mouse neurons (Lee *et al*. 2003; Castets *et al*. 2005). Profilin, a regulator of the actin cytoskeleton, and PPK1, a specialized sodium channel subunit, have been reported as targets of dFMRP in *Drosophila* neurons, although, so far, mammalian homologs have not been identified as FMRP targets (Reeve *et al*. 2005). These observations are consistent with dFMRP having a role in regulating the cytoskeleton as well as having common targets as mammalian FMRP in neurons.

Identifying additional targets will be important for elucidating the mechanism of FMRP regulation as well as the etiology of FXS. To this end we have used the cleavage stage *Drosophila* embryo as a system to study the mechanisms of FMRP function and the role of mRNA translational control in early embryonic morphogenesis.

## 1.2 THE *DROSOPHILA* CLEAVAGE STAGE

The initial cleavage divisions of embryogenesis in most animals are remarkably rapid and synchronous and have reduced or no gap phases. Following these unique divisions, animal embryos undergo a monumental transition, referred to as the midblastula transition (MBT), when the embryo shifts from dependence on maternal to zygotic genetic control. The hallmark of the MBT in *Drosophila* is the process of cleavage furrow formation, also referred to cellularization, which is unique to the insect cleavage stage. Although the mechanism for how the actual cleavage divisions occur varies greatly between animals, several of the known regulators of the MBT are functionally conserved throughout the animal kingdom suggesting that the molecular

mechanisms regulating the MBT are also conserved. In addition, the cleavage stage is characterized by a dramatic shift in post-transcriptional genetic control, making it well suited for the study of dFMRP function.

### 1.2.1 Cell cycles of the *Drosophila* cleavage stage

*Drosophila* embryos undergo superficial cleavage, wherein nuclear divisions occur within a common cytoplasm in the absence of cytokinesis. The first 9 nuclear cycles (NCs) are extremely fast and synchronous, lasting only about 8 minutes. During interphase of NC10 a small number of nuclei at the posterior pole of the embryo are cellularized and become pole cells, which will eventually give rise to the gametes of the adult fly. The somatic nuclei migrate to the cortex by NC10 where they undergo four additional divisions, which successively lengthen in duration (NC10 = 12 min, NC11 = 13 min, NC12 = 15 min, and NC13 = 26 min at 25°C) (Figure 1.2; Foe and Alberts 1983). During interphase of NC14, the cortically positioned nuclei are encapsulated by plasma membrane furrows, transforming the syncytial embryo into a cellular blastoderm through the process of cellularization. The mitosis of NC14 is the first completely asynchronous mitosis, with domains of cells progressing into mitosis at different rates, which is critical for determination of cell fate.

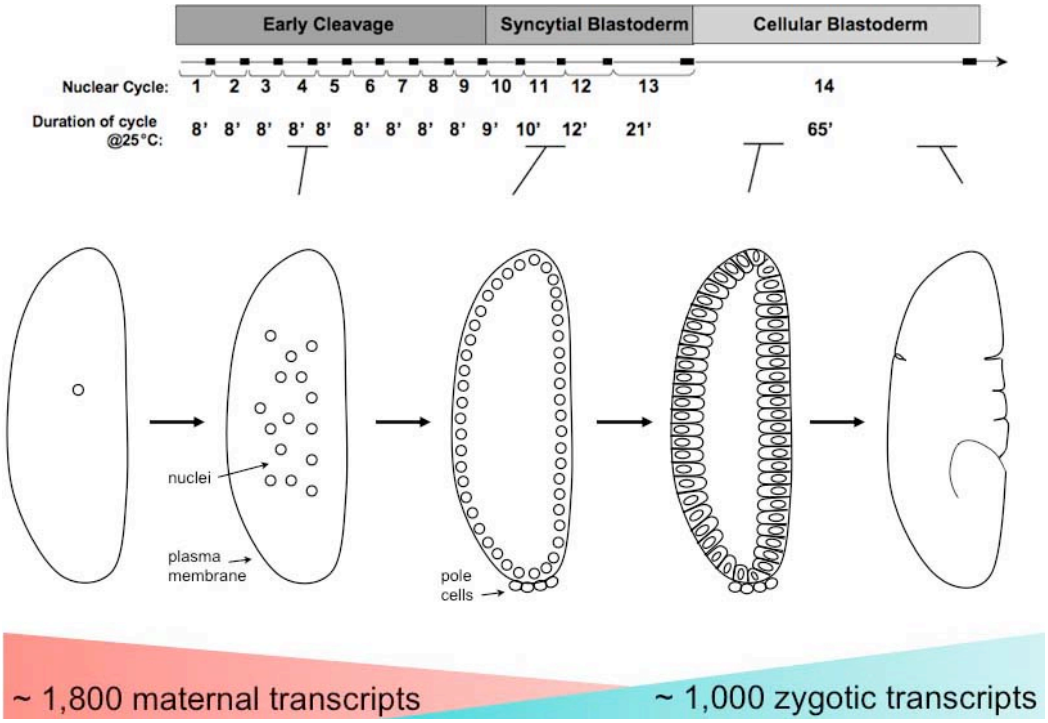


**Figure 1.2 Cell cycles lengthen at the MBT and a shift from maternal to zygotic genetic control occurs at nuclear cycle 14 during the cleavage stage**

Top grey bars indicate general phases of the cleavage stage. Nuclear cycle number and corresponding duration in minutes is shown under the black lines which indicate relative length of interphase (I) and black boxes which indicate relative length of mitosis (M). Duration of cycles at 25°C is indicated in minutes. Cartoon of embryo morphology at the different stages of cleavage and as a gastrula (far right). Red and green triangles show relative abundance of maternal transcripts that are degraded and zygotic transcripts that are activated during the MBT.

### 1.2.2 Cleavage furrow formation (cellularization)

Cleavage furrow formation is a specialized form of cytokinesis whereby cortically positioned nuclei are encapsulated by invaginating plasma membrane furrows. During this process, cleavage furrows ingress at two distinct rates. First, furrowing occurs slowly until the furrow front reaches the basal ends of nuclei. The rate then abruptly increases during the fast phase until the cells are formed and cellularization is complete. During the slow phase the nuclei elongate at a constant rate. This process requires a dramatic reorganization of the actin and MT cytoskeletons. F-actin is organized into an array of interlocking contractile rings under the plasma membrane and during furrow formation is positioned at the ingressing furrow front (Figure 1.3). At the onset of cellularization microtubule arrays emanate from pairs of cortically positioned centrosomes, extending their plus-ends into the interior of the embryo, forming 'inverted baskets' around individual nuclei (Figure 1.3). These microtubules are thought to provide some mechanical force required for nuclear elongation, as well as act as tracts for the secretory machinery (Foe and Alberts 1983). Cellularization is completed when furrows extend well past the basal ends of the nuclei into the basal cytoplasm and cleavage furrows constrict during basal closure. The embryo begins gastrulation prior to the completion of cellularization, and most cells retain an open cytoplasmic stalk well into gastrulation (Bate and Martinez Arias 1993).

Despite much effort, only a relatively small number of genes have been shown to be essential for *Drosophila* embryonic cleavage furrow formation (Mazumdar and Mazumdar 2002).

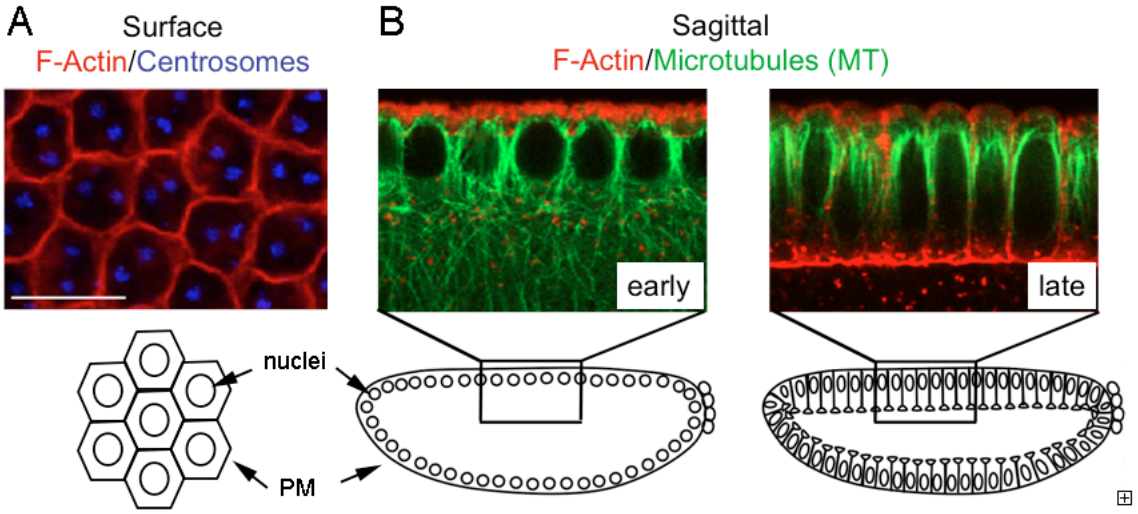


**Figure 1.3 Cleavage furrow formation depends on changes in the MT and Actin cytoskeletons**

Surface (A) and sagittal (B) immunofluorescence (IF) images of wild type (WT) embryos undergoing cleavage furrow formation showing F-actin (red), centrosomes (blue), and microtubules (MTs, green). Cartoons depict positioning of nuclei and plasma membrane (PM) in IF images.

### 1.2.3 MT and Actin regulators and furrow formation

As in conventional animal cell cytokinesis, many of the genes known to be required for cleavage furrow formation during cellularization are implicated in the regulation of the actin cytoskeleton (Glotzer 2001). Maternal-effect cleavage furrow formation defects have been described for mutations in many genes that are known to regulate the actin cytoskeleton, including *scraps* (*scra*, anillin), *peanut* (*pnut*, septin), *diaphanous* (*dia*), *Src oncogene at 64B* (*Src64*), and *Btk family kinase at 29A* (*Btk29A*) (Schupbach and Wieschaus 1989; Adam *et al*. 2000; Afshar *et al*. 2000; Thomas and Wieschaus 2004; Field *et al*. 2005). Mutations in *dia*, *scra* and *pnut* cause defects in contractile ring formation and furrow ingression (Adam *et al*. 2000; Afshar *et al*. 2000; Field *et al*. 2005). DIA, a Formin Homology protein involved in many actin-mediated cellular processes, is required to recruit actin, Anillin, and PNUT to the furrow front early in furrow formation (Afshar *et al*. 2000). In turn, Anillin and PNUT function together at the furrow front to assemble and organize the F-actin cytoskeleton, which is essential for the organization and ingression of new plasma membrane (Field *et al*. 2005; Sokac and Wieschaus 2008). Src64 and Btk29A are required for providing tension in cleavage furrows through the regulation of the actin cytoskeleton. In *Src64* and *Btk29A* mutants, furrows do not advance completely and basal closure of furrows does not occur (Thomas and Wieschaus 2004). In addition, three zygotic genes [*nullo, serendipity-a* (*sry-a*), and *bottleneck* (*bnk*)] are required for regulation of the actin cytoskeleton specifically during cellularization but not at any other time in development suggesting that they do not function during normal cytokinesis (Merrill *et al*. 1988; Wieschaus and Sweeton 1988; Schejter *et al*. 1992). Regardless, the mechanism for the activation of this unique set of genes may be important for a more complete understanding of the regulation that governs

the MBT (see section 1.3.4). While this list is hardly exhaustive of all the actin regulators that are required for cleavage furrow formation, it demonstrates that these actin regulatory genes are required for different aspects of furrow formation.

Although actomyosin based contraction has been considered to be a main driving force for furrow ingression during cellularization, it has been suggested that non-muscle Myosin II activity is dispensable for proper furrow ingression and is only required for constriction that occurs during basal closure (Royou *et al*. 2004). Many studies are now focused on possible roles for actin organization in targeted membrane secretion for providing the force required for furrow ingression.

### 1.2.4 Membrane trafficking and furrow formation

In addition to the reorganization of the actin cytoskeleton, MT-based targeted membrane secretion is also required for *Drosophila* embryonic cleavage furrow formation (Lecuit and Wieschaus 2000; Sisson *et al*. 2000). The amount of plasma membrane required to form the thousands of cells in the blastoderm is dependent on a huge increase in surface area, and it has been demonstrated that internal stores of membrane contribute to the formation of these furrows (Lecuit and Wieschaus 2000; Sisson *et al*. 2000). Furthermore, as mentioned above, it is possible that the addition of this new membrane drives furrows inward, rather than depending solely on actomyosin contraction (Lecuit and Wieschaus 2000; Royou *et al*. 2004; Thomas and Wieschaus 2004). Although many of the genes required for furrow formation that have been identified are involved in regulating the actin cytoskeleton, requirements for players in membrane trafficking and secretion have also been found. Specifically, Shibire (SHI), the *Drosophila* homolog of Dynamin and a protein implicated in endo- and exocytosis, is required for cleavage furrow formation (Swanson and Poodry 1981). In addition, proteins involved in recycling endosome (RE) trafficking [eg. Rab11 and Nuclear-fallout

(NUF)], Golgi trafficking [eg. Lava Lamp (LVA)], and targeted secretion (eg. Syntaxin1A) have also been shown to be necessary for cleavage furrow formation (Burgess *et al*. 1997; Rothwell *et al*. 1998; Sisson *et al*. 2000; Pelissier *et al*. 2003; Riggs *et al*. 2003). The requirement for these proteins in cleavage furrow formation underscores the importance of membrane trafficking mechanisms for this process, but the relationships between these different proteins and the mechanism of their regulation within the context of cleavage furrow formation are still not understood.

Identifying new genes involved in furrow formation will be essential to expand our understanding of the underlying mechanisms controlling the process as well as to contribute to our knowledge of conventional animal cell cytokinesis. As I will describe in the following chapters, in our efforts to identify these new genes, we found a requirement for dFMRP for cleavage furrow formation and cell cycle regulation during the MBT. This discovery has led us in many new directions, revealing previously unexplored regulatory pathways that depend on dFMRP.

### 1.3 THE *DROSOPHILA* MBT

The MBT varies among species with respect to its timing and duration, however it is generally characterized by a sudden onset in zygotic transcription and a desynchronization of the cell cycle. While in some animals this occurs during the midblastula stage (1000's of cells), others undergo the transition much earlier. The process was first described in amphibians where the transition occurs at the midblastula stage accompanied by the acquisition of cell motility and was originally termed the midblastula transition (MBT) (Newport and Kirschner 1982).

In *Drosophila,* zygotic gene expression begins prior to the MBT, with some transcripts beginning to be expressed as early as NC8 (Pritchard and Schubiger 1996).

Unlike the MBT described in *Xenopus* where the maternal to zygotic transition (MZT) is concomitant with the MBT, in *Drosophila* the MZT occurs prior to the MBT with maximal activation occuring during late interphase of NC14 (Edgar and Schubiger 1986). Microarray analysis of global gene transcription during the cleavage stage of *Drosophila* embryogenesis has revealed a highly dynamic program of mRNA expression (Arbeitman *et al*. 2002; Tadros and Lipshitz 2005; Pilot *et al*. 2006; De Renzis *et al*. 2007). These studies reveal that over half (~7800 genes) of the genome is maternally expressed and loaded into the embryo, and of the transcripts expressed during the transition, at least 1600 maternal transcripts (~20% of loaded mRNAs) are degraded and over 1000 zygotic transcripts increase in abundance at the MBT during cleavage furrow formation. In addition, much progress has been made in the identification of factors and description of the mechanisms involved in maternal and zygotic mRNA turnover prior to and during the MBT. In this section, I will discuss the progress that has been made towards understanding the non-RNA-based mechanisms that control the MBT in *Drosophila*, which include counting of the nucleocytoplasmic ratio, cell cycle control through fluctuations in activity of the cell cycle machinery, and activation of the DNA damage/replication checkpoint pathway as well as the mechanisms governing mRNA degradation, localization, and translational regulation during the MBT.

### 1.3.1 Nuclear to cytoplasmic ratio

The phenomena associated with the MBT (desychronization of individual cell cycles, activation of transcription, and acquisition of cell motility) respond to the nuclear to cytoplasmic ratio (N:C ratio) (Newport and Kirschner 1982; Newport and Kirschner 1982). It is thought that there is a cytoplasmic titrating factor that 'counts' the DNA content relative to cytoplasm. As the embryo undergoes successive rounds of replication, the factor is titrated out of the cytoplasm by the exponentially increasing content of DNA,

resulting in a lengthening of the cell cycle followed by the events of the MBT. It is likely that the general N:C ratio counting mechanism for controlling the timing of the MBT is well conserved. In *Drosophila*, mutations in *maternal haploid* (*mh*), a gene required for pronuclear fusion, give rise to haploid embryos (Edgar *et al*. 1986). Embryos derived from *mh* females progress through the first 13 nuclear cycles relatively normally, albeit at a slower rate. When the embryos reach interphase of NC14 they have the same number of nuclei as a wild type embryo at NC14, but they have half the amount of total DNA. Instead of lengthening interphase and cellularizing, almost all *mh* embryos undergo a metasynchronous mitosis 14 and then cellularize during interphase of NC15. Cleavage furrows often begin to form and ingress during the abbreviated NC14 but are interrupted and regress during the precocious mitosis 14. This observation demonstrates that the N:C ratio is one essential component in regulating the *Drosophila* MBT.

### 1.3.2 CDK activity and cell cycle regulation

Regulation of cell cycle control is also an essential aspect of the MBT and employs key conserved components. The classic studies of cell cycle progression first described by Hartwell, Hunt and Nurse found that the activity of Cyclin dependent kinases (CDKs) dictates the timing of cell cycle progression. CDK activity and substrate specificity is controlled in part by its association with a specific Cyclin protein (CYC) and its phosphorylation state. CDK protein levels remain constant through the cell cycle, but Cyclin protein levels alter causing a fluctuation in the activity of CDK. The system controlling CDK activity involves many additional regulatory factors that are able to integrate internal and external signals into an effect on CDK activity. In *Drosophila* embryos prior to NC10, nuclei proliferate with constant levels of CYC, and M-CDK (CDK that is associated with a mitosis specific Cyclin) activity presumably remains constant (Edgar *et al*. 1994). With regards to the MBT, CYC levels begin to oscillate at

NC10 with progressively higher percentages of total CYC being degraded with each successive nuclear division (Edgar *et al*. 1994). In order for interphase to lengthen long enough for furrow formation to occur, M-CDK activity needs to be inhibited. There are a number of factors that act to repress and activate M-CDK activity and their concerted regulation is important to achieve the appropriate state of M-CDK activity (Figure 1.4).

In *Drosophila*, the *cdc2* gene encodes CDK1, and its association with Cyclins A, B, and B3 are important for progression into and through mitosis during the cleavage divisions. In 10% of embryos that are maternally provided with 1X *CycA* and 1X *CycB*, mitosis of NC13 fails to initiate and embryos cellularize during an extended interphase of NC13 (Stiffler *et al*. 1999). On the other hand, ~8% of embryos expressing 4X *CycB* fail to elongate interphase of NC11-13 and cellularization never occurs (Stiffler *et al*. 1999). These observations suggest that the degradation of CYCB is essential for the elongation of interphase prior to the MBT. The dynamics of CYCB expression prior to and during the MBT are thought to result from degradation or translational repression of the *CycB* mRNA and the spindle-associated synthesis and degradation of CYCB (Huang and Raff 1999). The precise mechanism for controlling *CycB* mRNA metabolism is unknown, but appears to be independent of the major maternal degradation pathway controlled by Smaug protein discussed in section 1.3.4 (Tadros *et al*. 2007). It is known that the spindle-associated degradation of CYCB is APC-CDC20-dependent (Raff *et al*. 2002). Based on precedent from vertebrate studies and the localization of *CycB* mRNA to mitotic spindles in cleavage stage embryos, local polyadenylation-dependent translational activation may account for nuclear cycle-specific synthesis of CYCB during the MBT in *Drosophila*.

Two effectors of M-CDK1 activity include CDC25, a phosphatase that activates CDK1, and Wee1, a kinase that inactivates M-CDK1. In *Drosophila*, two genes encode

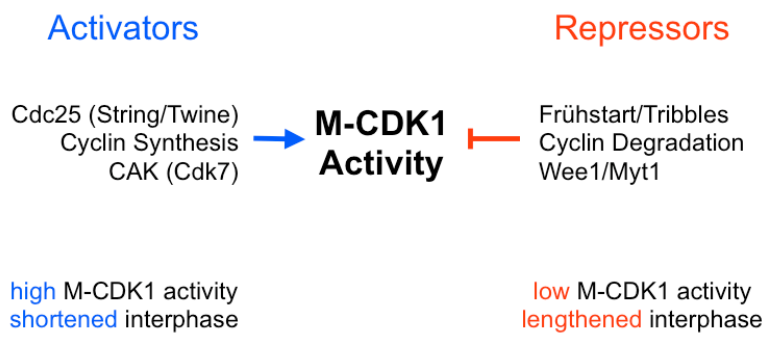


**Figure 1.4 Proper regulation of M-CDK1 activity during the MBT is essential for cleavage furrow formation**

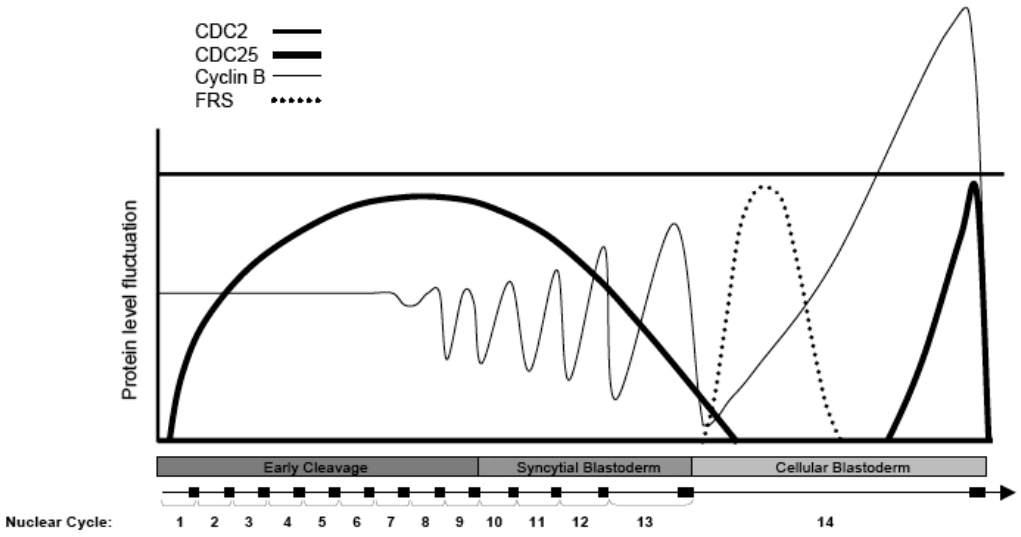


**Figure 1.5 Levels of cell cycle regulators fluctuate during the MBT**

Lines indicate fluctuations in protein levels over time as indicated at bottom. Figure adapted from Edgar *et al*. 1994.

CDC25, *string* (*stg*) and *twine* (*twe*), which are degraded during NC14. In a minor fraction (~2-5%) of embryos that contain 4X or 6X copies of either of these genes, embryos undergo a premature mitosis 14 and cellularize during interphase of NC15 (Edgar and Datar 1996). In 16% of embryos that are maternally provided with 1X *twe* and 0X *stg*, cellularization occurs during interphase of NC13 (Edgar and Datar 1996). These phenotypes are presumably due to a disruption in M-CDK1 activity during NC14. Prior to and during the MBT, Wee1 activity is constant, resulting in limited M-CDK1 activity during NC14. Loss of Wee1 activity results in abnormal cortical syncytial divisions and a failure to lengthen interphase due to a loss of M-CDK1 inhibition (Price *et al*. 2002).

In addition, there are zygotically encoded factors that affect M-CDK1 activity. Frühstart (FRS) and Tribbles (TRBL) are two zygotically encoded proteins that promote NC14 interphase lengthening (Grosshans and Wieschaus 2000). Although loss-of-function mutations in *frs* or *trbl* have no effect on divisions prior to NC13, they cause a premature mitosis 14 and cellularization during NC15 in ~8% of embryos (Grosshans and Wieschaus 2000). FRS is thought to inhibit the low levels of active M-CDK1 present at the start of NC14 by directly binding to CYCB, preventing specific substrate interactions (Gawlinski *et al*. 2007). TRBL, on the other hand, is required for CDC25 degradation (Mata *et al*. 2000). Introduction of ectopic *frs* or *trbl* mRNAs causes inhibition of mitosis at the sites of injection consistent with an inhibitory function (Grosshans and Wieschaus 2000).

Concerted regulation of these maternal and zygotic factors contributes to the inhibition of M-CDK1 activity and promotes the lengthening of interphase at NC14 through the degradation of CDC25 and directs inhibition of M-CDK1 through CYCB binding and inhibitory phosphorylation. Nearly all haploid embryos derived from

maternal haploid mutant females, where the N:C ratio is disrupted, fail to extend interphase of NC14 and attempt to cellularize in NC15. Yet, loss-of-function mutations in *frs* and *trbl* result in relatively low penetrance of premature mitosis of NC14, and the overexpression of CDC25 has a similar penetrance. Therefore, additional mechanisms beyond those already described are thought to regulate the timing of the MBT. In chapter 4, I will discuss how dFMRP is likely contributing to this regulation by impinging on M-CDK1 activity during the MBT.

### 1.3.3 DNA damage/replication checkpoint pathway

The lengthening of interphase after NC10 is also mediated by a cell cycle checkpoint mechanism. The DNA-replication damage checkpoint in *Drosophila* embryos can be considered to have been co-opted in order to gradually lengthen the cycle cycles after NC10. It is thought that during these later cycles S-phase takes longer to complete and a maternal replication factor is titrated out of the cytoplasm, resulting in a lengthening in interphase (Sibon *et al*. 1997). Meanwhile, the cell cycle oscillator controlling M-CDK1 activity continues to drive the cell cycle forward. Maternal expression of components of a conserved DNA-replication/damage checkpoint pathway, *grapes* (*grp*)/*checkpoint kinase-1* (*chk1*) and *meiosis-41* (*mei-41*), is required to respond to the state of DNA synthesis and delay M-phase (Sibon *et al*. 1997; Sibon *et al*. 1999). This checkpoint pathway is thought to mediate the inhibitory phosphorylation of CDK1 (CDC2), which inhibits its ability to initiate mitosis (Sibon *et al*. 1999). Checkpoint mutants cause severe mitotic spindle defects at NC12, block initiation of zygotic transcription, and fail to cellularize (Fogarty *et al*. 1994; Sibon *et al*. 1997; Sibon *et al*. 1999). In addition, it has been shown that GRP/CHK1 normally delays the nuclear accumulation of CYCB, preventing activation of CDK1 and delaying the cell cycle at the MBT (Royou *et al*. 2005).

### 1.3.4 Maternal and zygotic mRNA degradation pathways

In addition to cell cycle regulation and activation of zygotic transcription, regulation of mRNA degradation, localization, and translational control play key roles in the execution of the events of the MBT. Messenger RNA turnover is in part mediated by the precise coordination of maternally and zygotically encoded degradation pathways.

The maternal mRNA degradation pathway begins at or shortly following egg activation and does not require fertilization (Bashirullah *et al*. 1999). One of the major pathways that influences the degradation of unstable maternal mRNAs following egg activation is regulated by Smaug (SMG), a multifunctional RNA-binding protein that is able to translationally repress as well as direct the degradation of target transcripts (Tadros *et al*. 2007). Smaug protein accumulates after egg activation, and the mRNA and protein are degraded just prior to NC14 (Dahanukar *et al*. 1999). Prior to egg activation, *smg* mRNA is translationally repressed through its association with Pumilio and other repressive factors. Following egg activation, the Pan Gu Kinase acts through the *smg* 3'UTR to activate translation by relieving repression. SMG then mediates maternal transcript degradation by recruiting the CCR4-POP2-NOT deadenylase complex to a large number of the newly polyadenylated maternal mRNAs to mediate their deadenylation and subsequent degradation (Semotok *et al*. 2005). In addition, SMG can mediate translational repression by inhibiting initiation of translation via its known interaction with eIF4E and CUP (Nelson *et al*. 2004). Embryos derived from *smg* mutant females develop normally until NC11, at which point mitotic spindle defects are observed and cellularization fails to occur (Dahanukar *et al*. 1999). Analysis of gene expression in embryos from wild type and *smg-* females using microarray-based gene expression profiling shows that nearly 2/3rds of unstable maternal mRNAs are degraded in a SMG-dependent manner (Tadros *et al*. 2007). Messenger RNAs that are degraded in a SMG-

dependent manner are enriched for gene ontology terms related to the cell cycle, and the mis-expression of these mRNAs may be at least partially responsible for the *smg*- phenotypes. Although the interpretation of the *smg*- phenotype has focused on the demonstrable degradation of maternal mRNAs, it is possible that the SMG-mediated translational repression of some maternal mRNAs significantly contributes to the *smg*- phenotype. Despite this possibility, it remains clear that maternal mRNA degradation is required to execute the events of the MBT, and SMG-dependent degradation is a dominant pathway.

The zygotic degradation pathway becomes active 1.5-2hr after fertilization and functions with the maternal pathway to degrade specific mRNAs at the MZT/MBT (Bashirullah *et al*. 1999). The zygotic pathway is necessary to fully degrade mRNAs targeted by the maternal pathway as well as mRNAs that are unaffected by the maternal pathway. The identity of any zygotic factors that mediate the degradation of mRNAs at the MZT/MBT is unknown. Although recent progress has been made towards identifying these factors. In a set of elegant experiments, a combination of chromosome ablation and microarray analysis was used to determine what contribution the maternal and zygotic genomes make to the total amount of mRNA present at the MBT as well as how the degradation of maternal mRNAs is correlated with the activation of the zygotic genome (De Renzis *et al*. 2007). This analysis found that zygotically active genes at the MBT are enriched for transcription factors and that mRNAs that are first ubiquitously expressed maternally are 're-expressed' zygotically in localized patterns during the MBT. This observation is likely important for the subsequent determination of cell fate. In addition, *cis*-regulatory heptad DNA sequences, referred to as TAGteam sites, are enriched in genes zygotically expressed at the MBT. Bicoid stability factor (BSF), a protein previously implicated in translational regulation, was found to be capable of binding to

these sites and activate transcription (De Renzis *et al*. 2007). Recently it has also been shown that a transcriptional activator, Zelda (ZLD), is responsible for the activation of a large number of zygotic genes and also acts through binding to TAGteam sites (Liang *et al*. 2008). Embryos derived from *zld-* females are normal up to NC14 when then fail to cellularize or undergo cellularization with abnormal cleavage furrows. In addition, some embryos undergo what may be a premature mitosis of NC14 as seen in *frs* mutants. Indeed, the same study shows by microarray analysis that *frs* mRNA as well as mRNAs of other zygotically expressed genes required for proper cellularization (ie. *slam*, *nullo*, and *bnk*) are significantly downregulated in the *zld-* embryos. In the future, identification and further analysis of targets of BSF and ZLD transcriptional activation may reveal mediators of the zygotic degradation pathway as well as new effectors of the MBT.

Although this progress has been very important for identifying the major pathways and targets for maternal mRNA degradation at the MBT, these studies only focus on those mRNAs that are activated or degraded and have not identified mRNAs that are translationally repressed, which could represent a functionally important group of mRNAs.

### 1.3.5 Translational regulation

Degradation and transcriptional activation are clearly essential for the MBT, but there is also accumulating evidence that translational regulation also plays an important role in mediating the events of the MBT. Maternally expressed genes encoding conserved proteins that function in RNA translational control and localization such as *valois* (*vls*) and *staufen* (*stau*) have been shown to be required for pole cell formation and proper cleavage furrow formation during the MBT, although the context with which these translational regulators are functioning to mediate the events of the MBT is unknown (Schupbach and Wieschaus 1989; Sullivan *et al*. 1993). Given what we know about

dFMRP, it is an excellent candidate for also having a role in translational regulation during the MBT. I will present evidence for this in the following chapters.

There are also interesting links between the MBT and the RNA silencing pathways in *Drosophila*. Regulation of translation via silencing is used in many cellular and developmental processes in animals. Critical components of the RNA silencing pathway are members of the Argonaute protein family, and proteins of this family contain a PAZ domain, implicated in RNA-binding, as well as a PIWI domain, implicated in ribonuclease activity (Hutvagner and Simard 2008). Argonaute proteins associate with small, 22-25 nucleotide RNAs and guide them to their complementary mRNAs. About half of embryos derived from *ago2-* females have defects in pole cell formation and early nuclear divisions and migrations prior to the MBT (Deshpande *et al*. 2005; Meyer *et al*. 2006). In addition, *ago1* genetically interacts with an amorphic allele of *ago2* specifically during the MBT, suggesting that they have redundant activities at this time in development (Meyer *et al*. 2006). Though, it is unclear if this interaction is affecting the degradation or translational repression of mRNAs. It was originally thought that in *Drosophila* AGO1 functions in micro RNA (miRNA)-mediated RNA silencing via translational repression and AGO2 functions in small interfering RNA (siRNA)-mediated RNA silencing via mRNA degradation, although these relationships are likely more complex. Meyer *et al*., suggest that AGO1 and AGO2 are present in some type of mRNP degradation complex, possibly P bodies, and that the RNA silencing machinery is required for mediating the events of the MBT.

There is precedent for a requirement for miRNA-mediated translational regulation during vertebrate MBT. Zebrafish miR-430 is expressed at the MBT and is required for the downregulation of several hundred maternally expressed mRNAs (Giraldez *et al*. 2006). More direct studies have investigated the effects of miRNA loss-of-function

during the *Drosophila* MBT. Embryos injected with *miR-9* antisense oligos to disrupt *miR-9* function have severe defects in nuclear division and morphology, although it is unclear what the primary defect is in these embryos (Leaman *et al*. 2005). More recently, the *miR-309* cluster (containing *miR-3, miR4, miR5*, *miR6, miR286* and *miR-309*) was deleted in flies, and although there are no effects on embryonic development, microarray analysis reveals that a distinct set of maternal mRNAs is upregulated in the absence of the miRNAs (Bushati *et al*. 2008). The absence of an embryonic phenotype is possibly due to redundant function of miRNAs. It may be necessary to delete additional, redundant miRNA clusters that are specifically expressed during the MBT in order to detect embryonic phenotypes associated with disruptions in the MBT. The study suggests that a set of miRNAs is required to promote the deadenylation and clearence of maternal mRNAs at the MBT. Once again, this type of analysis would not identify mRNAs that are translationally repressed and not degraded in the absence of the miRNAs. Together these observations suggest that the RNA silencing machinery and miRNAs expressed at the MBT may represent the factors involved in the zygotic degradation pathway for the MBT.

As previously mentioned, there is evidence that FMRP functions with the RNA silencing pathways. Future studies exploring this relationship during the MBT could lead to a better understanding of RNA metabolism/translational regulation during the MBT as well as FMRP function.

# Chapter 2: dFMRP is required for cleavage furrow formation and controls *trailer hitch* expression

The data described in this chapter have been published in *The Proceedings of the National Academy of Sciences* (Monzo *et al*. 2006).

## 2.1 INTRODUCTION

During the cleavage stage of animal embryogenesis, cell numbers increase dramatically without growth, and a shift from maternal to zygotic genetic control occurs called the midblastula transition (MBT). Although these processes are fundamental to animal development, the molecular mechanisms controlling them are poorly understood. Here, we demonstrate that *Drosophila* fragile X mental retardation protein (dFMRP) is required for cleavage furrow formation and functions within dynamic cytoplasmic ribonucleoprotein (RNP) bodies during the MBT. dFMRP is observed to colocalize with the cytoplasmic RNP body components Maternal expression at 31B (ME31B) and Trailer Hitch (TRAL) in a punctate pattern throughout the cytoplasm of cleavage stage embryos. Complementary biochemistry demonstrates that dFMRP does not associate with polyribosomes, consistent with its reported exclusion from many cytoplasmic RNP bodies. By using a conditional mutation in *small bristles* (*sbr*), which encodes an mRNA nuclear export factor, to disrupt the normal cytoplasmic accumulation of zygotic transcripts at the MBT, we observe the formation of large, abnormal dFMRP/TRAL-associated structures, suggesting that dFMRP and TRAL dynamically regulate RNA metabolism at the MBT. Furthermore, we show that dFMRP associates with endogenous *tral* mRNA and is required for normal TRAL protein expression and localization,

revealing it as a previously undescribed target of dFMRP control. We also show genetically that *tral* itself is required for cleavage furrow formation. Together, these data suggest that in cleavage stage *Drosophila* embryos, dFMRP affects protein expression by controlling the availability and/or competency of specific transcripts to be translated.

## 2.2 RESULTS

### 2.2.1 *dfmr1* is required for female and male fertility

We tested the fertility of *dfmr1*$^{3}$*/Df(3R)Exel6265* (hereafter referred to as *dfmr1-*) females, which lack detectable dFMRP protein (Figure 2.1A), and examined their progeny for embryonic phenotypes. Wild type (WT, also referred to as *Oregon-R* in figures) and *dfmr1-* females were found to produce morphologically normal eggs at similar rates when crossed to WT males; however, fewer of the embryos from *dfmr1-* females hatch (Figure 2.1B). To test whether the embryos that hatch from *dfmr1-* females reflect partial rescue by the paternal chromosome containing a WT copy of *dfmr1*, *dfmr1-* females were crossed to heterozygous *fmr1*$^{3}$*/TM3-GFP* males and progeny were scored. Comparable numbers of *dfmr1-/dfmr1-* and *dfmr1-*/TM3-GFP embryos hatched, indicating that the viability of these embryos is determined by the maternal genotype (Figure 2.1B). We also verified that *dfmr1-* mutant males are sterile, as described in Zhang *et al*. 2004 (Figure 2.1B).

### 2.2.2 dFMRP activity is essential for cleavage furrow formation

Aside from a subtle effect on the duration of nuclear cycles 12 and 13 (see A2.1), a fully penetrant cleavage furrow formation phenotype was the first substantial defect

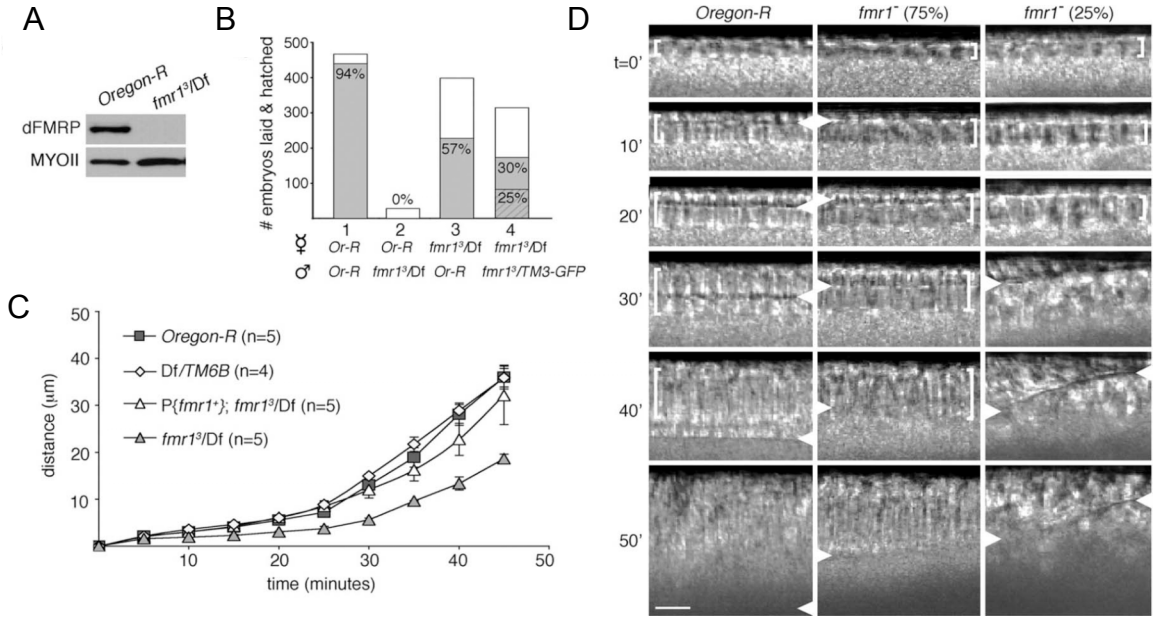


**Figure 2.1 Maternal expression of *dfmr1* is required for cleavage furrow formation**

(A) Immunoblots of 15 μg of *Oregon-R* (WT) and *dfmr1-* (*dfmr1*$^{3}$*/Df*) adult female extracts probed for dFMRP and Myosin II (MYOII, control). (B) The number of F1 embryos laid (white plus gray) and hatched (gray) are shown as bars for each cross. Hatch percentages (hatched/laid) are indicated on each bar. The striped region of bar 4 indicates the number of *dfmr1*$^{3}$*/TM3-GFP* hatchlings. (C) The average rate of furrow ingression is shown for embryos derived from the indicated female genotypes at 25°C. *dfmr1-* embryos with severe furrowing defects (D *Right*) were not quantified. Error bars and *n* indicate the standard deviation (SD) and number of movies measured, respectively. (D) Sequential frames from representative differential interference contrast movies of WT and *dfmr1-* embryos undergoing normal (*Left*), delayed (*Center*), and severely disrupted (*Right*) furrow formation at 25°C. The percentage of *dfmr1-* embryos in each phenotypic class is shown in parentheses. White arrowheads and brackets indicate the furrow front position and nuclear elongation, respectively. Times (*t* minutes) are relative to nuclear cycle 14 onset. Scale bar indicates 10 μm.

observed in live embryos derived from *dfmr1-* females crossed to WT males (hereafter referred to as *dfmr1-* embryos; Figure 2.1C and D). Approximately 75% of *dfmr1-* embryos display significant reduction in the rate of furrow ingression (Figure 2.1C and D), whereas the remaining 25% display dramatic furrowing defects characterized by abnormal nuclear morphology and uneven furrow ingression (Figure 2.1D). These phenotypes are rescued by maternal expression of a WT copy of *dfmr1* from a single P element transgene (Figure 2.1C) (Dockendorff *et al*. 2002). Immunofluorescence (IF) analysis of fixed cleavage stage *dfmr1-* embryos reveals no significant alteration in the appearance of MTs, Myosin II, Anillin, cortical F-actin, or Lava Lamp (LVA) associated Golgi bodies (Figure 2.5A). Together these observations suggest that dFMRP is required for proper cleavage furrow formation and that the phenotype is not likely due to gross defects in the MT or actin cytoskeletons.

### 2.2.3 dFMRP associates with cytoplasmic RNP bodies in cleavage stage embryos

Our phenotypic analysis indicates that the earliest measurable requirement for *dfmr1* occurs in the cleavage stage, hours before nervous system formation. To explore its function at this time, we examined the subcellular localization of dFMRP by indirect IF in fixed cleavage stage embryos. This analysis reveals a punctate distribution throughout the cytoplasm that increases in intensity over the course of furrow formation (Figure 2.2). Some dFMRP-associated structures associate with the advancing furrow front (Figure 2, arrow and bracket) and frequently are found adjacent to LVA-associated Golgi compartments but do not significantly colocalize with them (<2.5% of dFMRP puncta, $P > 0.5$; Table 2.1). Nuclear-localized dFMRP was not observed (Figure 2.2).

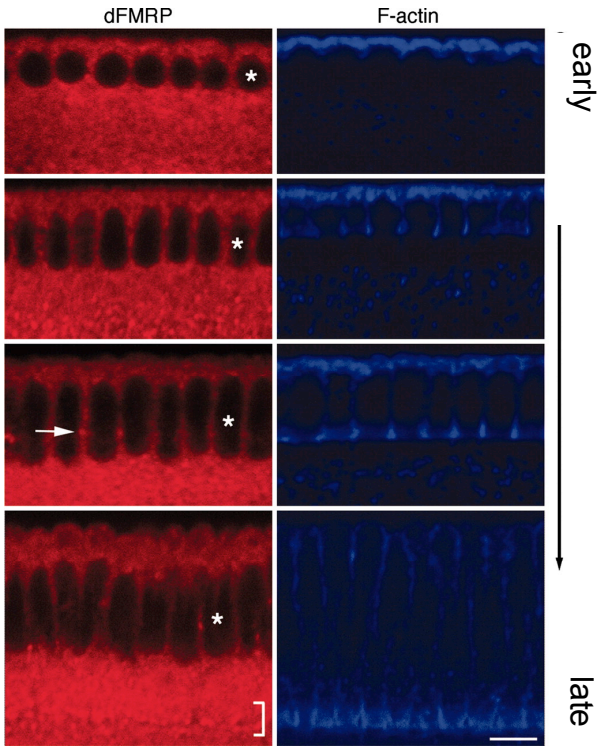


**Figure 2.2 dFMRP localizes to punctate cytoplasmic structures in cleavage stage embryos**

IF analysis of fixed WT embryos at progressive stages of cellularization shows punctate dFMRP localization throughout the cytoplasm (*Left*) and corresponding cortical F-actin marking plasma membrane furrows (*Right*). dFMRP puncta often are positioned at the furrow front (arrow and bracket). Asterisks indicate nuclei. Scale bar indicates 10 μm.

The localization pattern of dFMRP in embryos resembles the punctate localization described for the cytoplasmic RNP body protein components ME31B and TRAL in female germ-line cells, which are implicated in mRNA sequestration, transport, and translational suppression (Nakamura *et al*. 2001; Wilhelm *et al*. 2005). Also, RNase-treatment of fixed WT embryos causes a sharp and specific reduction in dFMRP detection by IF (Figure 2.3). Whether due to extraction of dFMRP or structural alteration of its epitope, this suggests that the dFMRP-associated structures contain RNA. Therefore, we assessed whether dFMRP colocalized with ME31B and TRAL in fixed embryos by IF. Indeed, quantification of IF images reveals a significant colocalization of dFMRP puncta with TRAL (42%, $P = 3.9 \times 10–17$) and ME31B (35%, $P = 2.6 \times 10–10$) puncta, particularly in the apical cytoplasm (Figure 2.4A; Table 2.1). Because dFMRP has been shown to associate with dAGO2 in Drosophila S2 cells (Caudy *et al*. 2002; Ishizuka *et al*. 2002) and mammalian argonaute proteins associate with cytoplasmic RNP bodies (Jakymiw *et al*. 2005; Liu *et al*. 2005; Sen and Blau 2005), we also tested whether dFMRP and dAGO2 colocalize. Punctate dAGO2 localization is seen almost exclusively in the basal cytoplasm where moderate colocalization of dFMRP puncta is observed with dAGO2 (Figure 2.4A, and 16%, $P = 8.8 \times 10–9$; Table 2.1).

To further explore the relationship between dFMRP, TRAL, ME31B, and dAGO2, we separated RNP complexes from cleavage stage embryos on sucrose density gradients and determined the sedimentation profiles for these proteins by immunoblot analysis. The majority of dAGO2 cosediments with polyribosomes (Figure 2.4B). By contrast, all detectable dFMRP sediments near the top of the gradient and does not associate with polyribosomes (Figure 2.4B), which are thought to be excluded from translationally quiescent cytoplasmic RNP bodies (Coller and Parker 2005).

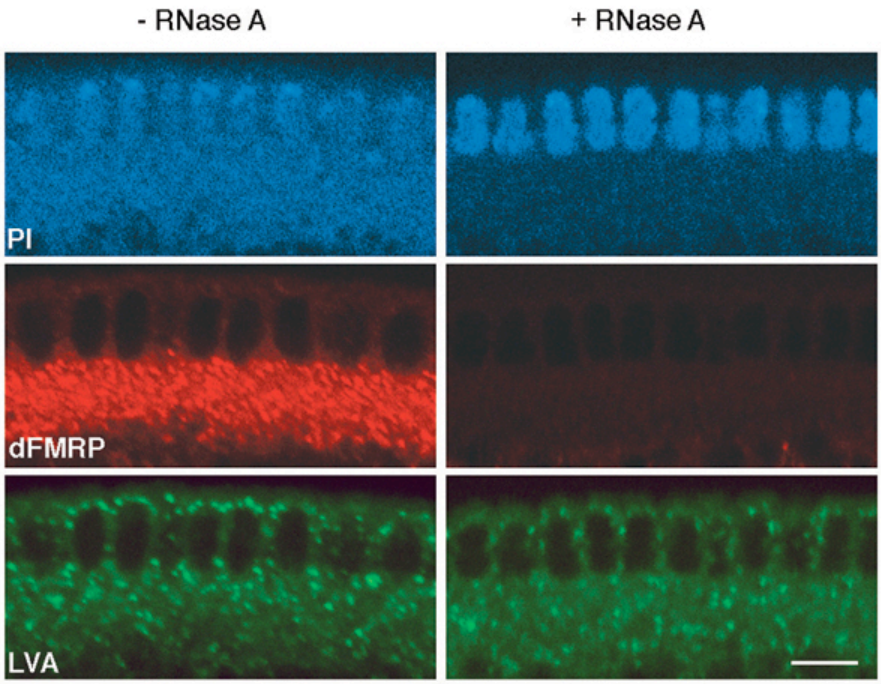


**Figure 2.3 dFMRP IF detection is RNase-sensitive**
Wild-type cleavage stage embryos were either not treated (*Left*) or treated (*Right*) with RNase A after fixation and before antibody incubation for IF. The RNase-treatment efficiently digested the cytoplasmic RNA (propidium iodide, PI), marginally affected LVA localization, and caused a significant reduction in dFMRP detection. The latter could result from the RNase-treatment extracting dFMRP or structurally altering the dFMRP epitope. In either case, these results suggest that the dFMRP-associated structures contain RNA. Scale bar indicates 10 μm.

| Measurement | TRAL (apical) | ME31B (apical) | dAGO2 (basal) | LVA (apical) | LVA (basal) |
|---|---|---|---|---|---|
| % dFMRP colocalizing | 42.2 | 34.9 | 15.8 | 0.9 | 2.4 |
| % control dFMRP colocalizing | 0.5 | 0.6 | 0.4 | 1.4 | 1.6 |
| Total no. of dFMRP puncta | 405 | 192 | 228 | 216 | 254 |
| Student's *t* test score (*P* value) | $4 \times 10^{-17}$ | $3 \times 10^{-10}$ | $9 \times 10^{-9}$ | 0.6 | 0.7 |

**Table 2.1 dFMRP significantly colocalizes with TRAL, ME31B, and dAGO2**

The percentages shown represent the number of dFMRP puncta that colocalize with either TRAL, ME31B, dAGO2, or LVA puncta in the apical or basal cytoplasm (as indicated) in original or control IF images. See A3.2.5 for method of quantification.

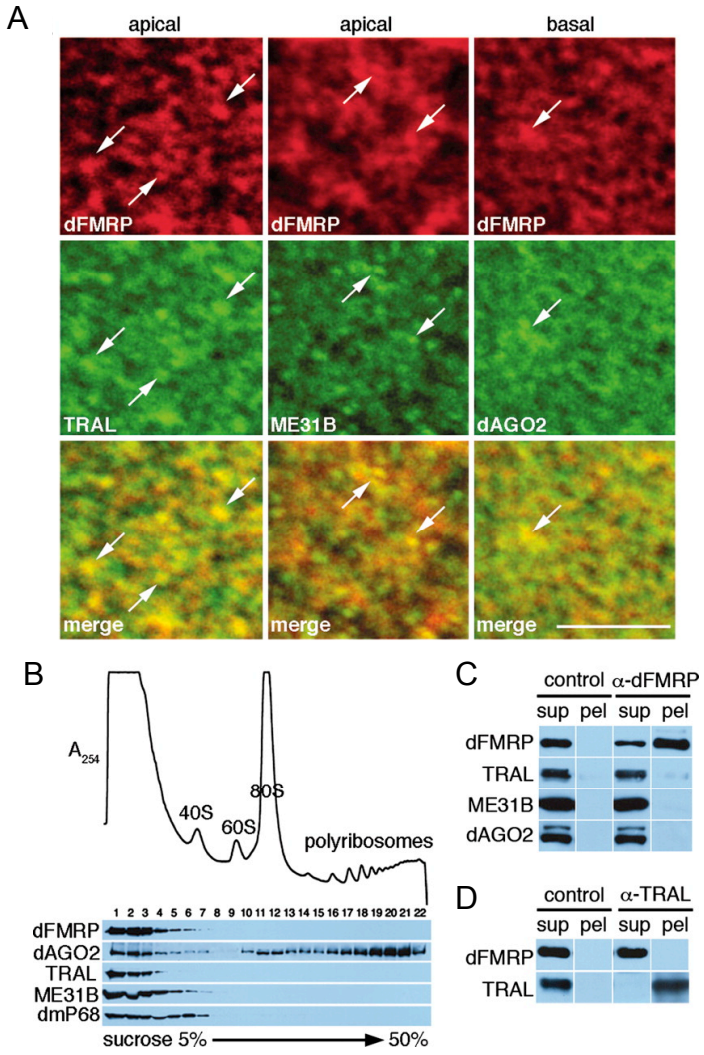


**Figure 2.4 dFMRP associates with cytoplasmic RNP bodies in cleavage stage embryos**

(A) IF analysis of fixed WT cleavage stage embryos shows considerable colocalization of dFMRP with TRAL and ME31B throughout the cytoplasm (apical cytoplasm shown) and partial colocalization with dAGO2 (only observed in the basal cytoplasm) in oblique optical sections. Arrows indicate examples of colocalization. Scale bar indicates 10 μm. (B) A UV absorbance trace (*A*254) indicates the positions of ribosomal subunits and polyribosomes across fractions 1–22 from a sucrose gradient. Immunoblots reveal the sedimentation profiles of proteins indicated at the left. (C and D) Immunoblots showing supernatant (sup) and pellet (pel) fractions from IPs performed with anti-FLAG (control) or anti-dFMRP antibodies (C) and BSA (control) or anti-TRAL antibody (D) by using WT embryo extracts. Blots were probed for the proteins indicated at the left. A weak nonspecific TRAL signal is observed in both pellets of C.

Similarly, TRAL and ME31B sediment near the top of the gradient as does dmP68, a DEAD-box-containing RNA helicase that associates with dFMRP and dAGO2 in Drosophila S2 cells (Ishizuka *et al*. 2002). These results are consistent with our IF data, indicating that dFMRP associates with translationally quiescent cytoplasmic RNP bodies. Although most dFMRP, TRAL, ME31B, and dmP68 cosediment in sucrose gradients, anti-dFMRP antibody does not coimmunoprecipitate (co-IP) TRAL, ME31B, or dmP68 (Figure 2.4C; dmP68 not shown), nor does anti-TRAL antibody co-IP dFMRP (Figure 2.4D). dAGO2 also does not co-IP with dFMRP in embryo extracts (Figure 2.4C). Therefore, dFMRP, TRAL, and ME31B probably exist in distinct complexes that associate with a common cytoplasmic structure.

### 2.2.4 dFMRP/TRAL-associated cytoplasmic RNP bodies are dynamic

If the dFMRP-associated cytoplasmic RNP bodies were metabolically active and associated with zygotic transcripts at the MBT, then a change in their composition and/or structure would be expected to occur upon disrupting the normal cytoplasmic accumulation of zygotic transcripts during the MBT. To test this possibility, we used a well characterized conditional mutation in *small bristles* (*sbr*), which encodes the Drosophila mRNA nuclear export factor NXF-1, to specifically block nuclear export of newly synthesized transcripts at the MBT (Wilkie *et al*. 2001). WT and $sbr^{ts148}$ embryos were either kept at the permissive temperature or shifted to the restrictive temperature for 25 min during the MBT, fixed, and examined by IF. Normal dFMRP, TRAL, and ME31B localization is observed in WT embryos at either temperature and in $sbr^{ts148}$ embryos at the permissive temperature (Figure 2.5). By contrast, temperature shifted $sbr^{ts148}$ embryos display a rapid and dramatic change in dFMRP and TRAL localization (Figure 2.4). Both proteins colocalize to large polymorphic structures (average

diameter= 2.8 μm) in the apical cytoplasm, which likely reflect the spatial coalescence of RNA processing intermediates containing dFMRP and TRAL. ME31B localization is unaffected in temperature-shifted *sbr*$^{ts148}$ embryos (data not shown), indicating that the effect on dFMRP and TRAL is specific.

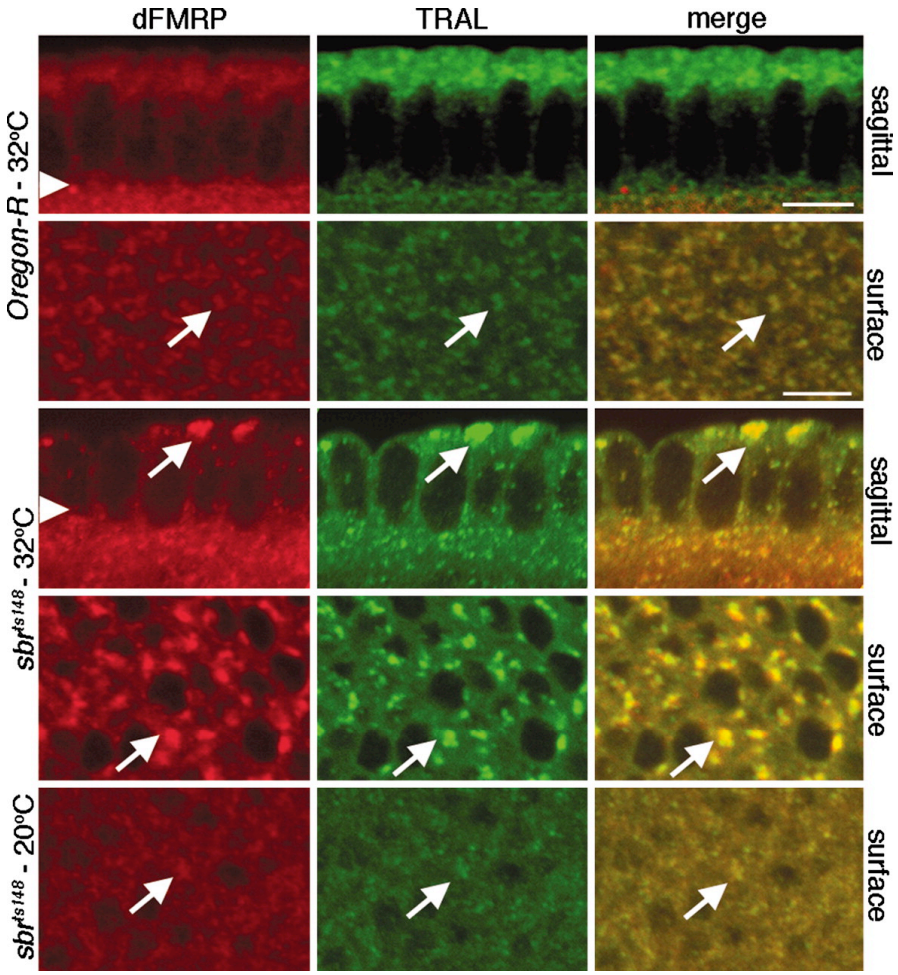


**Figure 2.5 dFMRP/TRAL cytoplasmic RNP bodies are dramatically affected by disrupting the MBT**

IF analysis of cleavage stage WT or *sbr*$^{ts148}$ embryos fixed at 32°C or 20°C (indicated at left) shows dFMRP and TRAL localization in sagittal and surface views (indicated at right). The WT and *sbr*$^{ts148}$ embryos were shifted to 32°C at 5 and 15 min into nuclear cycle 14, respectively. Arrows indicate colocalization. Arrowheads indicate the furrow front. Scale bar indicates 10 μm.

### 2.2.5 dFMRP associates with endogenous *tral* mRNA and is required for TRAL expression and localization

We next evaluated whether dFMRP is required for TRAL and ME31B expression in cleavage stage embryos. Because dFMRP binds *futsch* mRNA and suppresses its translation in Drosophila neurons (Zhang *et al*. 2001), we tested *futsch* expression in cleavage stage embryos as a control. As expected, quantitative reverse transcription PCR (qRT-PCR) showed comparable *futsch* mRNA levels between *dfmr1-* and WT embryos (Figure 2.6C), whereas quantification of Futsch protein revealed a 70% increase in fixed *dfmr1-* embryos over controls by IF (Figure 2.6A). Interestingly, in *dfmr1-* embryos TRAL localizes to numerous abnormal punctate structures in the apical cytoplasm (Figure 2.6B, 3.5 puncta per 10 $\mu m^2$). Although these structures are spherical and smaller (average diameter = 1.8 μm) than the polymorphic structures observed in $sbr^{ts148}$ mutants, they localize to the apical cytoplasm and lack detectable ME31B, as in $sbr^{ts148}$ embryos (data not shown). They are also observed before the MBT, but they are fewer in number (1.7 puncta per 10 $\mu m^2$), smaller (average diameter = 1.1 μm), and have no apparent phenotypic effect. Quantitative immunoblots show TRAL protein levels are reduced 2-fold in whole cleavage stage embryo extracts, whereas again ME31B is unaffected (Figure 2.6C). Paradoxically, instead of a decrease, we observe a significant increase in *tral* mRNA levels by quantitative PCR in *dfmr1-* embryos (Figure 2.6D). *me31b* mRNA levels are not significantly affected (Figure 2.6D). To test whether dFMRP associates with endogenous *tral* mRNA, we performed qRT-PCR on mRNA IPd from WT and *dfmr1-* embryo extracts using an anti-dFMRP antibody. Background levels of *RpL32* mRNA served as a control (Figure 2.6E). A nearly 10-fold enrichment of *tral* mRNA is observed in WT IPs over the background levels observed in *dfmr1-* IPs (Figure 2.6E).

These results suggest that in cleavage stage embryos dFMRP associates with a tral mRNP complex and possibly controls its competency and/or accessibility for translation.

To address whether the misexpression of TRAL might contribute to the furrow formation phenotype observed in *dfmr1-* embryos, we examined live *tral* mutant embryos undergoing cleavage furrow formation. Embryos laid by $tral^2/tral^3$, $tral^2/+$, $fmr1^3/+$, $tral^2/fmr1^3$, and *Df(3L)iro-2*/+ females crossed to WT males were examined and will be referred to using the female genotype for simplicity. The $tral^2$ and $fmr1^3$ are protein null alleles, $tral^3$ is a hypomorph, and *Df(3L)iro-2* removes the *tral* gene (*tral* alleles described in (Wilhelm *et al*. 2005). All $tral^2/tral^3$ embryos have a severe cleavage furrow formation phenotype that resembles the strong *dfmr1-* phenotype, and both $tral^2/+$ and *Df(3L)iro-2*/+ embryos have a moderate phenotype resembling the phenotype seen in most *dfmr1-* embryos (Figure 2.6; Figure 2.1; *Df(3L)iro-2* data not shown). Although $fmr1^3/+$ embryos furrow normally, the absence of a single copy of *dfmr1* in $tral^2/fmr1^3$ embryos mildly enhances the $tral^2/+$ phenotype (Figure 2.6). Together these observations suggest that dFMRP is required for the normal expression of TRAL and that the misexpression of TRAL likely at least partially contributes to the *dfmr1-* cleavage furrow formation phenotype.

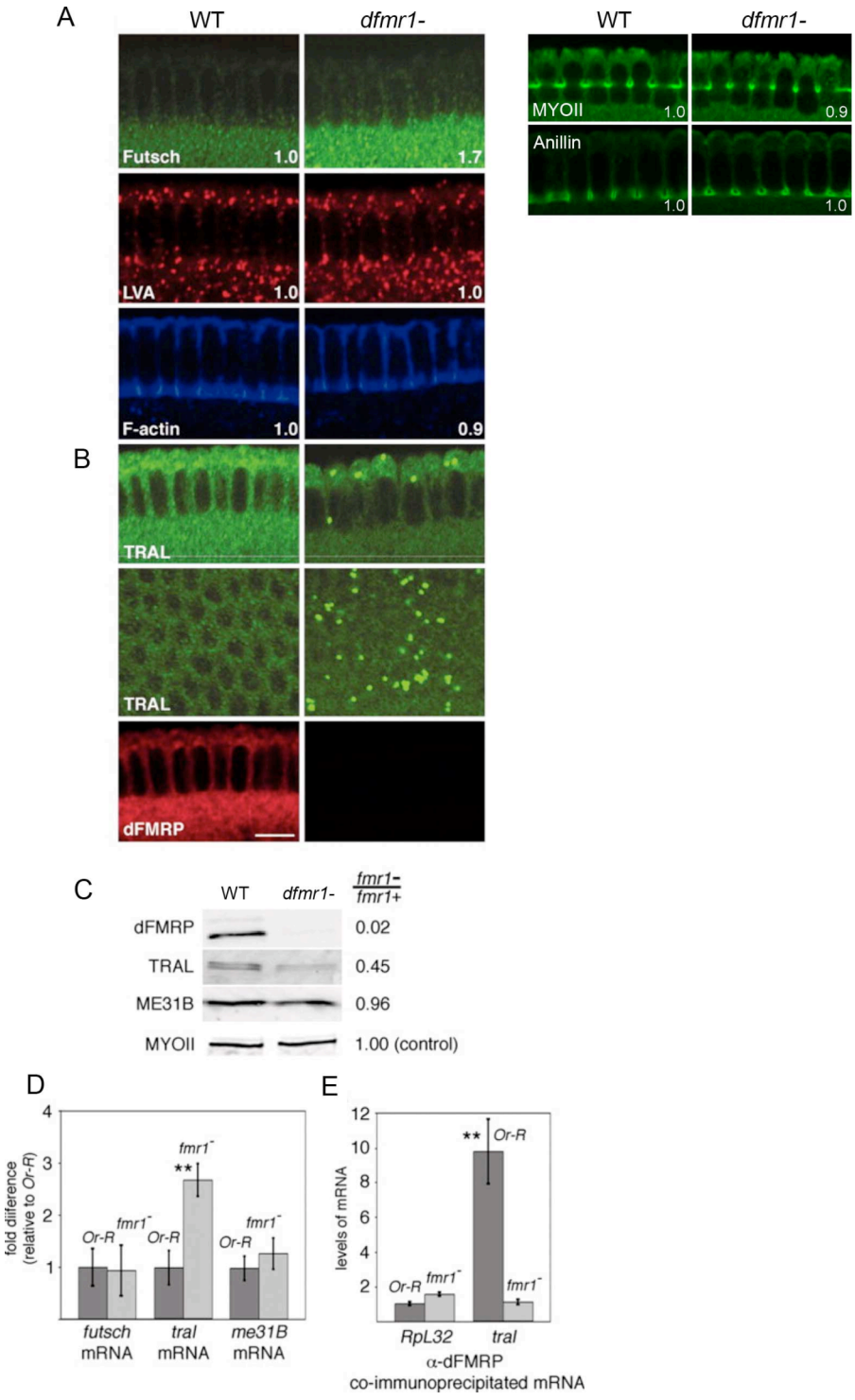


**Figure 2.6 *tral* mRNA is a target of dFMRP regulation**

Figure 2.6 on previous page.
(A and B) IF analysis of fixed WT and *fmr1* cleavage stage embryos show Futsch, Lava Lamp (LVA), F-actin, TRAL, and dFMRP localization. Quantified fluorescence signal intensity (level in *fmr1* / level in WT) is indicated in A *Lower Right*. (B) Sagittal (*Top*) and surface (*Middle*) optical sections show abnormal TRAL structures in the apical cytoplasm of *fmr1*- embryos. Scale bar indicates 10 μm. (C) Quantitative immunoblots show levels of the proteins indicated to the left in WT and *fmr1*- cleavage stage embryo extracts. Each signal was independently normalized to an internal loading control Myosin II (MYOII). The ratios of normalized signal intensities (*fmr1*- / WT) are shown to the right (dAGO2 ratio 0.85, data not shown). (D) Quantification of *futsch*, *tral*, and *me31B* mRNA levels in cleavage stage WT and *fmr1*- embryos by qRT-PCR shows a 2.7-fold increase in *tral* mRNA in *fmr*- embryos. *futsch* and *me31B* mRNA levels show no significant difference. (E) qRT-PCR of *RpL32* and *tral* mRNA in anti-dFMRP immunoprecipitates from cleavage stage WT and *fmr1*- embryo extracts. Significance was assessed by using the Student's *t* test (**, $P$ 0.005); $P$ 0.003 in *d*; and $P$ 0.001 in *e*). Error bars indicate SDs.

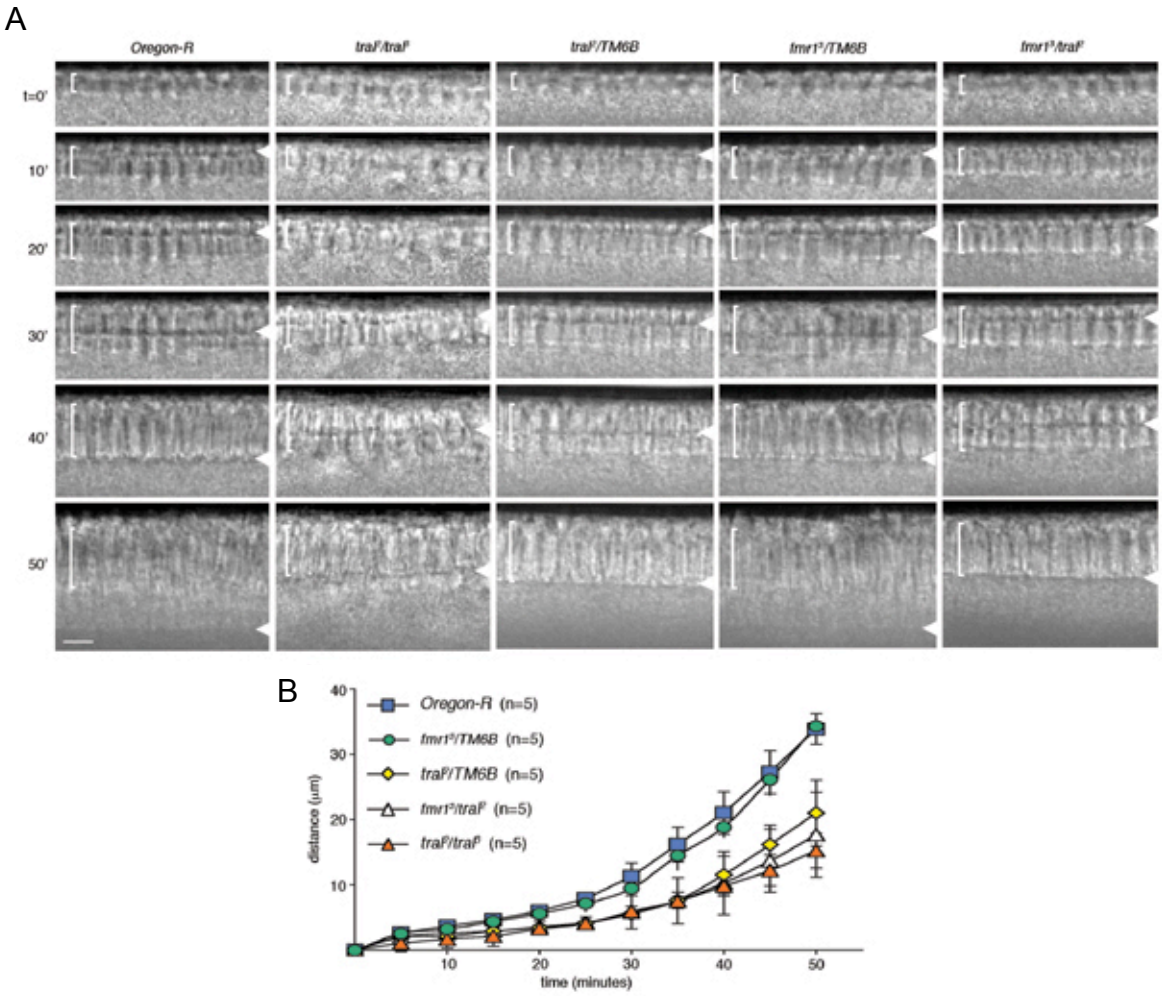


**Figure 2.7 Maternal expression of tral is required for cellularization**

(A) Sequential frames from representative DIC movies of embryos undergoing normal (WT and *fmr1*$^{3}$*/TM6B*) or disrupted (*tral*$^{2}$*/tral*$^{3}$, *tral*$^{2}$*/TM6B*, and *fmr1*$^{3}$*/tral*$^{2}$) furrow formation at 25°C. Arrowheads and brackets indicate the furrow front position and nuclear elongation, respectively. Times (*t*) in minutes are relative to nuclear cycle 14 onset. Scale bar indicates 10 µm. (B) Shown are the average rates of furrow ingression of embryos derived from WT, *fmr1*$^{3}$*/TM6B*, *tral*$^{2}$*/TM6B*, *fmr1*$^{3}$*/tral*$^{2}$, and *tral*$^{2}$*/tral*$^{3}$ females at 25°C. Error bars and n indicate the standard deviation and number of movies measured, respectively.

## 2.3 DISCUSSION

In this study, we demonstrate that maternal dFMRP activity is required for *Drosophila* cleavage furrow formation and functions within dynamic cytoplasmic RNP bodies at the MBT. Our data suggest that in cleavage stage Drosophila embryos, dFMRP affects translational initiation of specific mRNAs within cytoplasmic RNP bodies by controlling their availability and/or modulating their competency to be translated. dFMRP does not measurably associate with polyribosomes under a wide range of conditions in cleavage stage *Drosophila* extracts (Figure 2.4B), similar to results obtained for Drosophila S2 cells (Ishizuka *et al*. 2002), but in contrast to reports in other systems (Zalfa *et al*. 2006). Whether the cytoplasmic RNP bodies that dFMRP associates with are similar to P bodies or stress bodies or possibly a hybrid of the two is unknown and should be addressed in future studies. Instead, we observe dFMRP colocalize and cosediment with TRAL and ME31B, known components of translationally quiescent cytoplasmic RNP bodies (Nakamura *et al*. 2001; Wilhelm *et al*. 2005). Although dAGO2 cosediments with polyribosomes in cleavage stage embryo extracts and could directly suppress translational elongation or termination, a similar role for dFMRP is unlikely. In fact, there is no indication that endogenous dFMRP directly interacts with dAGO2 in cleavage stage Drosophila embryos, in contrast to their observed association in Drosophila S2 cell extracts (Caudy *et al*. 2002; Ishizuka *et al*. 2002). This discrepancy could result from a fundamental difference in RNA metabolism between S2 cells and cleavage stage embryos undergoing the MBT.

*tral* mRNA represents a previously undescribed *in vivo* target of dFMRP regulation. Although there is no direct evidence that dFMRP and TRAL form a stable complex in cleavage stage embryos, dFMRP activity is clearly required for normal TRAL protein expression *in vivo*. Mislocalization of TRAL but not ME31B in both *dfmr1*- and

*sbr*$^{ts148}$ embryos suggests that a specific functional relationship exists between dFMRP and TRAL. In *dfmr1-* embryos, TRAL protein levels also are reduced 2-fold (Figure 2.6C), indicating that TRAL does not simply get redistributed into abnormal structures, its rate of synthesis and/or degradation must also be affected. The co-IP of *tral* mRNA with dFMRP from WT embryo extracts demonstrates that dFMRP and *tral* mRNA form a stable RNP complex and suggests that dFMRP is involved in *tral* mRNA metabolism. Although we have not yet determined whether dFMRP directly binds *tral* mRNA, our analysis of the *tral* mRNA sequence, by using the algorithm RNABOB (www.genetics.wustl.edu/eddy/software) and search parameter guidelines described in Darnell *et al*. 2001 identified a single G-quartet stem-loop structure within the *tral* 3′ UTR, a motif that FMRP can bind with high affinity (Brown *et al*. 2001; Darnell *et al*. 2001). Regardless of whether dFMRP binds *tral* mRNA directly, dFMRP could control the assembly of a translationally competent *tral* mRNP complex and/or its localized delivery for translation. The transient association of *tral* mRNA with cytoplasmic RNP bodies in a translationally quiescent state might be required for dFMRP to promote the assembly of a translationally competent *tral* mRNP. Alternatively, the restricted translation of *tral* mRNA, controlled by dFMRP-dependent localized release from cytoplasmic RNP bodies, might promote the normal assembly of a functional TRAL RNP complex. In either case, lower steady-state TRAL protein levels resulting from decreased synthesis and/or increased degradation in *dfmr1-* embryos could be related to abnormal TRAL RNP complex assembly, observed as large structures by IF. Interestingly, the higher steady-state level of *tral* mRNA observed in *dfmr1-* embryo extracts is reminiscent of the increased levels of another dFMRP target, *pickpocket* mRNA, observed in *dfmr1-* embryo extracts and may reflect a common feature of dFMRP mRNA processing (Xu *et al*. 2004).

In conclusion, we believe that a system of cytoplasmic RNP bodies exists in cleavage stage embryos that associates with maternal and zygotic mRNAs to mediate their degradation or processing for subsequent release for translation during the MBT. It is likely that the cleavage furrow formation defect observed in *dfmr1-* mutants is at least in part the result of disrupting TRAL function. Indeed, we have shown that *tral-* embryos have a cleavage furrow formation phenotype that resembles that of *dfmr1-* embryos. TRAL has also been shown to associate with specific mRNAs at endoplasmic reticulum (ER) exit sites and is required for proper ER morphology and secretion during oogenesis (Wilhelm *et al*. 2005). Furthermore, depletion of the *C. elegans* homolog *car-1* causes defects in ER morphology as well as a defects in cleavage furrow formation during embryogenesis (Audhya *et al*. 2005). *tral* may represent a link between mRNA metabolism and the secretory pathway in cleavage stage embryos. Exploring the relationship between dFMRP and *tral* mRNA will be important for a better understanding of the function of FMRP in other systems as well as the process of cleavage furrow formation. However, as with FXS, it is likely that the altered expression of many targets is responsible for the full *dfmr1-* cleavage furrow formation phenotype.

# Chapter 3: Identification of new targets of dFMRP translational regulation

The following manuscript describing the work in this chapter is in preparation:
Monzo K, Dowd SR, Minden JS, and Sisson JC. The chaperonin containing TCP-1 (CCT) complex is a target of Fragile X mental retardation protein-dependent regulation in *Drosophila* cleavage stage embryos.

## 3.1 INTRODUCTION

We have previously demonstrated that dFMRP is required in early embryos for cleavage furrow formation during the midblastula transition (MBT). In an effort to identify new effectors of cleavage furrow formation and new targets of dFMRP-dependent regulation, we used two-dimensional difference gel electrophoresis (2D DIGE) combined with mass spectrometry to identify proteins that are misexpressed in *dfmr1-* embryos compared to stage-matched control embryos. Twenty-eight proteins were identified whose expression differs between control and *dfmr1-* cleavage stage embryos, and these proteins represent potential direct and indirect targets of dFMRP-dependent translational regulation. Of these candidates, three subunits of the chaperonin containing TCP-1 (CCT) show altered expression and the corresponding mRNAs specifically co-immunoprecipitate with dFMRP, suggesting that they are direct targets of dFMRP-dependent translational regulation. In addition, biochemical analysis reveals that the assembly of the CCT holocomplex is disrupted in *dfmr1-* embryo extracts. Genetic interaction tests between *cct* and *dfmr1* mutants strongly suggest that disrupted CCT function is relevant to the *dfmr1-* furrow formation phenotypes. Furthermore, we have found that the septin Peanut, a substrate of yeast CCT and a protein required for

cytokinesis, is mislocalized in both *cct* and in *dfmr1* mutant embryos, which may contribute to the *dfmr1-* cleavage furrow formation defects. Based on these results we propose that dFMRP-dependent translational regulation of specific CCT subunits is required for normal CCT holocomplex activity during the MBT and that at least one of its substrates required for cytokinesis is affected in *dfmr1-* embryos suggesting it may contribute to the *dfmr1-* cleavage furrow formation defect. Additional characterization of these candidate targets should provide insight into the mechanism of dFMRP-dependent regulation of cellular morphogenesis in early embryos and the etiology of FXS.

## 3.2 RESULTS

### 3.2.1 Comparative proteomic analysis of WT and *dfmr1-* cleavage stage embryos

The goal of this study was to identify direct and indirect targets of dFMRP-dependent translational regulation that contribute to the morphogenesis defects observed during cleavage furrow formation in *Drosophila* embryos derived from *fmr1*$^{3}$*/Df(3R)Exel6265* females (after this referred to as *dfmr1-* embryos) (Monzo *et al*. 2006). To identify proteins that are differentially expressed in *dfmr1-* compared to wild type cleavage stage embryos, a proteomic screen using 2D differential gel electrophoresis followed by mass spectrometry (2D DIGE/MS) (Viswanathan *et al*. 2006) was performed (Figure 3.1A), an approach that has been previously taken to identify dFMRP targets in fly brain and testis (Zhang *et al*. 2004; Zhang *et al*. 2005). This screen was a collaboration with Dr. Jonathan Minden. I performed the 2D DIGE/MS experiments in his laboratory at Carnegie Mellon University with assistance from Dr. Susan Dowd and Anupam Goyal. Forty-five protein spots were found to reproducibly change in *dfmr1-*

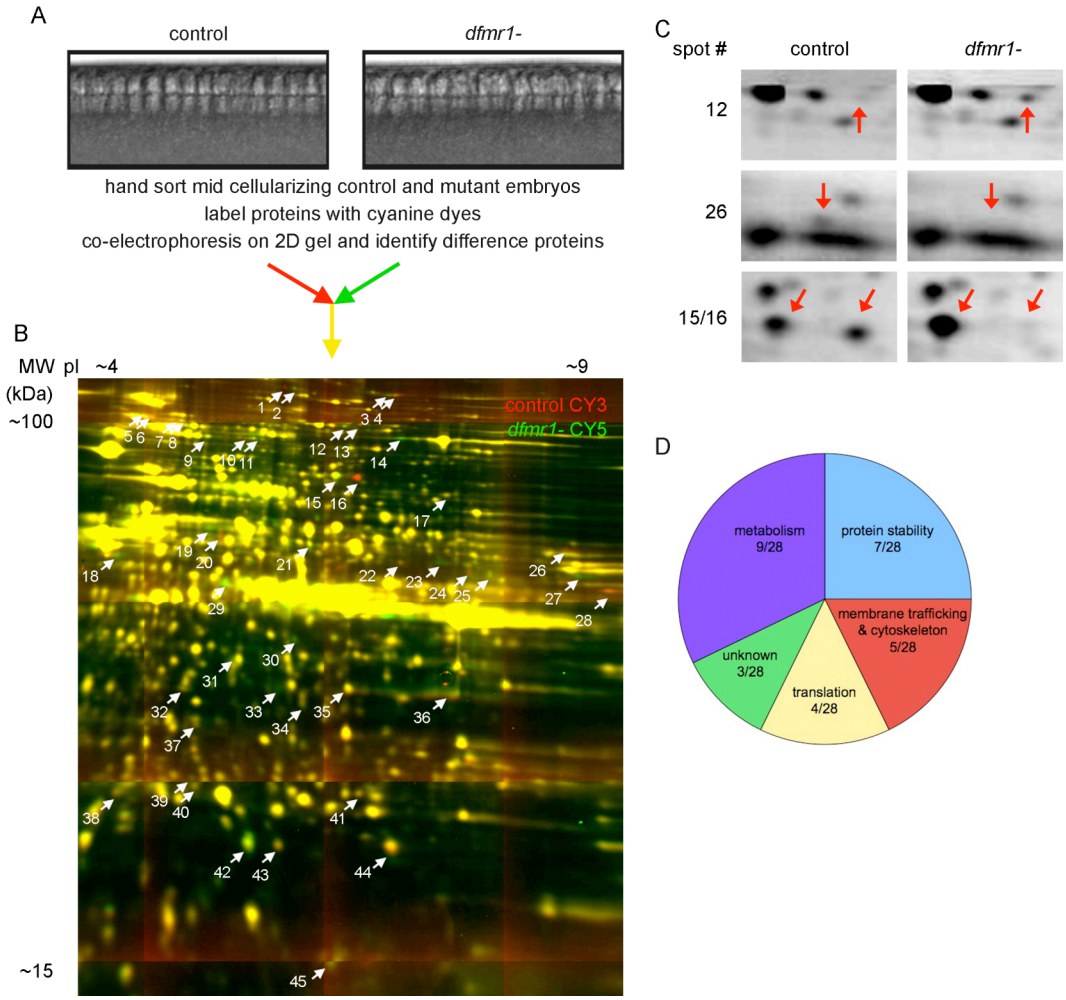


**Figure 3.1 Comparative proteomic analysis of control and *dfmr1-* cleavage stage embryos.**

(A) Schematic showing general procedure for 2D DIGE analysis. Differential interference contrast (DIC) images of control and *dfmr1-* embryos show the morphological stage of sorted embryos. (B) A master gel is pseudocolored with control extracts labeled with CY3 (red) and *dfmr1-* extracts labeled with CY5 (green). The approximate isoelectric point (pI) is indicated at the top of the gel and the approximate molecular weight (MW) is indicated to the left. Difference spots are indicated with white arrow and numbered. The labeled difference spots were observed in at least four gel replicates. (C) High magnification examples of difference spots are shown with red arrows, and corresponding spot number in (C) is indicated to left. (D) The 28 difference proteins identified by mass spectrometry are categorized by proposed gene ontology.

cleavage stage embryo lysates representing a small fraction of total protein spots observed in our gel conditions (Figure 3.1B). Twenty-eight proteins were identified by Maldi-TOF mass spectrometry with fold changes in abundance ranging from 1.3 to 56.7 (Table 3.1). The majority of proteins (13/28) increase in abundance in the mutant lysates, five decrease in abundance, and four shift in pI and/or molecular weight. The 28 proteins can be classified into five general gene ontology categories based on reported function: metabolism, protein stability, translation, cytoskeleton and membrane trafficking, and unknown (Figure 3.1D).

### 3.2.2 Secondary analysis of candidate targets to identify direct targets

The 28 proteins identified that reveal a difference in expression by 2D DIGE/MS represent potential direct or indirect targets of dFMRP-dependent translational regulation. To classify the candidate targets, a secondary screen was performed to identify the proteins whose mRNAs specifically associate with dFMRP and could be considered direct targets of dFMRP regulation. The amount of mRNA corresponding to the difference proteins in dFMRP immunoprecipitations (IPs) from WT and *dfmr1-* cellularizing embryo extracts was quantified and normalized to the amount of a standard control mRNA (*RpL32*) (Figure 3.2). An enrichment of at least two-fold of the mRNA in WT compared to *dfmr1-* IPs was considered significant and likely suggests that the mRNA is associated with a dFMRP complex and subject to direct translational regulation by dFMRP. The fold enrichment of a previously described target, *trailer hitch* (*tral*), was measured as a positive control (Monzo *et al*. 2006). In these experiments *tral* mRNA was found to be enriched 3.5 fold in WT IPs (Figure 3.2). The mRNAs for five candidates were found to be at least two-fold enriched: *CG5525*, *Cctγ*, *Tcp-1η*, *β'cop*, and *Aats-gly*. The mRNA sequence of all the potential candidates was analyzed using the

| Spot # (refer to Fig 1A) | CG Identifier | Gene name (Flybase) | Molecular function (Flybase) | MW (kDa) | pI | Mascot score | % Seq. cov. | # Pept. | Change of protein levels in *dfmr1*- | |
|---|---|---|---|---|---|---|---|---|---|---|
| 21 | CG8351 | *Tcp-1η Cct7* | Chaperonin-containing T-complex protein | 60.0 | 6.0 | 127 | 31 | 12 | increase | +1.38 |
| 39 | CG4463 | *Hsp23* | Heat shock protein chaperone/actin binding | 20.7 | 5.6 | 66 | 33 | 6 | increase | +3.71 |
| 35 | CG4904 | *Pros35* | Proteasome core complex | 31.0 | 6.1 | 158 | 60 | 12 | increase | +1.39 |
| 31 | CG18174 | *Rpn11* | Proteosome regulatory particle | 26.2 | 6.77 | 63 | 20 | 4 | increase | +1.51 |
| 12 | CG6699 | *β'Cop* | COP I vesicle coat/protein transporter activity | 102.7 | 5.1 | 153 | 30 | 17 | increase | +4.87 |
| 19 | CG8308 | *α-Tub67C* | α-Tubulin/Maternal and CNS specific | 51.9 | 5.1 | 101 | 32 | 10 | increase | +4.81 |
| 37 | CG7823 | *RhoGDI* | Rho GDP-dissociation inhibitor activity | 23.2 | 5.4 | 65 | 32 | 5 | increase | NR |
| 27 | CG3612 | *blw* | ATP-synthase subunit alpha | 59.6 | 9.1 | 112 | 28 | 11 | increase | +13.7 |
| 40 | CG1633 | *Jafrac1* | Thioredoxin peroxidase activity | 21.9 | 5.5 | 81 | 39 | 6 | increase | +2.13 |
| 29 | CG2985 | *Yp1* | Yolk protein | 48.7 | 7.2 | 90 | 25 | 6 | increase | +56.7 |
| 32 | CG8327 | *SpdS* | Spermidine synthase activity | 32.7 | 5.5 | 128 | 41 | 8 | increase | +1.41 |
| 45 | CG17820 | *fit* | unknown | 14.0 | 7.1 | 61 | 36 | 5 | increase | +4.11 |
| 18 | CG11596 | | unknown | 51.3 | 5.1 | 133 | 37 | 12 | increase | +2.83 |
| 26 | CG5525 | *Tcp-1δ Cct4* | Chaperonin-containing T-complex protein | 57.8 | 7.5 | 70 | 21 | 7 | decrease | -2.55 |
| 28 | CG7433 | | Amino acid biosynthesis, 4-aminobutyrate transaminase activity | 54.9 | 8.8 | 70 | 20 | 7 | decrease | -3.03 |
| 17 | CG6186 | *Tsf1* | Iron ion transporter activity | 72.9 | 6.7 | 158 | 29 | 12 | decrease | -1.40 |
| 43 | CG11793 | *Sod* | Superoxide dismutase activity | 15.2 | 5.7 | 96 | 57 | 6 | decrease | -1.45 |
| 38 | CG4381 | *GstD3* | Glutathione S transferase activity | 22.9 | 5.3 | 68 | 39 | 4 | decrease | -1.26 |
| 7, 8 | CG6603 | *Hsc70Cb* | Molecular chaperone | 89.0 | 5.31 | 209 | 33 | 17 | shift left | NR |

| | | | | | | | | | | |
|---|---|---|---|---|---|---|---|---|---|---|
| 42, 44 | CG4254 | *tsr* | Cofilin/actin depolymerizing factor-like | 17.4 | 6.74 | 149 | 60 | 9 | shift left | +1.6/-1.34 |
| 15, 16 | CG6778 | *Aat-gly* | Glycyl-tRNA synthetase | 76.6 | 6.0 | 82 | 15 | 7 | shift left | +1.88/-17.7 |
| 3, 4 | CG6045 | | Aldehyde oxidase/xanthine dehydrogenase | 139.6 | 6.15 | 222 | 31 | 22 | shift left | +2.32/-1.22 |
| 22, 23 | CG8977 | *Tcp-1γ Cct3* | Chaperonin-containing T-complex protein | 58.5 | 6.38 | 173 | 41 | 17 | shift right | NR |
| 24, 25 | CG3590 | | Adenylosuccinate lyase | 54.2 | 7.16 | 161 | 41 | 17 | shift right | -3.98/+1.60 |
| 10, 11 | CG12005 | *Mms19* | nucleic acid binding, transcription cofactor activity | 107.5 | 5.58 | 89 | 16 | 10 | shift right | -5.77/+2.32 |
| 36 | CG7490 | *RpLp0* | Ribosomal protein | 34.3 | 6.5 | 79 | 33 | 7 | shift up | NR |
| 34 | CG5269 | *vib* | Phosphatidylinositol transfer activity | 32.7 | 5.49 | 115 | 36 | 6 | shift down | NR |
| 5, 6 | CG32473 | | Aminopeptidase aminopeptidase activity | 102.7 | 5.0 | 92 | 10 | 7 | shift down and left | NR |

**Table 3.1 Identified difference proteins**

Table begins on previous page.
Flybase, www.flybase.org
Mascot score >59 considered significant (Perkins *et al*. 1999)
% Seq. cov., percent sequence coverage
# pept., number of peptides identified

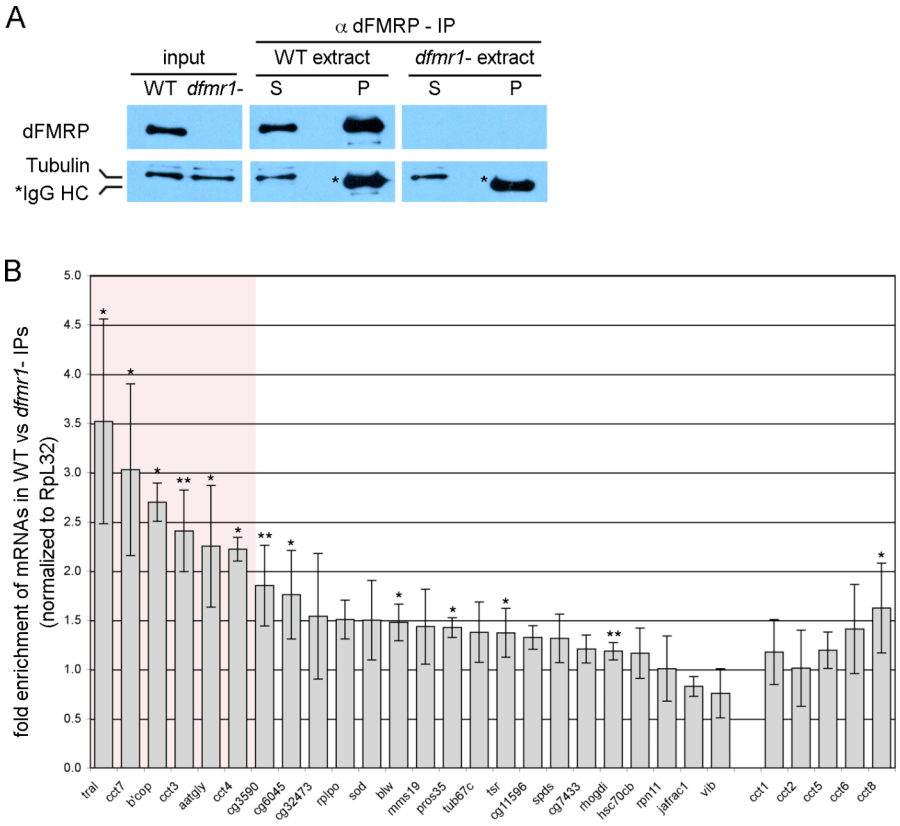


**Figure 3.2 Immunoprecipitation of candidate target mRNAs with dFMRP.**

(A) Immnuoblots showing input and supernatant (S) and pellet (P) fractions of IPs performed using an anti-dFMRP antibody with WT and *dfmr1-* extracts probed with dFMRP and Tubulin antibodies. Although no Tubulin co-IPd with dFMRP, IgG heavy chain (HC) was present in equal volumes in the P fraction of each IP as indicated with asterisks. (B) RNA was extracted from P fractions shown in (A) and subjected to qRT-PCR. Histogram shows the fold enrichment of each mRNA in WT vs. *dfmr1-* IPs normalized to *RpL32*. *tral* mRNA is a know target of dFMRP and its enrichment was tested as a positive control in these experiments. Error bars indicate standard deviations (SD). Significance was assessed using the Student's *t* test (*, $P \leq 0.05$ and **, $P \leq 0.005$). Red box highlights those mRNAs that are at least 2-fold in enriched.

algorithm RNABOB (www.genetics.wustl.edu/eddy/software) for G-quartet motifs, a known dMFRP binding motif. This analysis revealed putative G-quartets in the coding sequence of *CG5525*, *Cctγ*, *Tcp-1η*, and *β'cop* mRNAs, however we have not tested if these sequences contribute to their association with dFMRP. Together, these observations suggest that *CG5525*, *Cctγ*, *Tcp-1η*, *β'cop*, and *Aats-gly* are potential direct targets of dFMRP regulation.

### 3.2.3 Three subunits of the CCT complex are misregulated in *dfmr1-* embryos

Protein sequence analysis showed that *CG5525*, *Cctγ*, *Tcp-1η* encode three of the eight subunits of the Chaperonin Containing TCP-1 (CCT) complex (also referred to as TCP-1 or TCP-1 Ring Complex (TRiC)). The genes encoding the other five subunits were also identified within the *Drosophila* genome based on protein sequence homology (Figure 3.4). I will refer to the complex as CCT and the independent eight subunits as CCT1-8 for simplicity. CCT is a group II chaperonin that assists in the folding or in the assembly of protein substrates in an ATP-dependent manner (Liou and Willison 1997). The CCT holocomplex is composed of two rings containing eight distinct subunits (Figure 3.3). Each subunit is expressed stoichiometrically from an individual gene. The eight different cct genes encode conserved regions and a variable region, termed the apical domain, which confers substrate specificity (Liou and Willison 1997). Although CCT was initially thought to exclusively fold actin and tubulin, between 2-7% of cytosolic proteins have been recently identified to interact with CCT in yeast and mammalian cells (Dekker *et al*. 2008; Yam *et al*. 2008). Most of these newly identified CCT substrates are functionally and structurally diverse and cannot be easily predicted based on function or sequence alone. All eight of the cct genes are essential for eukaryotic cell viability, and it has been shown that temperature sensitive (ts) alleles of *cct4* in budding yeast cause cytokinesis defects, a cellular process analogous to

*Drosophila* cellularization (Dekker *et al*. 2008). A comprehensive comparison of the *D. melanogaster* CCT protein sequences with those of *S.cerevisiae* and *H. sapiens* reveals a high degree of conservation for each (Figure 3.4), suggesting conserved functionality. Interestingly, the *D. melanogaster cct* sequences are more conserved with the *cct* sequences of *H. sapiens* than *S.cerevisiae* (Figure 3.4). Although CCT protein levels for all eight subunits were not assessed by immunoblot analysis due to availability of antibodies, we tested for the association of dFMRP with the mRNAs for five subunits not identified in the screen (*cct1, 2, 5, 6* and *8*) and found that they do not associate with dFMRP during the cleavage stage (Figure 3.2). Because three subunits (CCT3, CCT4, and CCT7) of this complex are misexpressed in *dfmr1-* mutant embryos, we chose to focus on the potential relevance of the misregulation in the *dfmr1-* mutant phenotype.

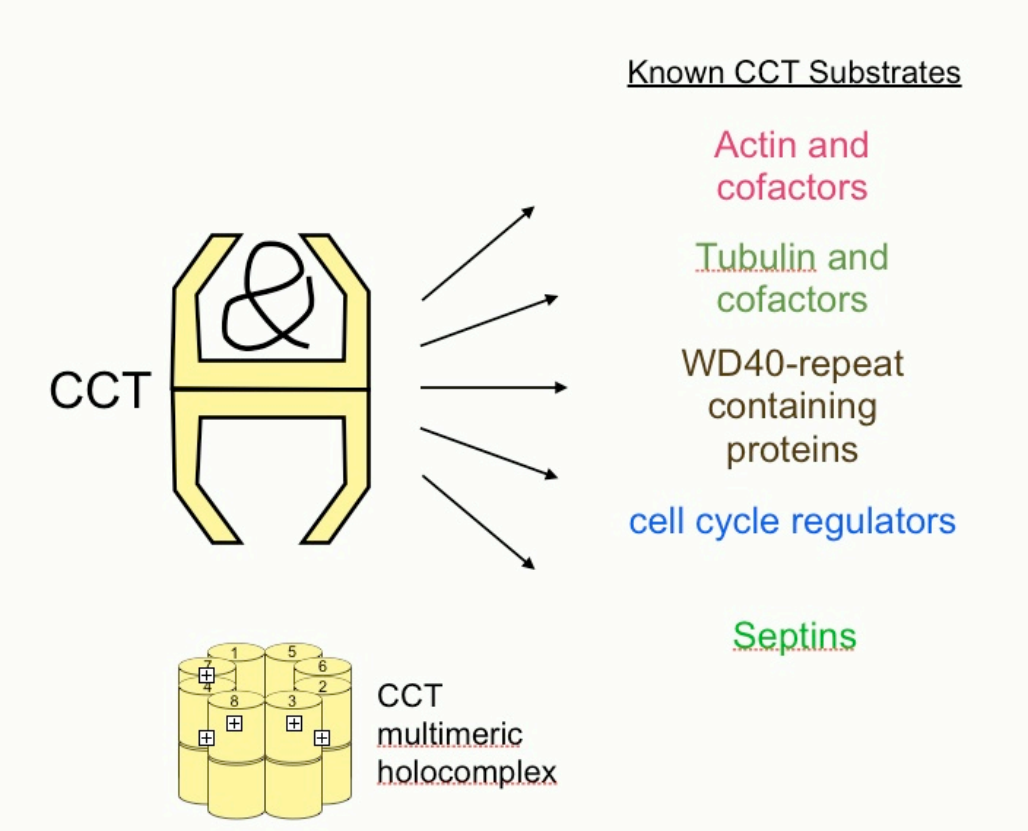


**Figure 3.3 The CCT complex and known substrates.**

Shown is a cartoon of the general double barrel structure of the CCT complex along with a subset of the known classes of substrates. Lower cartoon shows one orientation for each of the eight different CCT subunits in context of the 16-subunited multimeric holocomplex.

A

| Chaperonin Containing T-Complex (CCT) or TCP-1 Ring Complex (TRiC) subunite | | | | | | | | | |
|---|---|---|---|---|---|---|---|---|---|
| Flybase gene name | CG Identifier | Subunit | | MW (kDa) | PI | cytological position | %identity/similarity to *S. cerevisiae* homologs | %identity/similarity to human homologs | change in *dfmr1-* |
| *Tcp1-like* | CG5374 | CCT1 | TCP-1α | 59.6 | 6.3 | 3R: 94B1 | 63 / 79 | 73 / 85 | |
| | CG7033 | CCT2 | TCP-1β | 58.1 | 5.6 | X: 8C8 | 63 / 79 | 71 / 84 | |
| *Cctγ* | CG8977 | CCT3 | TCP-1γ | 59.4 | 6.9 | 3R: 89D6 | 59 / 76 | 69 / 83 | shift right |
| | CG5525 | CCT4 | TCP-1δ | 57.1 | 7.6 | 2L:33F3 | 58 / 79 | 70 / 86 | decrease |
| *Cct5* | CG8439 | CCT5 | TCP-1ε | 59.3 | 6.1 | 2R: 48E4 | 61 / 79 | 71 / 88 | |
| *T-cp1ζ* | CG8231 | CCT6 | TCP-1ζ | 58.2 | 6.6 | X: 13E13-14 | 52 / 71 | 69 / 85 | |
| *Tcp-1η* | CG8351 | CCT7 | TCP-1η | 59.4 | 6.3 | 3R: 85B1-2 | 62 / 79 | 76 / 87 | increase |
| | CG8258 | CCT8 | TCP-1Θ | 59.4 | 4.9 | 2R: 44F5 | 42 / 64 | 62 / 79 | |

B

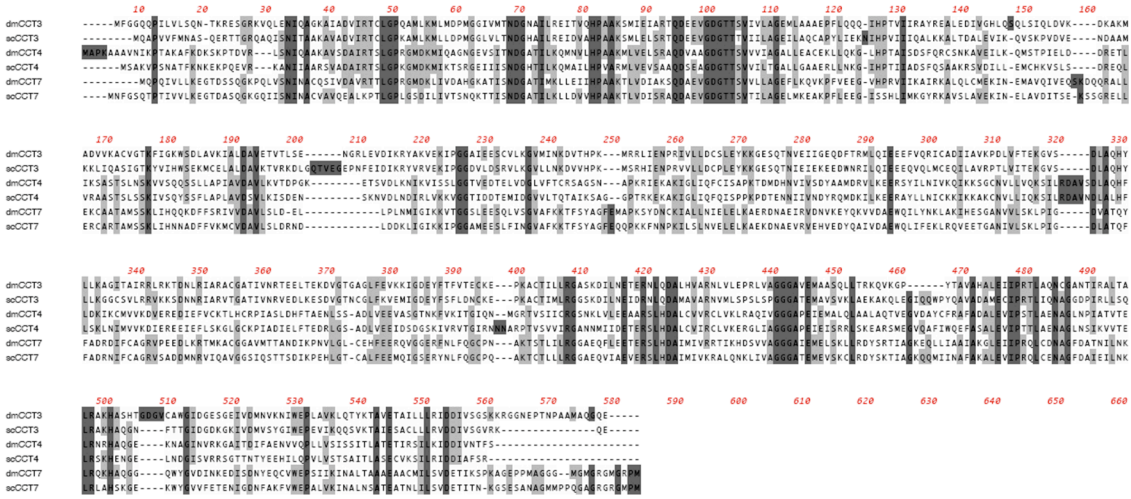


**Figure 3.4 CCT subunits in *Drosophila melanogaster*.**

(A) Table shows known genetic and molecular information for each of the eight CCT subunits in fly. Percentages of identity and similarity in protein sequence for each of the subunits was compared between fly and budding yeast and fly and human. The protein difference detected in *dfmr1-* embryos the 2D DIGE gels is indicated for those proteins identified in the screen. (B) A Clustal-W alignment of the protein sequences of the fly (dm) and budding yeast (sc) CCT subunits affected in *dfmr1-* embryos shows regions of high conservation.

### 3.2.4 CCT is required for proper cleavage furrow formation

In order to assess the requirement for CCT during fly development, cleavage furrow formation was examined in embryos laid by females lacking a single copy of one or three different cct genes. While all WT embryos complete furrow formation in about 55 minutes, half of the embryos examined from females lacking a copy of *cct1*, *cct4*, and *cct6* display a delay in furrowing rate (Figure 3.5A) similar to what is observed in the majority of *dfmr1-* embryos (Figure 2.1). One embryo displayed moderate disruptions in nuclear morphology although furrowing rates appeared normal. Furrowing proceeded normally in embryos derived from heterozygous females of *cct1*, *cct3*, *cct4*, *cct6*, *cct7*, and *cct8* (data not shown). Significantly, when a single copy of *cct4* is removed in a *dfmr1-* background, the percentage of embryos displaying severe disruptions in furrow formation is enhanced from 25% (*dfmr1-*) to 75% (*cct4-/+, dfmr1-/-*) (Figure 3.5B). This is the expectation if the decrease in CCT4 levels are relevant to the *dfmr1-* phenotype. A similar effect was observed in *cct6-/+, dfmr1-/-* (Figure 3.5B). This interaction appears to be specific as removing a copy of a general translational regulator, ribosomal protein gene (*RpS13*), or a known effector of cleavage furrow formation, the scraps gene, which encodes Anillin, does not enhance the *dfmr1-* severe furrow formation phenotype (Figure 3.5B). Together, these observations suggest that the misregulation of CCT in *dfmr1-* embryos is an important contributing factor to the furrow formation phenotype.

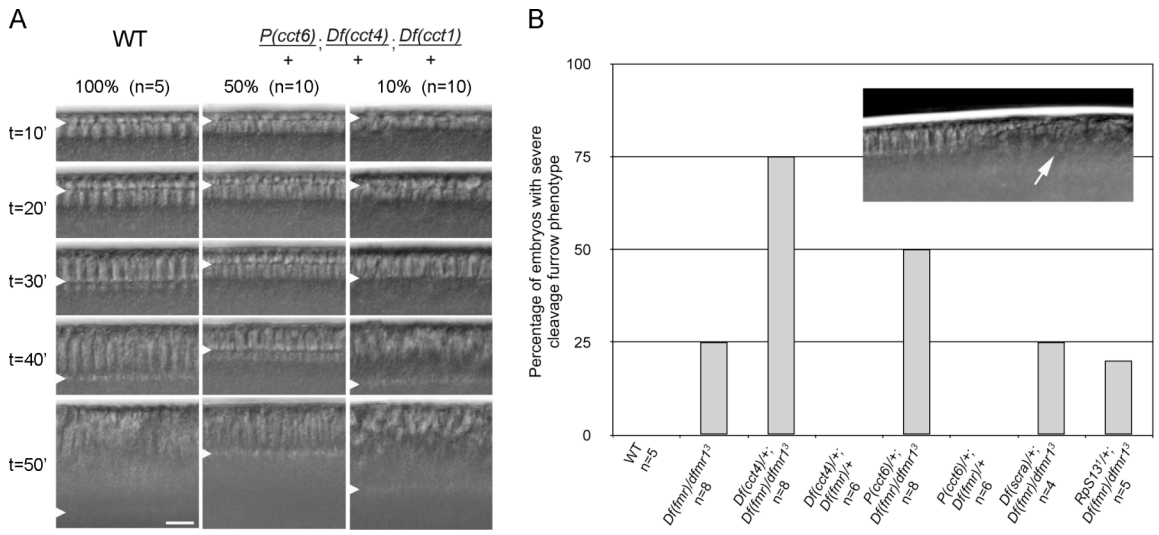


**Figure 3.5 CCT is required for proper cleavage furrow formation and loss of *cct* enhances *dfmr1-* phenotype.**

(A) Frames from representative DIC movies of WT and *cct-* cleavage stage embryos. Time (t) is in minutes from the start of interphase of nuclear cycle 14. Percentage and number of embryos examined (n) with shown phenotype is indicated at top. Arrowheads and brackets indicate the furrow front position and nuclear elongation, respectively. Scale bar indicates 10 μm. (B) Bar graph shows percentage of embryos with severe cleavage furrow phenotype. Genotypes are indicated at the bottom with the total number of embryos observed (n). The inset is a representative DIC image of an embryo with a severe furrowing phenotype. Arrow indicates where furrow is completely disrupted.

### 3.2.5 CCT holocomplex assembly is disrupted in *dfmr1-* embryos

Based on the initial observation that dFMRP is required for the proper expression of CCT subunits and that CCT is required for proper cleavage furrow formation, I expected that CCT function is compromised in *dfmr1-* embryos. To test if the CCT holocomplex is disrupted in *dfmr1-* cleavage stage embryos, embryonic extracts were separated by gel filtration chromatography and immunoblot analysis. The CCT1 antibody used in this study was generated against a rat CCT1 peptide and detects a single band with a molecular weight of the predicted size of approximately 60 kDa in cleavage stage embryo extracts (Figure 3.6A). The abundance of CCT1 is not affected in *dfmr1-* embryos, as quantified in 1D SDS-PAGE gels (Figure 3.6A). The majority of CCT1 in WT and *dfmr1-* extracts fractionates near 660kDa (fraction 11/20, Figure 3.6B). Interestingly, about 40% of CCT1 in *dfmr1-* extracts fractionates near 60kDa (Figure 3.6B). This fractionation profile was observed in 3 of 5 experiments. Consistent with these results, it was previously shown that reduction of a single CCT subunit by siRNA in mouse fibroblasts disrupts assembly of the other CCT subunits into the holocomplex (Grantham *et al*. 2006). These observations suggest that in WT cleavage stage embryos the vast majority of CCT1 is incorporated into a large holocomplex, and in *dfmr1-* embryos the assembly of CCT holocomplex is at least partially disrupted with some CCT1 left in monomeric or unassembled form.

To further characterize the nature of the disruption of the CCT complex in *dfmr1-* embryos, cleavage stage *dfmr1-* embryos were fixed and stained to assess subcellular localization of the CCT complex. In WT embryos CCT, as detected with the antibody against CCT1, is seen in a diffuse punctate pattern throughout the cytoplasm and to a

somewhat lesser extent in the nuclei (Figure 3.6C). This general pattern is very similar in *dfmr1-* embryos except that larger ectopic puncta of CCT are observed in the apical cytoplasm (Figure 3C). These ectopic puncta are never observed in WT and may represent CCT1 that is not assembled into CCT holocomplex, consistent with the fractionation profile of CCT1 in *dfmr1-* embryos. Although much smaller, the ectopic CCT apical puncta are reminiscent of how the previously described target, TRAL, is misexpressed in large aggregates in the apical cytoplasm in *dfmr1-* embryos. Double immunofluorescence of TRAL and CCT1 reveal that the two proteins are mislocalized to different compartments in the apical cytoplasm of *dfmr1-* embryos (data not shown). Together the results of the CCT fractionation and fixed analysis of *dfmr1-* embryos suggest that CCT holocomplex does not assemble properly in *dfmr1-* due to a misregulation of individual subunit stoichiometry which may lead to reduced or abnormal CCT function.

### 3.2.6 The septin Peanut is mislocalized in *cct-* and *dfmr1-* cleavage stage embryos

As previously mentioned, CCT substrates are functionally diverse. Recently, the septins and septin effectors were identified as a new class of physiologically relevant substrates in yeast by virtue of their physical association and genetic interaction with CCT and cct genes (Dekker *et al*. 2008). Conditional alleles of cct genes cause ectopic localization of the septin Cdc3p and have low penetrance cytokinesis defects (Dekker *et al*. 2008). In addition, CCT loss of function in yeast does not affect *de novo* septin polypeptide folding, and it appears to be involved in regulating the assembly of septin filaments (Dekker *et al*. 2008). To test if the septins are conserved substrates of CCT in the fly, Septin localization was assessed in cleavage stage embryos from females lacking a copy of *cct1*, *cct4*, and *cct6* (*cct-*). In fixed WT embryos, the septin PNUT tightly localizes to the leading edge of the furrow front along with F-actin. In fixed *cct* loss of function

embryos, the majority of PNUT localizes to the furrow front as it does in WT, in addition to ectopic accumulation along the lateral membranes (Figure 3.7A). This ectopic accumulation is reminiscent of what is observed in yeast *cct4* ts mutants. In WT budding yeast cells undergoing division septins tightly localize to the neck between the mother and bud. In *cct4* ts mutants expressing a Cdc3p-GFP at the restrictive temperature, the GFP is seen as the neck as well at other parts of the plasma membrane (Dekker *et al.* 2008). PNUT localization was also assessed in *dfmr1-* embryos. Again, PNUT was seen localized to the furrow front as in WT embryos but also ectopically localized along the lateral membranes to an even greater extent than what was observed in *cct-* embryos (Figure 3.7B). Importantly, F-actin and other F-actin binding proteins, such as Anillin and Myosin II, that normally localize to the furrow front are not affected in these mutants (Figures 2.6A, 3.6A and B and data not shown), suggesting that the effect on PNUT localization is specific and is not a secondary effect from a general disorganization of the cortical membrane. Finally, to further investigate the possibility that PNUT is a bona fide substrate of CCT in flies, IPs were performed to test if CCT and PNUT physically associate. A small amount of CCT1 specifically co-IPs with PNUT in WT cleavage stage embryos, consistent with PNUT being a substrate of CCT (Figure 3.7C). This interaction appears to be slightly disrupted in *dfmr1-* embryos as the amount of CCT that co-IPs with PNUT is slightly decreased (Figure 3.7C). Together, these observations suggest that septins are a likely conserved substrate of CCT in flies and that the ectopic localization of PNUT in *dfmr1-* embryos is due to the misregulation of CCT and may at least partially contribute to the *dfmr1-* cleavage furrow formation phenotype.

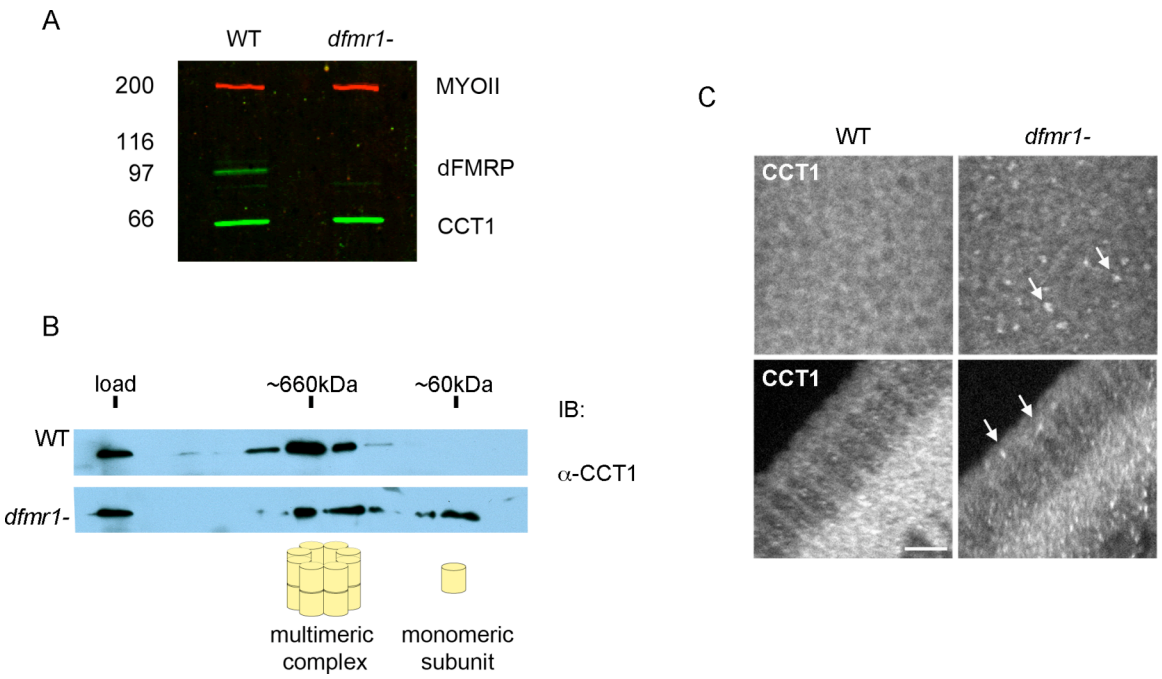


**Figure 3.6 CCT holocomplex assembly is disrupted in *dfmr1-* embryos.**

(A) Quantitative immunoblot (IB) of WT and *dfmr1-* cleavage stage embryo extracts probed with antibodies against CCT1, dFMRP, and Myosin II (MYOII, loading control) indicated to right. MW in kDa is indicated to the left. (B) IB of fractions collected from 1.3 mg of WT and *dfmr1-* cleavage stage embryo extracts separated using a Superose 6 column and probed with anti-CCT1 antibody. 10mg of protein loaded onto column is indicated at far left of blots. 660kDa complex was present in fraction 11 of 20. Cartoon representation of possible state of CCT complex formation indicated below blots. (C) Immunofluorescence analysis of fixed cleavage stage WT and *dfmr1-* embryos shows CCT1 localization in surface (top) and sagittal (bottom) views. Arrows indicate abnormal accumulation of CCT1. Scale bar indicates 10 μm.

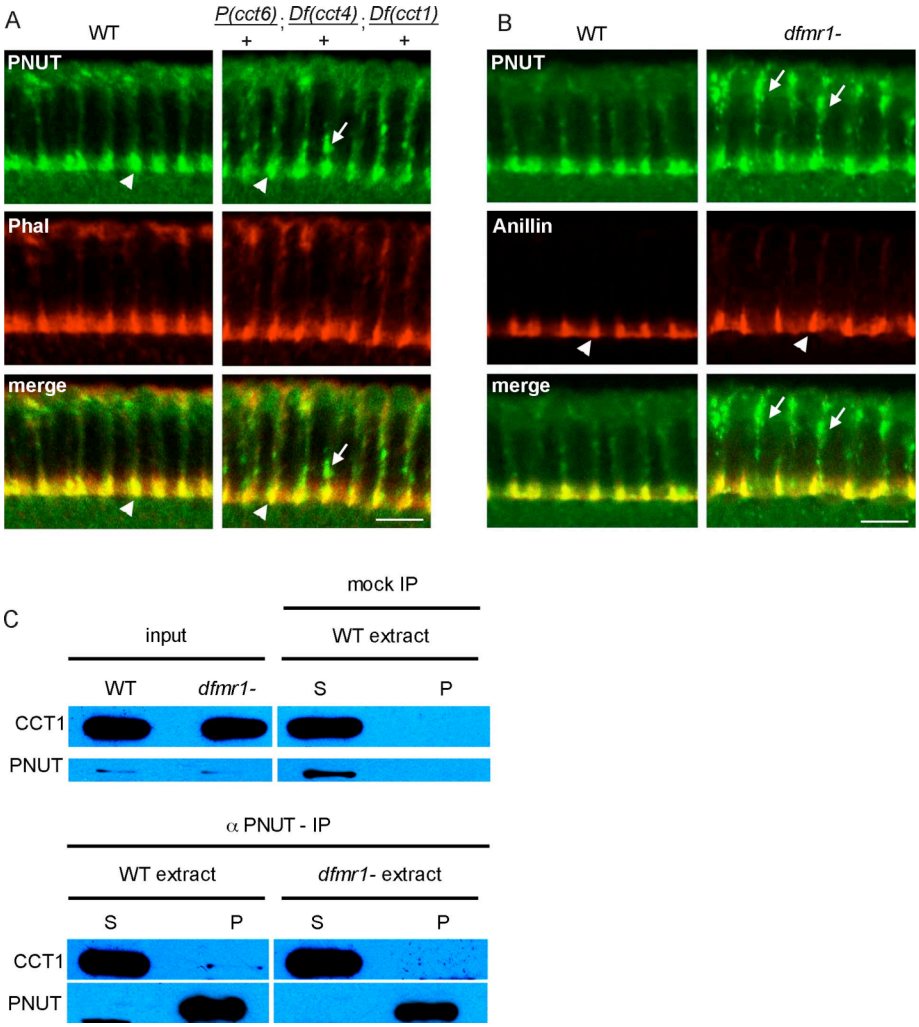


**Figure 3.7 PNUT localization is dependent on CCT and is a likely substrate of CCT**

(A) IF analysis of fixed cleavage stage WT and *cct*- embryos shows PNUT and F-actin (Phalloidin) localization. (B) IF analysis of fixed WT and *dfmr1*- embryos shows PNUT and Anillin localization. Arrow heads indicate normal localization of PNUT and Anillin to furrow fronts, and arrows indicate abnormal accumulation of PNUT along lateral membrane. Scale bar indicates 10 μm. (C) Immunoblots showing PNUT IPs from WT and *dfmr1*- extracts. 5 μg starting extract was loaded in input lanes (2% of total input). 10 μg of supernatants (S) and 50% of pellet (P) from mock and anti-PNUT IPs was loaded in indicated lanes. Proteins probed for indicated to left.

## 3.3 DISCUSSION

Here, a comparative proteomic approach was used to identify new targets of dFMRP-dependent regulation. Twenty-eight proteins showed differences in abundance between WT and *dfmr1-* embryos, representing potential direct and indirect targets of dFMRP. The majority of the identified proteins function in metabolic pathways, some of which have previously been implicated in FMRP regulation. Many of the identified proteins are also involved in regulating the actin and MT cytoskeletons and membrane trafficking, and the majority of the genes known to be required for proper furrow formation are involved in regulating these pathways (see sections 1.2.3 and 1.2.4). Other interesting classes of identified proteins have roles in translational regulation and protein stability. Identification of these classes of targets suggests a tiered or hierarchical mode of regulation by FMRP, whereby modulation of expression of one of these targets affects the expression of an additional class of targets. Consistent with this, we have previously shown that dFMRP regulates the expression of a known translational regulator, *tral*, whose targets are at this point unknown (Monzo *et al*. 2006). We chose to follow-up on the misregulation of the chaperonin CCT in *dfmr1-* cleavage stage embryos because three of the eight CCT subunits are misregulated, suggesting significant regulation of this complex is potentially relevant during the cleavage stage. The identification of the CCT complex as a target of dFMRP regulation is also consistent with a hierarchal mode of regulation by dFMRP as CCT has a complex set of substrates itself.

### 3.3.1 dFMRP and classes of targets

The majority of targets identified in this screen are generally involved in metabolism, which could be a result of an inherent property of this type of analysis. Many of the proteins that can be easily and reproducibly identified using 2D DIGE/MS are present at relatively high abundance and include many metabolic proteins. Such

targets are still potentially relevant based on observations made in other studies. Three targets identified in this screen were also identified in 2D DIGE screens performed using *Drosophila* testis or heads (Table 1). One of these proteins, Jafrac1 or Thioredoxin, is involved in oxidative stress response, and it has been observed that *FMR1* mutant mice are sensitive to oxidative stress suggesting that the stress response is perturbed in the mutants (El Bekay *et al*. 2007). Two other proteins with known or predicated roles in oxidative stress response, Superoxide dismutase (SOD) and the protein encoded by CG6045, were found to be misregulated in *dfmr1-* embryos in this screen, suggesting that modulation of the oxidative stress response pathways may be regulated at least in part by FMRP. Furthermore, *SOD1* was previously identified as a target of FMRP in mouse neurons (Miyashiro *et al*. 2003). The identification of these targets is consistent with reported observations of known FMRP targets.

About 18% of the identified targets are involved in regulation of the actin and MT cytoskeletons and membrane trafficking, pathways that are known to be important for cleavage furrow formation and neuron morphology. *β'cop* represents a potentially interesting target of dFMRP. β'COP is a subunit of the COPI coat which is required for forming vesicles that are destined for retrograde trafficking from the Golgi to the endoplasmic reticulum (Girod *et al*. 1999). The amount of plasma membrane required to form the thousands of cells during cleavage furrow formation is dependent on a huge increase in surface area, and it has been demonstrated that internal stores of Golgi-derived membrane contribute to the formation of these furrows (Sisson *et al*. 2000). Proper trafficking between the various endomembrane compartments is crucial for proper furrow formation, and this trafficking also seems to be important in the maintenance of neuronal morphology and function (Kennedy and Ehlers 2006). An effector of COPI vesicle formation, the GTPase activating protein Arf1 GAP, is essential for dendritic

growth and outbranching (Moore *et al*. 2007). FMRP is also involved in dendritic growth and branching, suggesting a possible connection between the two pathways. Validation and further characterization of *β'cop* as a target of dFMRP could be important for understanding how FMRP affects membrane trafficking.

*Aats-gly*, also known as *glycyl-tRNA synthetase* (*gars*), was also identified as a target of dFMRP regulation. In the screen, Aats-gly was identified as a protein that shifts in pI in *dfmr1-* embryos, and overall protein abundance decreases in the mutant. We also showed that the *Aats-gly* mRNA likely associates with a dFMRP complex, suggesting it is a direct target of dFMRP. Glycyl-tRNA synthetase is important for catalyzing tRNA aminoacylation, a critical step in protein translation. *Aats-gly* is the ortholog of the human *GARS* gene that is associated with Charcot-Marie-Tooth neuropathy type 2D (CMT2D), a heritable disease that causes defects in motor and sensory neurons (Chihara *et al*. 2007). Similar to *dfmr1* mutants, *Aats-gly* mutants have defects in dendritic arborization as a result of perturbing protein translation (Chihara *et al*. 2007). The relationship between FMRP and Aats-gly expression may be relevant for both cleavage furrow formation during the MBT as well as aspects of development in the nervous system.

Together, these findings suggest that genes normally thought of as functioning in a general 'housekeeping' capacity, such as those functioning in metabolic processes and protein synthesis, may have more specific functions during development and cell maintenance and their precise regulation is important for cellular processes.

### 3.3.2 CCT and dFMRP regulation

The manner in which the three CCT subunits are affected in *dfmr1-* is complex. CCT3 was identified as shifting in pI to a more basic state in the mutant extracts, CCT4 was identified as decreasing 2.6 fold in mutant extracts, and CCT7 was identified as

increasing 1.4 fold in mutant extracts (Table 1). It should be noted that overall abundance of CCT3 was difficult to assess because the labeled spots were not well resolved. Despite the differences in how protein abundance is affected, dFMRP appears to associate with all three mRNAs suggesting that dFMRP is conferring different types of regulation on the different transcripts. In addition, nearly 70% of FMRP-associated mRNAs identified in a microarray screen contain putative G-quartet motifs (Brown *et al*. 2001), and the mRNA sequences of *cct3*, *cct4*, and *cct7* contain G-quartets. The increase in abundance of CCT7 is most consistent with the prevailing idea that FMRP primarily functions as a repressor of translation. If dFMRP directly regulates the expression of CCT4 or any of the proteins identified as decreasing in abundance in the mutant, it would suggest that dFMRP normally activates the translation of these targets. There is evidence for activation by FMRP, but translational competency of specific transcripts will be the focus of future work. Many (~35%) of the proteins, including CCT3, identified shift in molecular weight and/or pI suggesting that normal post-translational modification is altered in the mutant lysates. This would likely result from indirect regulation by dFMRP. Given our observation that dFMRP associates with the *cct3* mRNA, an alternative hypothesis is that *cct3* represents a normal direct target of dFMRP that is translated inappropriately in the wrong subcellular compartment. The inappropriate translation leads to CCT3 being abnormally modified post-translationally in the absence of dFMRP. Alternatively, the overall abundance of the protein may be affected although this is difficult to discern due to the resolution of the different protein spots. Again, detailed biochemical analysis on the nature of the association of dFMRP and these targets and its affect on translation will be the focus of future studies.

### 3.3.3 Septins and CCT

The septins are a known class of CCT substrates in yeast and are themselves required for cytokinesis and cleavage furrow formation (Field *et al*. 1996; Adam *et al*. 2000). I have found that the septins are a conserved family of CCT substrates in fly, and specifically, that the septin PNUT depends on CCT and dFMRP for its proper localization in the fly embryo. This observation is consistent with previous reports that in early *dfmr1*- embryos PNUT is mislocalized (Deshpande *et al*. 2006), although it is still unclear if the misregulation of the septin contributes to the furrow formation defects observed in both *cct*- and *dfmr1*- embryos. It is known that PNUT associates with Septin 1 (SEPT1) and Septin 2 (SEPT2) and is required for SEPT1 localization to the furrow front in cleavage stage embryos (Field *et al*. 1996). Although the effect on the mislocalization of PNUT in *dfmr1*- embryos appears specific, I have not been able to confidently assess if there are also effects on other septins expressed during the cleavage stage due to unavailability of effective reagents. Preliminary results suggest that at least SEPT1 localization is normal in *dfmr1*- embryos (data not shown), but further analysis should be done to confirm these results. An interesting low penetrant phenotype that I have observed in *dfmr1*- embryos that was also reported to occur in *pnut*- embryos (Adam *et al*. 2000) is a defect in the migration of the posterior midgut. Normally when furrow formation is almost complete the posterior midgut migrates over the dorsal side of the embryo, however in the mutants the migration occurs ventrally or to either lateral side. These observations are consistent with the idea that the misregulation of PNUT in *dfmr1*- has morphological consequences.

The genetic and biochemical relationships between FMRP, CCT, and septins may have significance in the nervous system as septins are known to localize to dendritic protrusions and branch points. Misregulation of septins also causes defects in dendritic

morphology, similar to what is observed in FMRP mutants and FXS patients (Tada *et al*. 2007; Xie *et al*. 2007). It is tempting to speculate that misregulation of CCT could cause septin defects in neurons of *dfmr1* mutants and possibly in FXS patients.

Our work suggests that three of the eight *cct* mRNAs are misregulated in *dfmr1*- cleavage stage embryos. This appears to alter the normal stoichiometry of CCT subunits and in turn affects CCT complex assembly. The aberrant expression of CCT holocomplex in turn affects the assembly of some number of its substrates that are required for proper furrow formation, suggesting a multi-tiered regulatory system. We have identified at least one of these substrates as the septin PNUT. The misregulation of PNUT results in ectopic accumulation of PNUT to lateral membranes, where is may be affecting/impeding how the furrow forms and ingresses. It seems likely that the cleavage furrow formation phenotypes observed in *dfmr1*- embryos are not due to the misregulation of a single transcript or protein but rather the cumulative misregulation of many factors that are regulated in a hierarchical manner that contributes to the phenotype. Although this screen revealed an important set of targets, it was certainly not to saturation. Other strategies will need to be employed to get closer to identifying as many relevant targets as possible (see Appendix 2.2). The identification and characterization of new targets of FMRP will certainly be important for a more complete understanding the function of FMRP and the etiology of FXS.

# Chapter 4: dFMRP and cell cycle regulation at the MBT

The data described in this chapter were generated in collaboration with Ophelia Papoulas, a Research Associate in the Sisson Lab and the following manuscript describing this work is in preparation:

Papoulas O*, Monzo K*, Cantin GT, Ruse C, Yates JR, and Sisson JC. Synaptic plasticity regulators control the cell cycle machinery at the midblastula transition. *equal contributing authors.

## 4.1 INTRODUCTION

A complex system of regulatory mechanisms governs the events of the MBT. In addition to mRNA degradation and transcriptional activation there also are non-RNA based mechanisms that are clearly essential for the MBT in *Drosophila* which include counting of the nucleocytoplasmic ratio (N:C), cell cycle control through fluctuations in activity of the cell cycle machinery, and activation of the DNA damage/replication checkpoint pathway. There is also accumulating evidence that translational regulation plays an important role in mediating the events of the MBT. Our studies suggest that dFMRP functions as a translational regulator during the MBT to affect some of the non-RNA based mechanisms that control the timing of the MBT.

As previously described, dFMRP functions in dynamic mRNP bodies and is required for cellular morphogenesis during the cleavage stage at the MBT in *Drosophila* embryos. In an effort to further understand how dFMRP functions during this time in development, a biochemical screen was performed to identify proteins that associate with dFMRP specifically during the cleavage stage. Two proteins were identified: eukaryotic initiation factor 4G (eIF4G) and a previously uncharacterized protein that is homologous to vertebrate Caprin (CAPR). eIF4G is an essential component of the eIF4F initiation complex which associates with mRNAs and allows them to be assembled into a

translation initiation complex (Gebauer and Hentze 2004). CAPR is a ubiquitous RNA-binding protein that controls progression through the cell cycle in proliferating cells (Wang *et al*. 2005). It is enriched in the nervous system where it localizes to neuronal granules and is involved in translational control (Solomon *et al*. 2007). dFMRP has also been shown to localize to neuronal granules in mouse and fly where it functions as a translational regulator (Kanai *et al*. 2004; Barbee *et al*. 2006). In this chapter, I will describe our efforts to identify new dFMRP-associated proteins and understand how one of these proteins, Caprin, functions together with dFMRP to control cell cycle timing and mediate the events of the MBT.

## 4.2 RESULTS

### 4.2.1 Identification of dFMRP-associated proteins

In order to understand the role of dFMRP in early embryonic morphogenesis a biochemical screen was carried out to identify dFMRP-associated proteins by performing IPs of dFMRP from extracts of cleavage stage *Drosophila* embryos coupled with multidimensional protein identification technology (MudPIT) mass spectrometry. Because the embryo is highly enriched in ribosomal material, dFMRP was resolved from bulk ribosomal subunits and polyribosomes on sucrose gradients prior to IPs in order to avoid ribosomal contamination. Soluble extracts from WT and *dfmr1-* embryos were fractionated in parallel, and the fractions enriched for dFMRP were pooled. The pooled fractions from WT were used to IP dFMRP (Figure 4.1, sample A) and the pooled fractions from *dfmr1-* embryos were used to mock-IP dFMRP as a control for non-

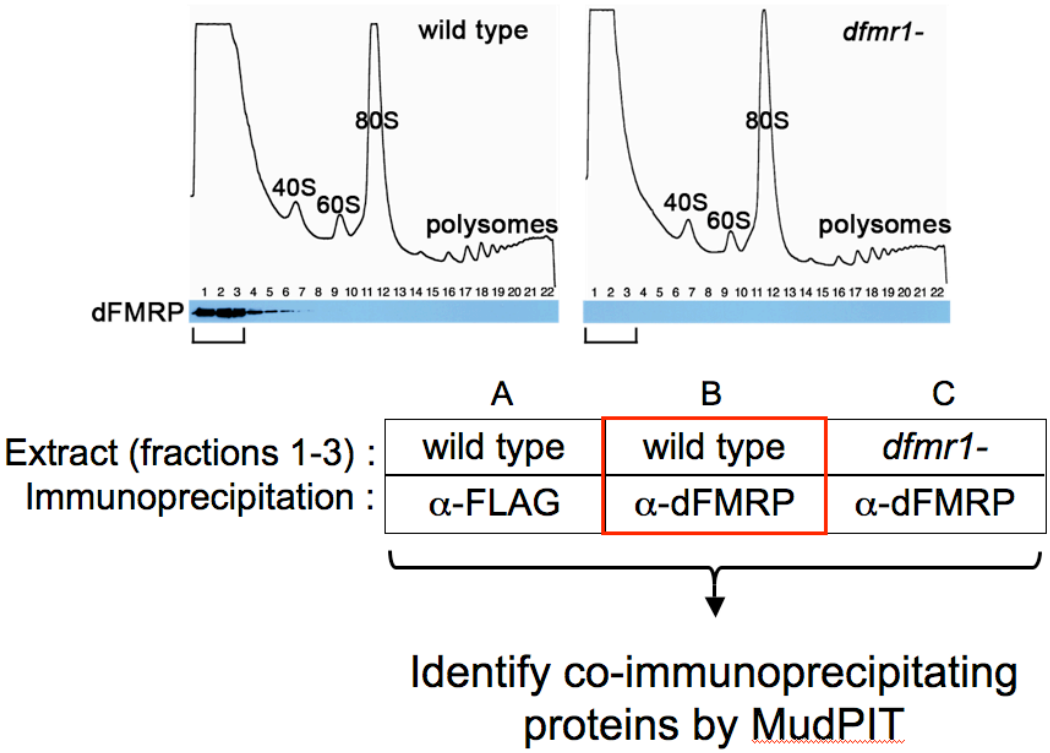


**Figure 4.1 Identification of dFMRP-associated proteins by co-IP and MudPIT**

Top panel shows a UV absorbance trace (*A*254) indicating the positions of ribosomal subunits and polyribosomes across fractions 1–22 from a sucrose gradient of WT and *dfmr1-* cleavage stage embryo extracts. Immunoblots reveal the enrichment of dFMRP in fractions 1-3 and the absence of dFMRP in *dfmr1-* extracts. Lower schematic describes the procedure for identifying proteins that specifically co-IP with dFMRP. Proteins identified in Sample B but not A or C were considered to be associated with dFMRP. This figure is adapted from data and a figure generated by Ophelia Papoulas.

specific binding (Figure 4.1, sample C). An additional control was performed with anti-FLAG antibody and WT extracts (Figure 1, sample A). Proteins that co-IPd with dFMRP were identified by MudPIT mass spectrometry in collaboration with Dr. John Yates (Scripps Research Institute).

Only two proteins specifically co-IPd with dFMRP: eukaryotic initiation factor 4G (eIF4G) and a previously uncharacterized protein in fly encoded by the gene CG18811 homologous to vertebrate Caprin (CAPR). eIF4G mediates the binding of all translationally-competent mRNAs to the 40S ribosome to form a pre-initiation complex and is a scaffolding protein that serves as a major target of translational control (Gingras *et al*. 1999). The association of eIF4G and dFMRP and the previous observation that dFMRP does not associate with active polyribosomes in cleavage stage embryos (Figure 2.4B), suggests that dFMRP may act as a regulator of translational initiation during the cleavage stage. The characterization of eIF4G and dFMRP will be the focus of future studies. Only eIF4G and CAPR were specifically identified as being associated with dFMPR in our experiments, likely due to the stringency of the screen. Interestingly, both are clearly implicated in translational regulation suggesting that this screen has likely identified proteins relevant to the mechanism of dFMRP function. In this study, we focused on how dFMRP and CAPR function together during the MBT.

### 4.2.2 Characterization of *Drosophila* Caprin

The CG18811 gene in the *Drosophila* genome is related by protein sequence homology to two vertebrate RNA-binding proteins termed Cytoplasmic activation/proliferation-associated proteins (Caprins) that are thought to regulate the translation of specific mRNAs. Vertebrate Caprins have been shown to localize to neuronal granules and repress the translation of mRNAs through an unknown mechanism within dendrites (Wang *et al*. 2005; Solomon *et al*. 2007). Neuronal granules are

important sites of post-translational regulation that are believed to sequester specific mRNAs for later release and translation at dendritic synapses in response to external cues (Anderson and Kedersha 2006). The protein and RNA composition of neuronal granules is complex, and is thought to include quiescent ribosomal subunits as well as many proteins involved in RNA metabolism including FMRP, ME31B, and TRAL (in fly) (Anderson and Kedersha 2006; Barbee *et al*. 2006). However, Caprin 1 was originally identified in proliferating tissues as a mitotic phosphoprotein in *Xenopus* and is required for normal progression through the $G_1$ phase of the cell cycle suggesting it is capable of regulating translation in neuronal and non-neuronal tissues (Stukenberg *et al*. 1997; Wang *et al*. 2005).

Primary amino acid sequence analysis of CG18811 revealed the presence of a highly conserved HR1 (Homology Region 1) domain, apparent G3BP binding motif and C-terminal RGG RNA-binding domains suggest CG18811 is related to vertebrate Caprins 1 and 2 (Grill *et al*. 2004) however the absence of a CRD domain (C1q-related domain) suggests it is more closely related to Caprin 1 (Figure 4.2). The HR1 domain is the most highly conserved domain among the Caprin family members, but its function is unknown. Because CG18811 is the only HR1-containing gene in the *Drosophila* genome we named it *caprin* (*capr*).

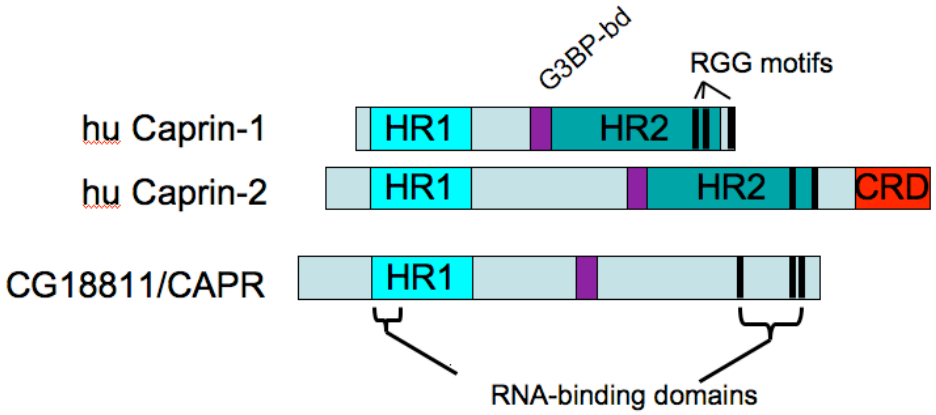


**Figure 4.2 CG18811 is homologous to vertebrate Caprin 1**

Schematic of human Caprin 1 and Caprin 2 and fly CG18811/CAPR protein domains. Homology Region 1 (HR1), G3BP binding motif (G3BP-bd), C1q-related domain (CRD), and arginine-glycine rich RNA-binding motifs (RGG). This figure was generated by Ophelia Papoulas.

### 4.2.3 Functional analysis of Caprin

To begin to address the relevance of the CAPR/dFMRP association *in vivo*, IF analysis of fixed WT embryos was performed using an antibody against a CAPR peptide that was generated in the lab. The anti-CAPR antibody is highly specific for a single band of 140 kD in extracts from adult flies or embryos and absent in mutant extracts (Figure 4.3B). IF analysis of fixed wild type embryos showed that CAPR localizes to the cytoplasm and extensively colocalizes with dFMRP prior to cleavage furrow formation in the apical cytoplasm (Figure 4.3C). In gastrulated embryos CAPR and dFMRP are highly expressed in the central nervous system consistent with the reported roles of vertebrate FMRP and Caprin 1 (Figure 4.4; O'donnell and Warren 2002; Solomon *et al*. 2007). These observations indicate that dFMRP and CAPR associate *in vivo* and may function together to regulate mRNA expression during the MBT.

To examine the function of CAPR in *Drosophila* embryos a protein null allele $capr^{2}$ was generated by imprecise transposon excision (Figure 4.3A). $capr^{2}/Df(3L)Cat$ (hereafter refered to as *capr-*) flies are viable and show no obvious morphological defects, however females are semi-fertile and when mated to WT males, produce embryos (*capr-* embryos) with a cleavage furrow phenotype strikingly similar to the furrowing delay seen in *dfmr1-* embryos (Figures 4.5 and 2.2). Specifically, *capr-* embryos develop normally until the onset of cleavage furrow formation at NC14 when furrows appear morphologically normal but progress at a slower rate compared to WT.

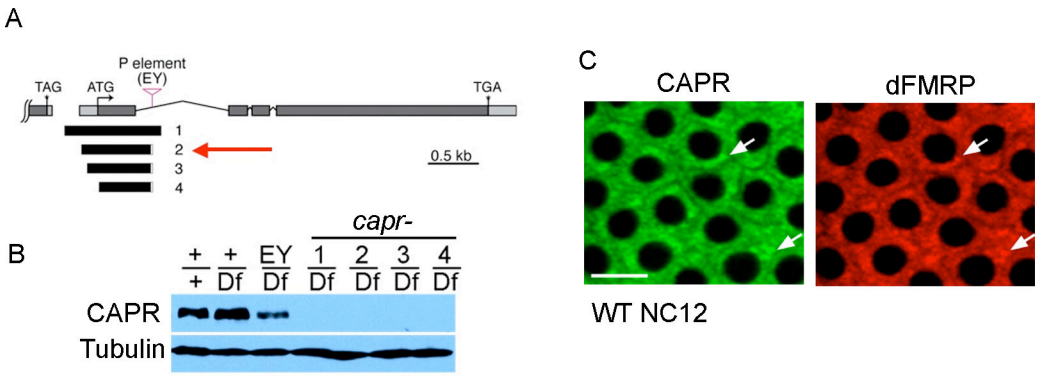


**Figure 4.3 CAPR colocalizes with dFMRP in cleavage stage embryos**

(A) Schematic of genomic region containing *capr*. Four small deletions removing the predicited ATG were generated by imprecise excision of a P-element inserted into an intron of the gene. The red arrow indicates that the *capr2* allele was used for all subsequent functional studies. (B) Immunoblot analysis of WT, +/Df, EY/Df, and the four *capr* deletions alleles in trans to the deficiency. The deficiency, *Df(3L)Cat*, is indicated by Df and completely removes *capr* and other surrounding genes. (C) IF analysis of WT fixed embryo in interphase of NC12 shows cytoplasmic distribution of CAPR and colocalization with dFMRP as indicated with arrows. Scale bar indicates 10 μm. Parts A and B of this figure were generated by Ophelia Papoulas.

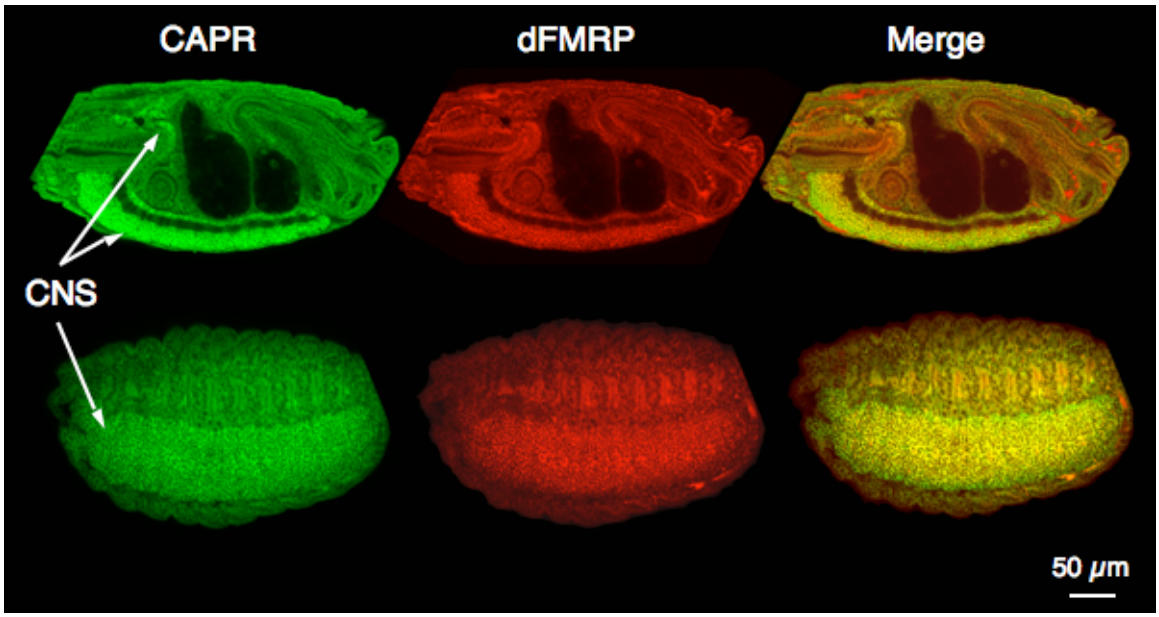


**Figure 4.4 dFMRP and CAPR colocalizes in the CNS**

IF images of sagital (top) and oblique (bottom) WT embryos showing CAPR (green) and dFMRP (red) enriched in CNS as indicated with arrows. Figure was generated by John Sisson.

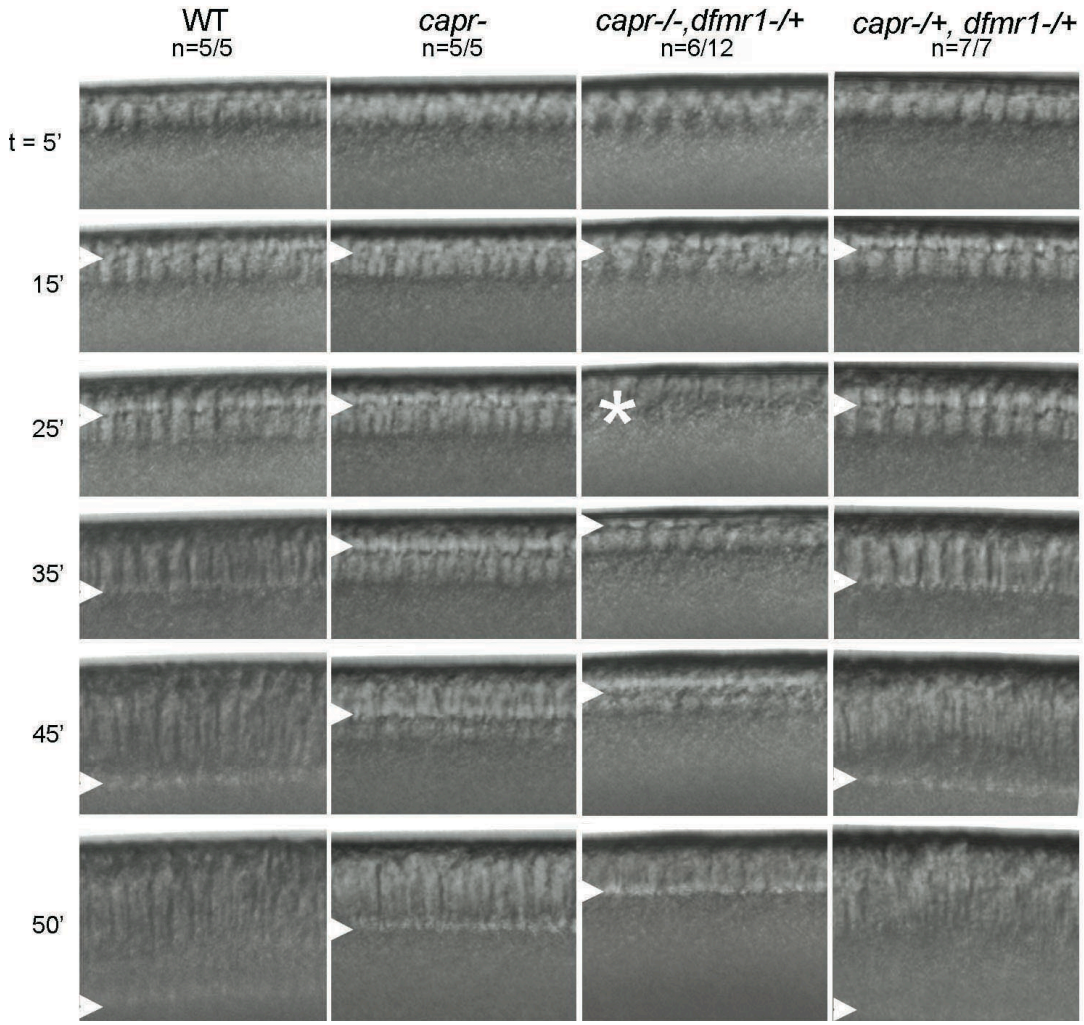


**Figure 4.5 *capr* is required for proper furrow formation and controls cell cycle timing with *dfmr1***

Frames from representative DIC movies of WT and different mutant cleavage stage embryos. Mutant type is indicated at top. Total number of embryos examined (n) with those with shown phenotype is indicated at top. Time (t) indicating in minutes after start of interphase of nuclear cycle 14. Arrowheads and brackets indicate the furrow front position and nuclear elongation, respectively. Asterisk indicates nuclei in mitosis. Scale bar indicates 10 μm.

### 4.2.4 *dfmr1* and *capr* interact during the MBT

The similarity in *capr*- and *dfmr1*- cleavage furrow phenotypes suggested that the proteins could be functioning to regulate the same process and/or the same target mRNAs. If so, then double mutants would be predicted to show enhanced defects. To test this, embryos from double mutant females of the genotype $capr^{2}$, +/ *Df(3L)Cat,* $dfmr1^{3}$ mated to WT males (hereafter refered to as *capr*-/-, *dfmr1*-/+ embryos) were examined. A significant portion of the embryos (approximately 50%, data not shown) examined by live imaging showed a decreased furrowing rate relative to WT, however the remaining showed a distinct phenotype that was never observed in either *capr*-/- or *dfmr1*-/+ alone. The first observation was that many of the *capr*-/-, *dfmr1*-/+ embryos underwent cleavage furrow formation with an increased nuclear density or patches of increased density suggesting that the normal nuclear division cycle was disrupted. A more detailed analysis showed that approximately 50% of *capr*-/-, *dfmr1*-/+ embryos underwent a premature mitosis approximately 20 minutes into interphase of NC14 and completed cleavage furrow formation during interphase of NC15 (Figure 4.5 and 4.6). In many of these embryos, cleavage furrows formed but regressed during the premature mitosis and then reformed to complete furrow formation with a higher nuclear density. An interesting feature of this phenotype is that the rate of furrow ingression in mutants during NC15 is faster than the rate in WT embryos during NC14. This may be because factors required for furrow formation were able to accumulate to certain levels during the abbreviated interphase of NC14 allowing the furrowing machinery to assemble and mediate furrow ingression faster than normal.

The same phenotype was observed in embryos from females of the genotype +, *Df(3R)Exel6265*/ *Df(3L)Cat,* $dfmr1^{3}$ (*capr*-/+, *dfmr1*-/-) but not from $capr^{rvt}$, +/ *Df(3L)Cat,* $dfmr1^{3}$ (*capr*-/+, *dfmr1*-/+) control females where $capr^{rvt}$ is a precise excision

of the transposon indicating that the new phenotype arises from simultaneous reduction of *dfmr1* and *capr*. The premature mitosis was sometimes synchronous throughout the embryo but frequently in patches with only a portion of the embryo undergoing a premature mitosis prior to attempting furrow formation (Figure 4.7 for patch phenotype). Quantification of interphase lengths of live embryos from nuclear cycles 10 through 14 revealed that the duration of all prior nuclear cycles was unaffected and that the earliest observable defect in *capr*-/-, *dfmr1*-/+ embryos was the premature mitosis during NC14 (Figure 4.6). The disruption of the timing of cell cycle and furrow formation during the MBT in *capr*-/-, *dfmr1*-/+ embryos is a phenotype not observed in either *dfmr1*- or *capr*- embryos and indicates that these gene products functionally interact to affect some aspect of the cell cycle regulatory machinery. Spindle morphology and chromosome segregation appeared largely normal in *capr*-/-, *dfmr1*-/+ embryos (Figure 4.7), suggesting that of the known regulators of the timing of the MBT it is unlikely that the *Smg* or the DNA damage checkpoint proteins are affected since mutations in *smg, grp* or *Mei41* produce dramatic defects in those processes (see sections 1.3.3 and 1.3.4). The premature mitosis of NC14 phenotype is also seen for genes that regulate M-CDK1 activity during the MBT, however it should be noted that the phenotype is much more penetrant in *capr*-/-, *dfmr1*-/+ embryos (see section 1.3.2). Together these observations suggest that dFMRP and CAPR are likely acting together to affect expression of regulators of M-CDK1 activity known to affect nuclear cycle lengthening specifically during NC14 of the MBT.

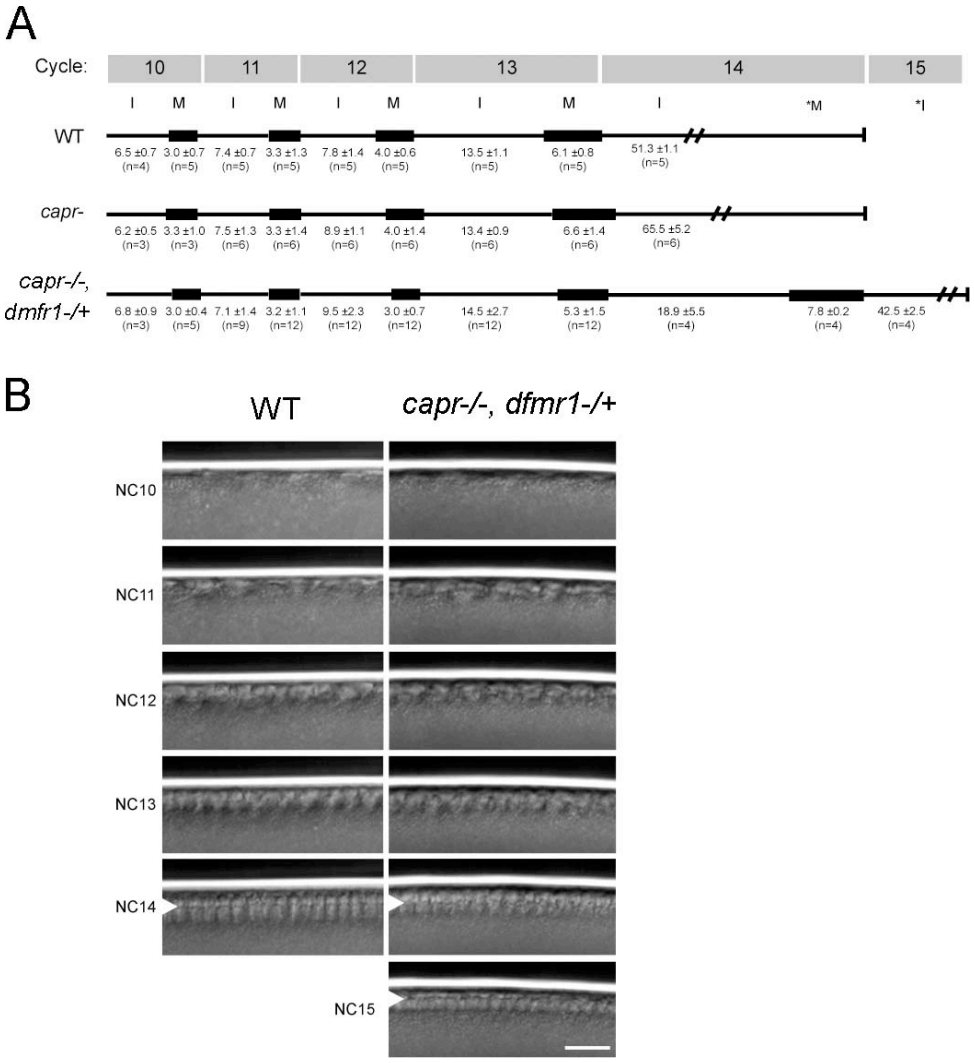


**Figure 4.6 *capr* and *dfmr1* are required for cell cycle lengthening at NC14**

(A) Summary of quantification of nuclear cycle lengths from DIC movies of WT, *capr*-, and *capr*-/-, *dfmr1*-/+ embryos. Bars next to cycle indicate nuclear cycle number. Number under black lines indicates length of interphase (I) with standard error and number under black box indicates length of mitosis (M) with standard error. The number of embryos quantified at any given cycle (n) is under each time. The duration of furrow formation was quantified for interphase of NC14 in WT and *capr*-. Note, normal NC14 mitosis is the first asynchronous mitosis and duration can not be quantified. Abnormal NC14 mitosis and furrow formation in NC15 in *capr*-/-, *dfmr1*-/+ embryos is marked with an asterisk. (B) Stills from DIC movies showing nuclear densities during interphase of different nuclear cycles (left) in WT and *capr*-/-, *dfmr1*-/+ embryos. Arrow heads indicate position of furrow front. Scale bar indicates 10 μm.

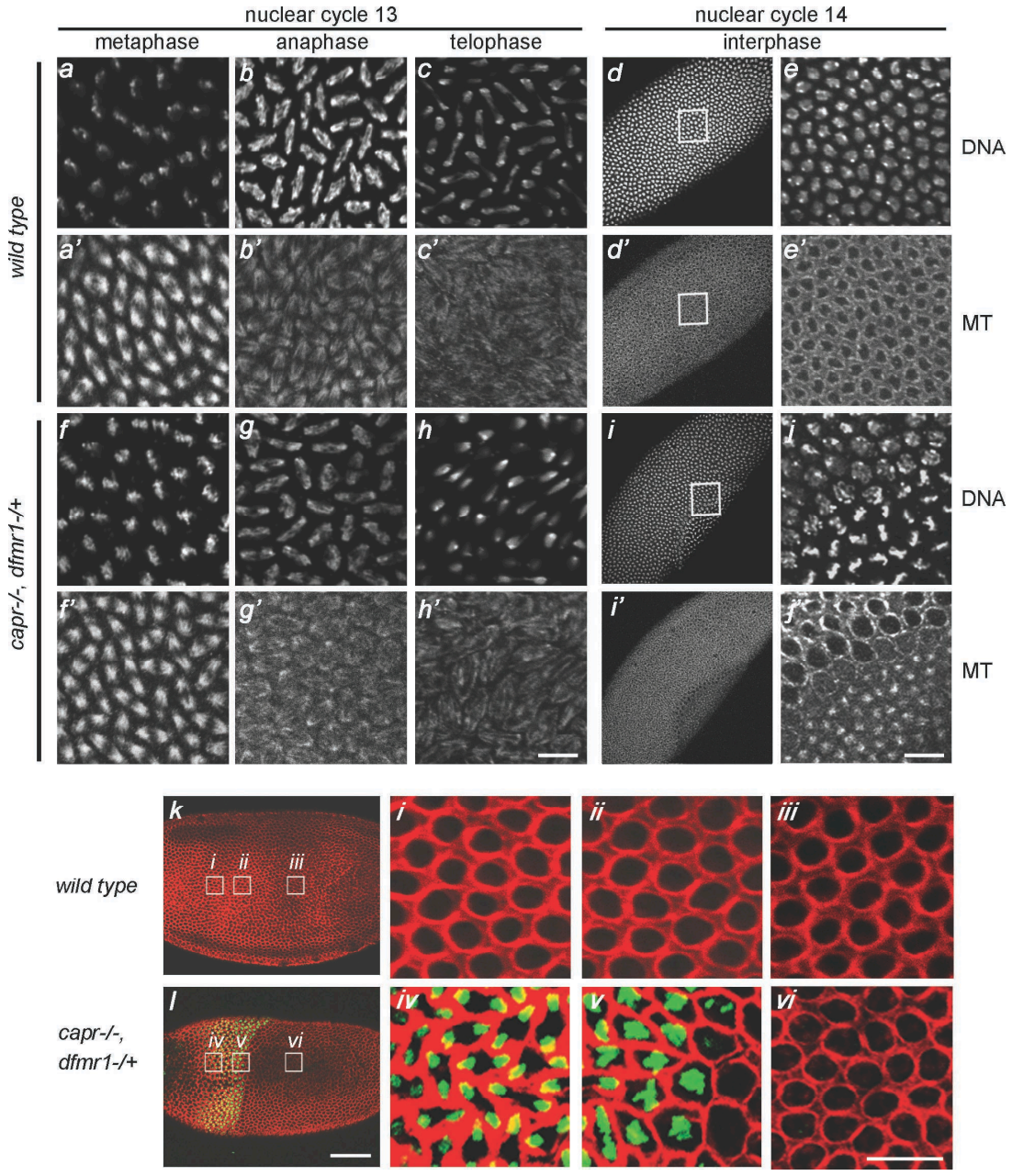


**Figure 4.7** ***capr -/-, dfmr1 -/+*** **mutants complete the events of mitosis normally**

Figure 4.7 on previous page.
IF images of the surface of fixed WT (a-e, k) and *capr-/-, dfmr1-/+* (f-j, l) embryos stained to reveal DNA (a-j) and MT (a'-j') localization during the different stages of mitosis of NC13 and interphase of 14 as indicated at top. Low magnification images of embryos in interphase of NC14 (d and i) show an even pattern of nuclei at the surface of the embryos. Higher magnification shows normal mitotic figures of NC14 in *capr-/-, dfmr1-/+* embryos undergoing premature mitosis of NC14 (j and j'). Lower panel shows an example of a *capr-/-, dfmr1-/+* embryo undergoing premature mitosis 14 non-uniformly. Embryos in k and l are stained to reveal F-actin (red) and phospho-histone H3 (a marker for mitosis, green). Regions *i, ii*, and *iii* show uniform actin rings which delineate the position of the cortical nuclei. Region *vi* shows nuclei in interphase of NC14, region *v* shows nuclei in metaphase, and region *iv* shows nuclei in anaphase and telophase. All mitotic figures appear normal. Scale bar indicates 10 μm in high magnification images and 50 μm in low magnification images.

### 4.2.5 dFMRP and CAPR control expression of CYCB and FRS at the MBT

To identify which regulators of the cell cycle might be affected in *capr-/-, dfmr1-/+* embryos, immunoblot analysis was performed using hand sorted staged WT, *capr-*, and *capr-/-, dfmr1-/+* embryos. While the phosphorylation state of M-CDK1 appeared normal throughout the transition from interphase of NC13 to NC14, the levels of two other regulators of M-CDK1 activity were specifically altered in the double mutant embryos (Figure 4.8). Levels of CYCB were inappropriately elevated in mitosis of NC13 (M13) and early NC14 as compared to WT (Figure 4.8). In addition, FRS, a zygotic inhibitor of CYCB, did not accumulate to appropriate levels until mid NC14 as compared to WT (Figure 4.8). Consistent with the live analysis, this disruption of CYCB and FRS expression was not detected in *capr-* embryos which undergo delayed furrow formation but never a premature mitosis during NC14.

If the inappropriate CYCB expression detected by immunoblot analysis contributes to the phenotype observed in live embryos, reducing the dosage of *CycB* should suppress the premature mitosis phenotype. Whereas 50% of *capr-/-, dfmr1-/+*

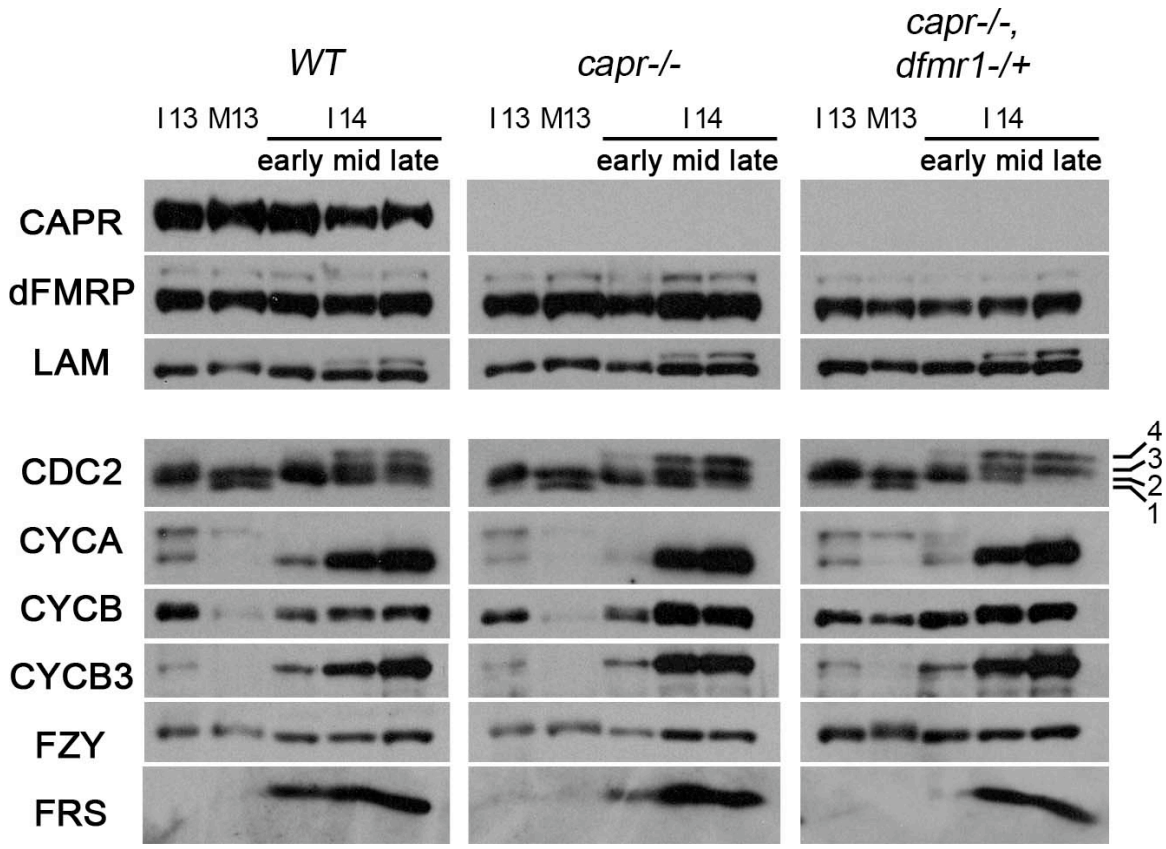


**Figure 4.8 CYCB and FRS expression is perturbed in *capr-/-, dfmr1-/+* embryos**

Immunoblots of handsorted WT, *capr-/-*, and *capr-/-, dfmr1-/+* embryos show abundance of proteins (left) as embryos progress from NC13 to NC14 as indicated at top. I14 embryos were sorted into three stages based on progression of furrow front. The four phosphoisoforms of CDC2 (CDK1) are indicated to the right. Form 1 has an activating phosphate (T161P), form 2 is unphosphorylated, form 3 and 4 have inhibitory phosphates (Y15P and T14P, Y15P) as first described in Edgar and Datar, 1996. NC13 interphase (I13), NC13 mitosis (M13), NC14 interphase (I14). The data and figure was generated by Ophelia Papoulas. I prepared and assisted in handsorting of embryos.

embryos showed a premature mitosis in NC14, loss of one maternal copy of *CycB* was able to significantly rescue this phenotype. Only 17% of embryos from *CycB*$^{2}$/+; *capr*$^{2}$, +/ *Df(3L)Cat, dfmr1*$^{3}$ (*CycB*-/+, *capr*-/-, *dfmr1*-/+) females mated to WT males underwent premature mitosis in NC14 (Figure 4.9). Because half the embryos produced by *CycB*-/+, *capr*-/-, *dfmr1*-/+ females are zygotically heterozygous for *CycB* it remained possible that elevated CYCB levels could arise from premature aberrant expression of the zygotic *CycB* gene and thus only be sufficient to produce premature mitosis in half the progeny of the previous test cross. To rule out the possibility that zygotic misexpression of *CycB* accounts for the premature mitosis observed in embryos from *capr*-/-, *dfmr1*-/+ females, females were mated to *CycB*$^{2}$/*CYO-GFP* males and embryos were observed for premature mitosis and scored for the presence of GFP, indicating that the embryo received a WT copy of *CycB*. Reduction of the zygotic contribution of CYCB was unable to rescue the premature mitosis phenotype indicating that the elevated levels we see are due to misexpression of the maternal *CycB* mRNA (GFP- bar, Figure 4.9). We do not believe that the observed elevated CYCB levels at mitosis 13 are due to impaired degradation by the Anaphase Promoting Complex (APC) because other known targets of APC (CYCA and CYCB3) are appropriately degraded at M13, and the CDC20 subunit of the APC complex (FZY) is expressed at levels comparable to that in wild type embryos (Figure 4.8). Furthermore, proper degradation of CYCB is necessary for progression through the cell cycle (Su *et al*. 1998; Glotzer 2001), and *capr*-/-, *dfmr1*-/+ embryos appear to progress through mitosis normally (Figure 4.8). These observations suggest that the premature mitosis in NC14 in *capr*-/-, *dfmr1*-/+ embryos is due to premature translation of maternal *CycB* mRNA.

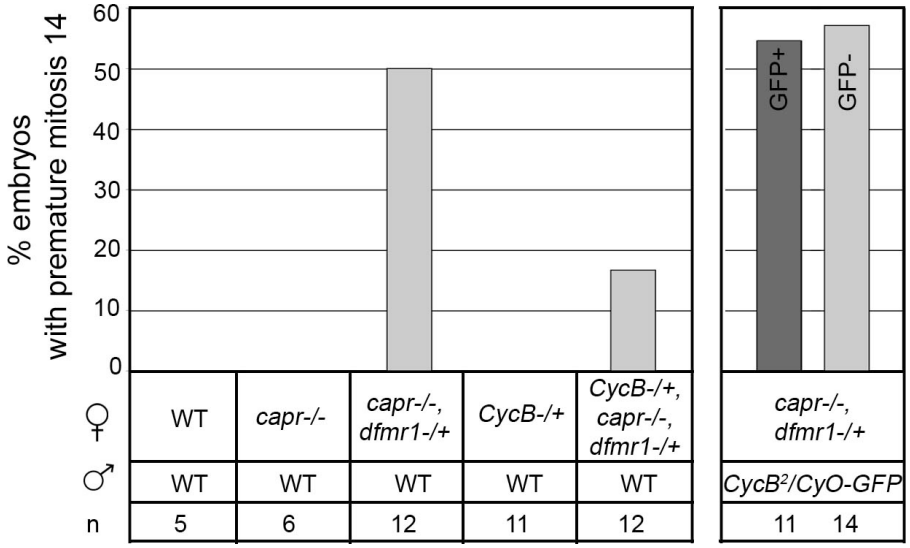


**Figure 4.9 Loss of maternal *CycB* rescues premature mitosis 14 phenotype in *capr-/-, dfmr1-/+***

Bar graph shows percentage of embryos laid by females (♀, top row) mated to males (♂, bottom row) that displayed a premature mitosis 14. 'n' indicates total number of embryos observed from each cross. The two bars to the right represent embryos fromthe same cross and were distinguished by the presence or absence of GFP. The presence of GFP indicates that embryos were *CycB*+/+, and the absence of GFP indicates that embryos were *CycB*-/+.

Our phenotypic analysis argues that CAPR and dFMRP function together and affect expression of *CycB*. To determine whether *CycB*, *fr*s, or other cell cycle regulators are themselves direct targets of CAPR/dFMRP translational regulation we tested whether any of the candidate mRNAs specifically associate with CAPR or dFMRP at this time in development. CAPR or dFMRP IPs were conducted from wild type extracts of embryos staged to span NC13 to early NC14, and mock IPs were conducted from correspondingly staged mutant embryos (with either *capr*-/- or *dfmr1*-/- embryos respectively). Co-IPd RNA was isolated and levels of specific mRNAs in the starting extract (steady-state

levels) and in the IPs were determined by qRT-PCR. While steady-state levels of *CycB* and *frs* were not altered in mutant embryos prior to the start of NC14 (2-2.5hr, Figure 4.10), both mRNAs were enriched in IPs performed from wild type extracts suggesting that they are part of a dFMRP and CAPR-containing mRNP *in vivo* and are likely to be direct targets of translational regulation (Figure 4.11). Interestingly, the levels of *CycB* mRNA are significantly higher in 3-3.5hr *capr*-/-, *dfmr1*-/+ embryos compared to WT embryos of the same age (Figure 4.10). One possible explanation is that the maternal *CycB* mRNA is normally repressed in a WT situation, which may destabilize the transcript. In the *capr*-/-, *dfmr1*-/+ embryos, the *CycB* mRNA is not repressed which may then result in the stabilization and accumulation of transcript which is apparent at the later stage. Future studies assessing the stability of dFMRP and CAPR target mRNAs will potentially be able to address this observation.

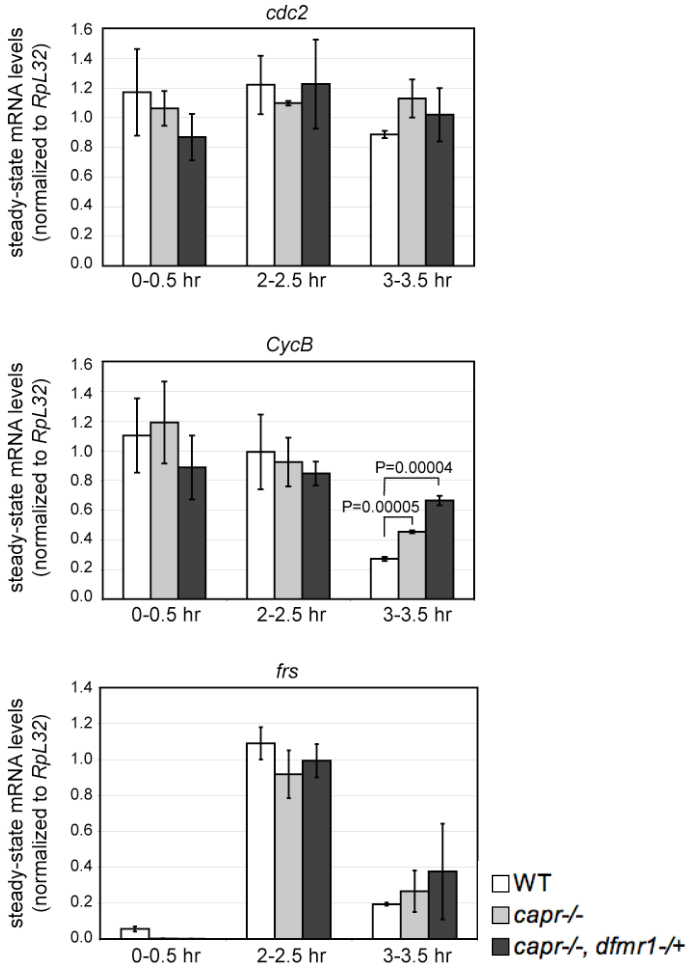


**Figure 4.10 Steady state mRNA levels are not affected prior to NC14 in *capr-/-, dfmr1-/+* embryos**

Bar graph of *cdc2*, *Cycb*, and *frs* mRNA levels quantified by qRT-PCR from 30 minute collections of WT (white bar), *capr*-/- (grey), and *capr*-/-, *dfmr1*-/+ (black) embryos. 0-0.5 hr embryos are enriched for early NCs well before the onset of zygotic transcription. 2-2.5 hr embryos are enriched for syncytial stages just prior to NC14. 3-3.5 hr embryos are enriched for mid- and late-furrowing cleavage stage. Error bars indicate standard deviations (SD). Significance was assessed using the Student's *t* test and significant P - values are shown.

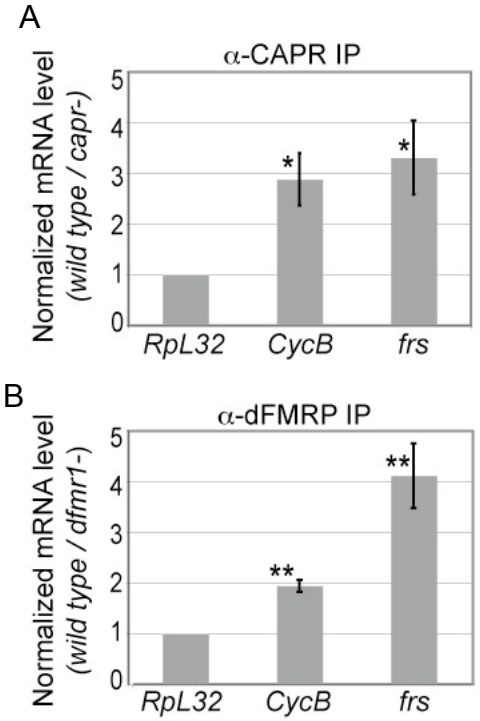


**Figure 4.11 CAPR and dFMRP associate with *CycB* and *frs* mRNAs**

Bar graph shows the fold enrichment of each mRNA in WT vs. *capr-* anti-CAPR IPs (A) and WT vs. *dfmr1-* anti-dFMRP IPs (B) normalized to *RpL32* measured by qRT-PCR. Error bars indicate standard deviations (SD). Significance was assessed using the Student's *t* test (*, $P \leq 0.05$ and **, $P \leq 0.005$). The data and figure were generated by Ophelia Papoulas.

## 4.3 DISCUSSION

To broaden our understanding of how FMRP functions, a stringent biochemical screen was performed to identify proteins that associate with dFMRP during the cleavage stage at the *Drosophila* MBT. Two dFMRP-associated proteins previously implicated in translational regulation were identified: eIF4G and Caprin. This study focused on the genetic interaction between dFMRP and CAPR during the MBT. We have shown that CAPR is required on its own for forming proper cleavage furrows. In addition, we have found that dFMRP and CAPR are required together to lengthen the cell cycle during interphase of NC14 by likely responding to changes in the N:C and in turn modulating the expression of CYCB and FRS (Figure 4.12).

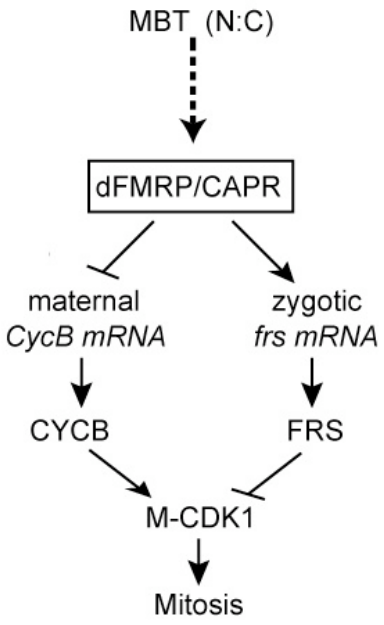


**Figure 4.12 Model for dFMRP and CAPR regulation of the cell cycle at the MBT**

Figure generated by John Sisson.

### 4.3.1 dFMRP and CAPR regulate multiple cell cycle regulators

The specific nature and relatively high penetrance of the premature M14 phenotype together with what is known about other genes that also display this phenotype when altered, lead us to believe that dFMRP and CAPR regulate the expression of a number of different proteins involved in cell cycle control during the MBT. As described in Chapter 1, altering levels of *CycB* has been shown to affect the timing of cleavage furrow formation but at a low penetrance. About 8% of embryos expressing 4X *CycB* fail to elongate interphase of NC11-13 and furrowing never occurs, and 10% of embryos that are maternally provided with 1X *CycB* fail to initiate mitosis of NC13 and embryos attempt to form cleavage furrows during an extended interphase of NC13 (Stiffler *et al*. 1999). In addition, loss-of-function mutations in *frs* and *trb*, normal inhibitors of M-CDK1 activity required for the lengthening of interphase of NC14, result in a relatively low penetrance of the premature mitosis 14 phenotype (Grosshans and Wieschaus 2000). Over expression of *cdc25/twe*, an activator of M-CDK1 activity has a similar effect (Edgar and Datar 1996). Together with these previous observations, our findings that CYCB and FRS levels are disrupted in the *capr-/-, dfmr1-/+* embryos and that dFMRP and CAPR both associate with the *CycB* and *frs* mRNAs suggest that the premature mitosis phenotype is due to the disruption of the expression of multiple cell cycle regulators.

### 4.3.2 Do dFMRP and CAPR spatially regulate *CycB* expression?

As discussed in section 1.3.2, the temporal as well as spatial regulation of *CycB* expression is important for progression through the cell cycle, although the specific mechanism for controlling *CycB* mRNA metabolism is unknown. We have shown that the basis for the misregulation of CYCB during the transition from mitosis of NC13 to

interphase of NC14 in *capr*-/-, *dfmr1*-/+ embryos is likely due to the inappropriate translation from maternal *CycB* mRNA (Figures 4.7 and 4.8). We attempted to address whether the misregulation is of only a subpopulation of *CycB* mRNA, by assessing the subcellular localization of *CycB* mRNA by fluorescent in situ hybridization (FISH) (data not shown generated by Gerrit van der Ende) and protein by IF in fixed embryos (data not shown). Results for both experiments were inconclusive, as we were unable to detect spindle-associated mRNA or protein during mitosis of NC13. These results were most likely due to insufficient fixation of spindle MTs and associated proteins and mRNAs. The outstanding question of whether dFMRP and CAPR spatially regulate the expression of *CycB* will be interesting to address in future studies.

### 4.3.3 dFMRP and CAPR regulate the expression of zygotic genes

In order for interphase of NC14 to lengthen to allow for cleavage furrow formation, Frs protein needs to accumulate shortly after interphase of NC14 is initiated to repress M-CDK1 activity. dFMRP and CAPR are required for the apparent activation of the zygotically expressed *frs* mRNA. It has been reported that the transcriptional activation of the *frs* gene is dependant on the transcriptional regulator, Zelda (Liang *et al*. 2008). Because the temporal regulation of FRS expression is very strict, it seems reasonable that *frs* mRNA expressed prior to the onset of interphase of NC14 may be in a translationally incompetent state and requires activation in order to accumulate the protein to sufficient levels to mediate inhibition of M-CDK1. The premature mitosis of NC14 phenotype suggests that M-CDK1 activity is not repressed properly in *capr*-/-, *dfmr1*-/+ embryos during interphase of NC14. Our observations that FRS protein levels do accumulate normally and that the *frs* mRNA associates with both dFMRP and CAPR suggest that dFMRP and CAPR are likely the proteins responsible for this activation.

In conclusion, we have identified new previously unknown dFMRP-associated proteins. One of these proteins, CAPR, functions with dFMRP during the cleavage stage to mediate the timing and morphological events of the MBT in *Drosophila* embryos. In addition, we have shown that CAPR is expressed in the fly CNS where vertebrate Caprins have also been shown to function to regulate the expression of specific mRNAs. Future studies in the nervous system may reveal possible functional interactions between the two proteins where FMRP loss of function is known to cause many of the neurological phenotypes seen in FXS patients.

# Appendix 1: A characterization of conditional mutants affecting *Drosophila* cleavage furrow formation

## A1.1 INTRODUCTION

It is known that maternal gene products are sufficient to mediate the events of the first phase of cleavage as shown in studies using pharmacological agents to block zygotic transcription and a genetic screen using *Drosophila* embryos completely lacking entire chromosome arms (Edgar and Schubiger 1986; Merrill *et al*. 1988; Wieschaus and Sweeton 1988). It was also demonstrated that the process of cellularization only requires zygotic transcription from six discrete genetic loci (Merrill *et al*. 1988; Wieschaus and Sweeton 1988). Thus, the majority of gene products required for proper cellularization are likely to be maternally derived, and some of these gene products may be required for viability. For this reason, conventional loss-of-function genetic screens have a limited ability to identify genes required during the cleavage stage. Conditional mutants offer a unique opportunity to identify new genes required for *Drosophila* cleavage furrow formation because any effects of the mutation can be studied during a particular stage of development. Consequently, we obtained a collection of EMS-induced, temperature-sensitive (ts) zygotic lethal mutants residing on the X-chromosome (W. Sullivan and H. Francis-Lang, University of California Santa Cruz). In this appendix, I describe a screen I performed to identify X-linked mutations that affect *Drosophila* embryonic cleavage furrow formation. I began this work as an undergraduate in the Sisson lab and continued to work on it as a graduate student before the FMRP project became my main focus.

## A1.2 RESULTS

### A1.2.1 Live analysis screen of temperature sensitive mutants

To identify conditional mutants that affect cellularization I screened an existing collection of temperature-sensitive (ts) mutants originally identified as X-linked mutants that cause zygotic lethality at a restrictive temperature of 29°C. From the original collection consisting of 158 stocks, 38 stocks were shown to retain ts zygotic lethality and also to be ts maternal sterile (W. Sullivan, B. Zhang, UT Austin, and H. Kramer, UT Southwestern). I analyzed cellularizing embryos derived from wild type (WT) and homozygous mutant females using time-lapse differential interference contrast (DIC) microscopy. Embryos were collected and allowed to age at the permissive temperature on a temperature controlled microscope stage until the onset of interphase of nuclear cycle 14 when they were shifted to the restrictive temperature and imaged until gastrulation (Figure A1.1). Rates of nuclear elongation and furrow ingression were calculated from live time-lapse recordings. Five mutants were identified that display cellularization defects at the restrictive temperature (Figure A1.2). These mutants can be classified into two distinct phenotypic categories based on either primary disruptions in the rates of furrow ingression with relatively normal morphology or severe disruptions in furrow ingression, nuclear morphology, and cytoplasmic movements.

During normal cellularization cleavage furrows ingress at two distinct rates. First, furrowing occurs slowly until the furrow front reaches the basal ends of nuclei. The rate then abruptly increases during the fast phase until the cells are formed and cellularization is complete. During the slow phase the nuclei elongate at a constant rate. In wild type embryos at 32°C (the restrictive temperature for this screen), nuclei begin to elongate within the first 10 min of interphase of nuclear cycle 14. Membrane furrows begin to form soon after, and the furrow front can be seen as a refractive structure along

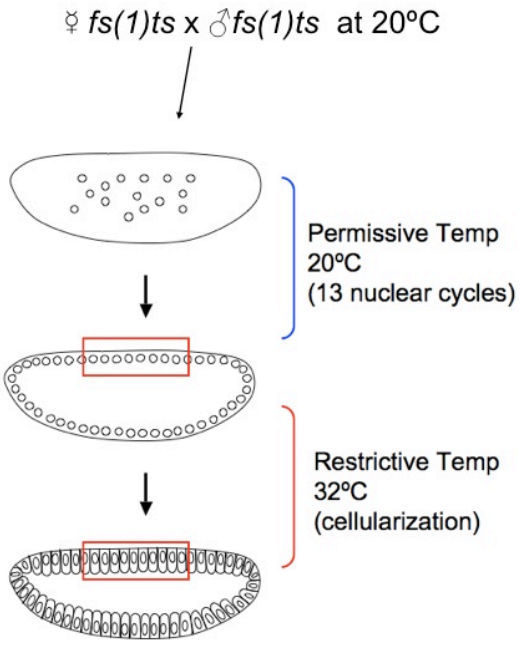


**Figure A1.1 Schematic of screen to identify ts cellularization defects**
Virgin *fs(1)ts* females were mated to males of the same genotype. Embryos collected from this cross were allowed to develop at the permissive temperature in a perfusion incubator until the onset of NC14, when they were shifted to the restrictive temperature and imaged.

the entire inner surface of the embryo that ingresses at two distinct rates. Initially, the furrow front ingresses at a rate of ~0.3 μm/min, referred to as the slow phase. Once the furrow front approaches the basal tips of the elongated nuclei, after approximately 30 min, the rate of ingression increases to ~1.2 μm/min, referred to as the fast phase. The furrow continues to grow until the membrane surrounding individual nuclei pinches off to form individual cells.

### A1.2.2 Moderate cellularization mutants

Two mutants were found to have defects during both phases of furrow ingression and nuclear elongation. Cellularization in *fs(1)ts448* and *fs(1)ts567* embryos show uniform and significant delays in furrow ingression at the restrictive temperature compared to WT (Figure A1.2). The average rates of slow phase furrow ingression in *fs(1)ts448* and *fs(1)ts567* embryos are 2-fold slower than WT (*fs(1)ts448* = 0.11 μm/min, *fs(1)ts567* = 0.13 μm/min and WT = 0.25 μm/min; Table A1.1). Although the furrowing rate of *fs(1)ts448* embryos increases 2-fold during the transition from slow phase to fast phase, the rate of ingression remains delayed compared to WT (*fs(1)ts448* = 0.23 μm/min and WT = 1.14 μm/min, Table A1.1). Nuclei also fail to completely elongate in these mutants. After 50 min into cellularization, the ends of nuclei in *fs(1)ts448* and *fs(1)ts567* embryos only reach about half the distance from the cortex (~10 μm) compared to WT embryos (20 μm) (Figure A1.1; Table A1.1). Although embryos derived from both *fs(1)ts448 and fs(1)ts567* females appear cellularized and initiate gastrulation, they fail to hatch at the restrictive temperature. *fs(1)ts448* and *fs(1)ts567* homozygous females have decreased egg production at both permissive and restrictive temperatures (Table A1.2). However, the hatch rates are significantly lower at the restrictive temperature

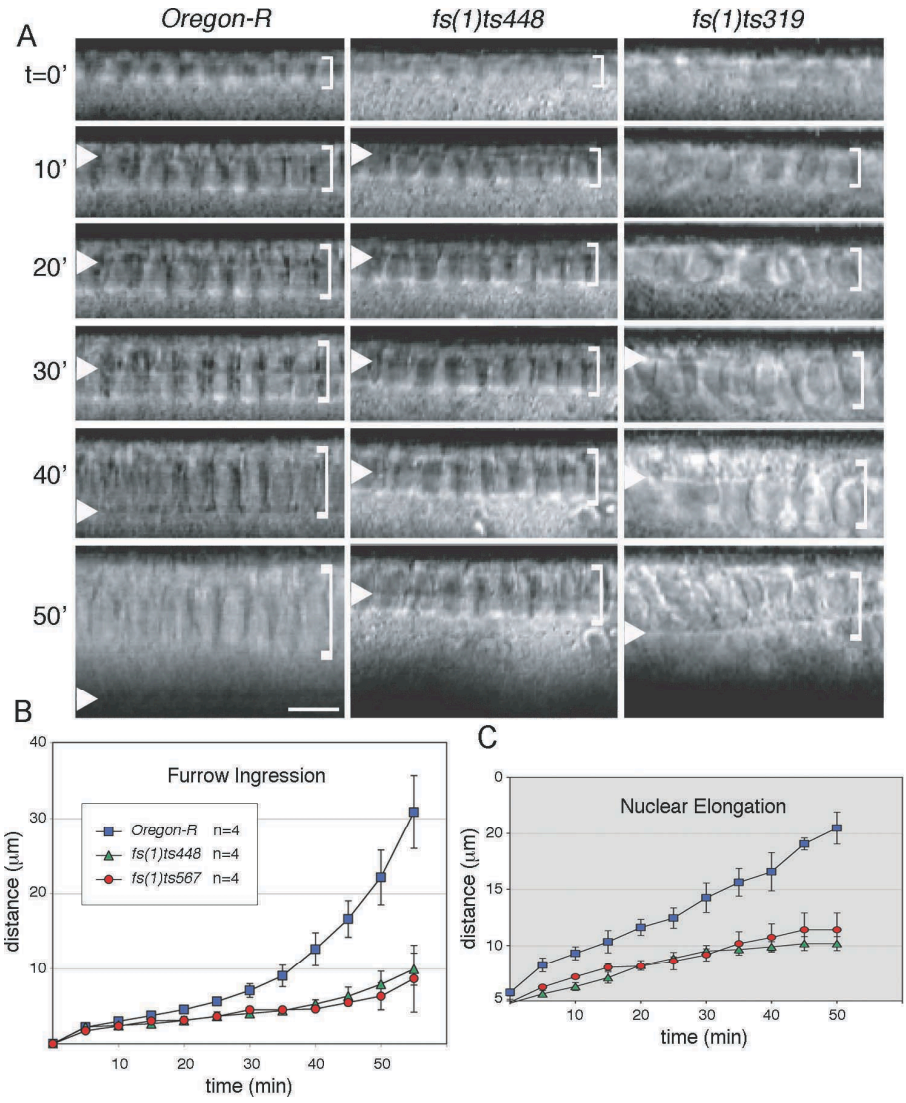


**Figure A1.2 Time-lapse imaging reveals temperature-sensitive cellularization defects**

Sequential frames (A) from representative DIC movies of WT and ts mutant embryos undergoing normal (left panel) and abnormal (middle and right panels) cellularization at 32°C. White arrowheads and brackets indicate the furrow front position and nuclear position and elongation, respectively. Times (*t*) in minutes are relative to onset of nuclear cycle 14. Scale bar represents 10 $\mu$m. The average rates of furrow ingression (B) and nuclear elongation (C) in embryos derived from WT, *fs(1)ts448*, and *fs(1)ts567* homozygous females mated to WT males. Error bars and n indicate the standard deviation and number of movies measured, respectively.

| Maternal Genotype | Slow Phase (μm/min) | Fast Phase (μm/min) | Nuclear Elongation (μm/min) | n |
|---|---|---|---|---|
| *Oregon-R* | 0.25 ± 0.03 | 1.14 ± 0.19 | 0.28 ± 0.02 | 4 |
| *fs(1)ts448* | 0.11 ± 0.02$^{***}$ | 0.23 ± 0.09$^{***}$ | 0.11 ± 0.03$^{***}$ | 4 |
| *fs(1)ts448/Df(1)HF396* | 0.10 ± 0.03$^{***}$ | 0.35 ± 0.10$^{***}$ | 0.15 ± 0.03$^{***}$ | 3 |
| *fs(1)ts567* | 0.12 ± 0.01$^{***}$ | 0.17 ± 0.18$^{***}$ | 0.13 ± 0.03$^{**}$ | 4 |
| *fs(1)ts567/Df(1)DA622* | 0.10 ± 0.02$^{***}$ | 0.17 ± 0.15$^{***}$ | 0.15 ± 0.03$^{***}$ | 3 |
| *fs(1)ts148/small bristles* | 0.13 ± 0.03$^{**}$ | 0.35 ± 0.16$^{***}$ | 0.16 ± 0.01$^{***}$ | 4 |
| *fs(1)ts242* | 0.20 ± 0.07 | 0.89 ± 0.29 | 0.18 ± 0.05$^{*}$ | 4 |
| *fs(1)ts242/Df(1)JC70* | 0.14 | 0.60 | 0.12 | 3 |
| *fs(1)ts319* | 0.10 ± 0.05$^{*}$ | 0.49 ± 0.32 | 0.16 ± 0.03$^{*}$ | 4 |
| *fs(1)ts319/RA37* | n.d. | n.d | n.d. | |

**Table A1.1 Rates of furrow ingression and nuclear elongation**

Rates from embryos laid by females with indicated geneotype mated to WT males. Standard error shown next to rates. Total number of movies quantified indicated by 'n'. Not determined, n.d. Significance measured by Student's *t*-test, $^{*}P<0.01$, $^{**}P<0.001$, $^{***}P<0.0001$.

(7-fold lower for *fs(1)ts448* and 10-fold lower for *fs(1)ts567*, Table A1.2). This may reflect mutations that are non-conditional with respect to oogenesis but conditional with respect to embryogenesis. In addition, progeny derived from *fs(1)ts448* and *fs(1)ts567* adults fail to eclose at the restrictive temperature, with lethal phases during larval or pupal stages as indicated in Table A1.2.

### A1.2.3 Severe cellularization mutants

Three mutants were identified that display severe defects in nuclear morphology and furrow ingression. Live cellularizing *fs(1)319* embryos show severe disruptions in nuclear morphology and cytoplasmic movements throughout cellularization (Figure A1.2). The majority of the nuclei appear to remain attached to the cortex and increase in volume but fail to elongate. The shapes of nuclei become irregular, possibly due to their failure to elongate and the disruptions in the cytoplasm. Despite the turbulent cytoplasmic movements, the birefringence pattern of the furrow front suggests that an apparently intact contractile apparatus forms and is capable of ingression. *fs(1)ts242* and *fs(1)ts148* also display severe disruptions in nuclear morphology and furrow ingression during cellularization at the restrictive temperature. Although the furrow front in cellularizing *fs(1)ts242* embryos is locally abnormal, it ingresses globally at rates similar to wild type (Table A1.1). Rates of furrow ingression in cellularizing *fs(1)ts319* and *fs(1)ts148* embryos show significant departures from wild type (Table A1.1).

The overall numbers of eggs deposited by *fs(1)ts242* and *fs(1)ts319* mutant females of the severe class are not significantly different at the restrictive compared to the permissive temperature or wild type, but the hatch rate is significantly lower at the restrictive temperature (3-fold lower for *fs(1)ts242* and 7.5-fold lower for *fs(1)ts319*; Table A1.2). Homozygous *fs(1)ts148* females display an almost 5-fold reduction in egg

| Maternal Genotype | Hatch Percentage [a] (n) | | Relative Eclosure [b] (n) | | |
|---|---|---|---|---|---|
| | 20°C | 29°C | 20°C | 29°C | lethal phase |
| *Oregon-R* | 94.4 (213) | 86.7 (279) | 1.00 (220) | 0.80 (175) | |
| *fs(1)ts448* | 63.6 (66) | 9.1* (11) | 0.55 (122) | 0.05 (10) | L,P |
| *fs(1)ts567* | 60.9 (23) | 5.9* (34) | 0.59 (130) | 0.00 (0) | L |
| *fs(1)ts148* | 85.9 (142) | 0.0* (29*) | 0.99 (219) | 0.00 (0) | E |
| *fs(1)ts242* | 66.4 (265) | 22.1* (181) | 0.74 (163) | 0.00 (0) | L,P |
| *fs(1)ts319* | 66.9 (260) | 8.9* (123) | 0.82 (181) | 0.38 (84) | L,P |

**Table A1.2 Mutants display temperature-sensitive maternal sterility and zygotic lethality**

[a] females were mated to *FM7a* males. [b] females were mated to *fs(1)t*s males of the same genotype. n indicates total number of embryos laid (hatch percentage) or total numbers of F1 adults obtained from cross (relative eclosure). Hatch percentages or total number of embryos laid at 29°C significantly different from those at 20°C as measured by Student's *t*-test are indicated with asterisks, $^{*}P<0.01$. Lethal phase indicates stage that development is arrested. E embryonic, L larval, P pupal

production at the restrictive temperature, and none of the embryos laid at the restrictive temperature hatch (Table A1.2). Progeny derived from *fs(1)ts148* and *fs(1)ts242* adults completely fail to eclose at the restrictive temperature, with lethal phases during embryonic, larval, or pupal stages as indicated in Table A1.2. *fs(1)ts319* F1 adults eclose at the restrictive temperature but do so at a decreased frequency (0.38) compared to wild type (1.00) and *fs(1)ts319* (0.82) at the permissive temperature. The majority of *fs(1)ts319* F1 progeny arrest development as larvae or pupae.

### A1.2.4 *fs(1)ts319* embryos display ts MT defects during cellularization

Due to its strong maternal sterility and cellularization phenotype, I initiated a phenotypic characterization of *fs(1)ts319* cellularizing embryos. Analysis of live *fs(1)ts319* embryos suggests that the contractile apparatus is intact and able to advance during cellularization. Normally, F-actin forms an array of interlocking contractile rings under the plasma membrane and during furrow formation is positioned at the ingressing furrow front (Figure A1.3). *fs(1)ts319* embryos fixed at the restrictive temperature and stained with fluorescent phalloidin, reveal relatively normal F-actin accumulation at the ingressing furrows compared to WT at the restrictive temperature (Figure A1.3). In addition, localization of Myosin II and Anillin at the leading edge of the furrow front is normal in *fs(1)ts319* embryos at the restrictive temperature (data not shown). In contrast, the microtubule cytoskeleton appears disrupted in mutant embryos fixed at the restrictive temperature and analyzed by immunofluorescence (IF). At the onset of cellularization microtubule arrays emanate from pairs of cortically positioned centrosomes, extending their plus-ends into the interior of the embryo, forming 'inverted baskets' around individual nuclei (Figure A1.3), and are thought to provide some mechanical force required for nuclear elongation (Foe and Alberts 1983). Microtubule arrays surrounding individual nuclei often appear diffuse and do not extend into the basal cytoplasm (Figure

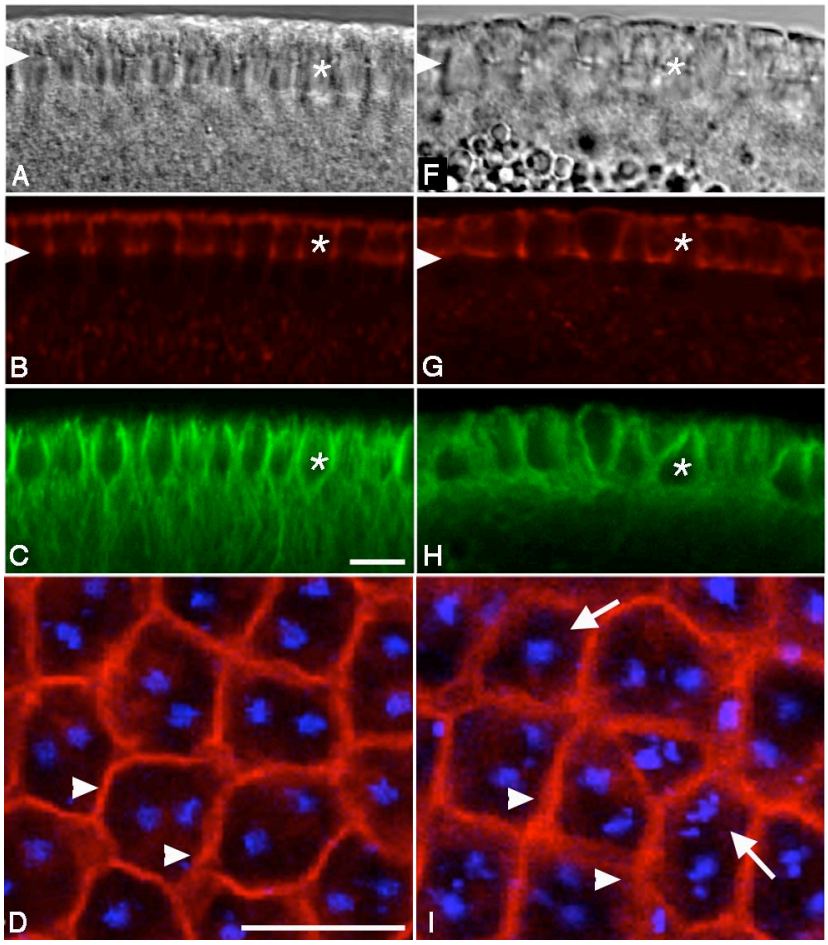


**Figure A1.3 The microtubule cytoskeleton is disorganized and centrosome morphology is abnormal in *fs(1)ts319* mutant embryos at the restrictive temperature**

IF analysis of WT (A-D) and fs(1)ts319 (E-I) cellularizing embryos fixed at 32°C shows relatively normal cortical F-actin localization by phalloidin (arrowheads in B, G, D, I) and disrupted microtubules in mutant embryos (C and H). Oblique images through the apical cytoplasm (D and I) show abnormal centrosome morphology, including fragmentation, uneven spacing, and lone centrosomes associated with single hexagonal rings (arrows). Asterisks indicate nuclei. Scale bars represent 10 μm.

A1.3). In WT cellularizing embryos, normal microtubule arrays are observed at the restrictive temperature (Figure A1.3). In addition, centrosome morphology is abnormal in *fs(1)ts319* embryos at the restrictive temperature. In cellularizing wild type embryos, pairs of centrosomes are evenly spaced above individual nuclei within hexagonal actin cleavage furrows. The centrosomes are normally discrete structures as indicated by the localization of the centrosomal protein, Centrosomin (CNN), in fixed cellularizing embryos (Figure A1.3). In *fs(1)ts319* embryos cellularizing at the restrictive temperature, the centrosomes are often fragmented and not evenly spaced with respect to the actin rings (Figure A1.3). Furthermore, the live analysis of *fs(1)ts319* embryos cellularizing at the restrictive temperature shows that nuclei increase in volume, fail to elongate, and the majority remain attached to the cortex. The nuclei that no longer remain at the cortex appear to be ripped off the surface by the dramatic cytoplasmic movements rather than falling in as is seen when actin is depolymerized (Edgar *et al*. 1987). These observations are consistent with a microtubule-based rather than an actin-based defect affecting cellularization in *fs(1)ts319* embryos.

### A1.2.5 *fs(1)ts319* embryos display ts defects in endoplasmic reticulum morphology

Given the observed microtubule and furrow formation defects in *fs(1)ts319* cellularizing embryos, I assessed the morphology of various endomembrane compartments (RE, Golgi, and ER) in *fs(1)ts319* embryos. Vesicles trafficked through the RE are thought to be involved in membrane addition and recruitment of actin to cleavage furrows during cellularization (Pelissier *et al*. 2003; Riggs *et al*. 2003). The localization patterns of Rab11 and Nuclear Fallout (NUF), two proteins that localize to the RE during cellularization, are relatively normal in *fs(1)ts319* at the restrictive temperature (data not shown). During cellularization, Golgi bodies are normally observed as punctate structures dispersed in the basal cytoplasm that tend to undergo

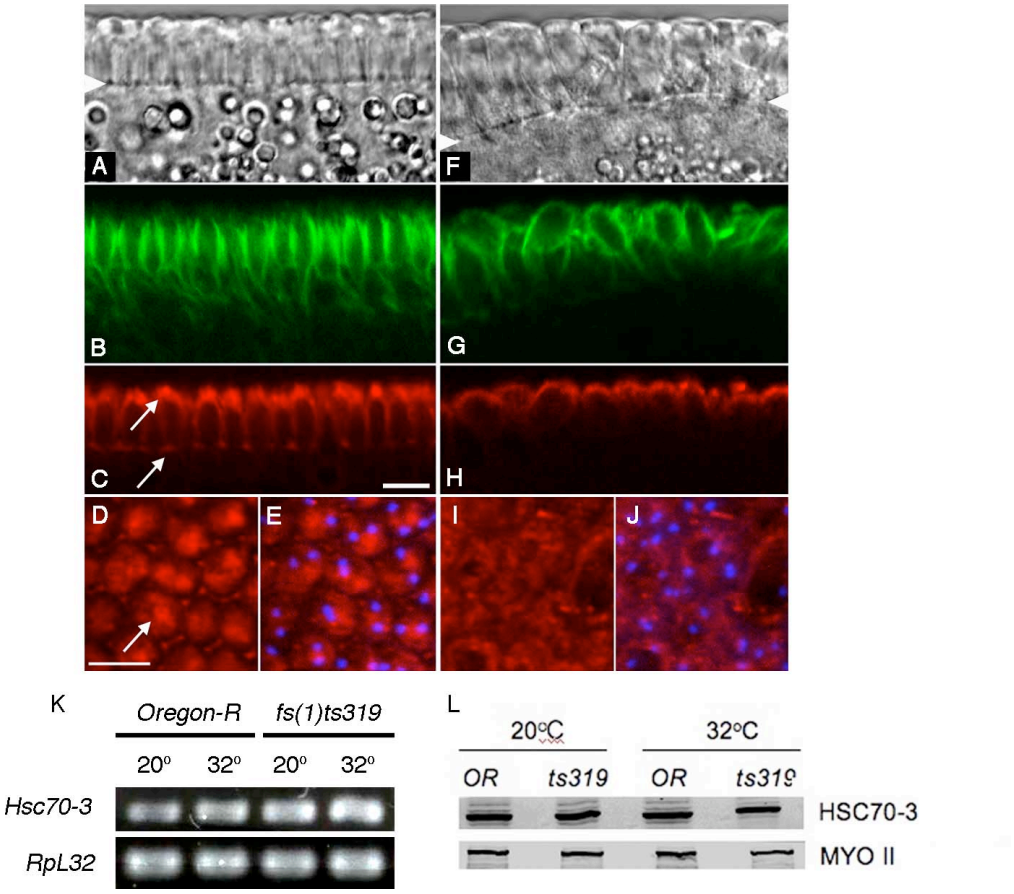


**Figure A1.4 ER morphology is disrupted in *fs(1)ts319* mutant embryos at the restrictive temperature**

IF analysis of WT (A-E) and *fs(1)ts319* (F-J) cellularizing embryos fixed at 32°C shows failure of the lumenal ER chaperone HSC70-3 to accumulate normally (arrows) in mutant embryos in sagittal (A-C, F-H) and surface projections through the apical cytoplasm (D-E, I-J). Centrosome pairs indicate location of individual nuclei relative to ER in merged image (E and J). Scale bars represent 10 μm. (K) Quantification of *Hsc70-3* and *RpL32* (control) mRNA levels by RT-PCR from total RNA extracted from WT and *fs(1)ts319* embryos subjected to the permissive (20°C) or restrictive (32°C) temperature during cellularization.

microtubule-based apical movement during the fast phase (Papoulas *et al*. 2005). Although fixed *fs(1)ts319* embryos cellularizing at the restrictive temperature have relatively normal Golgi morphology, their distribution between the apical and basal cytoplasm in late cellularizing embryos is abnormal. Less LVA-associated Golgi are observed in the apical cytoplasm of *fs(1)ts319* than in WT under the same conditions (Figure A1.4). The possible disruption of Golgi bodies to undergo apical movement in the mutant embryos may be due to the disruptions seen in the microtubule cytoskeleton. Finally, I assessed the morphology of the ER in *fs(1)ts319* cellularizing embryos at the restrictive temperature. The lumenal ER chaperone, Heat shock protein cognate 3 (HSC70-3), is normally concentrated at the apical perinuclear region with some localization extending to the ingressing furrow front of late cellularizing WT embryos. In *fs(1)ts319* embryos, HSC70-3 localization is more diffuse in the apical perinuclear region than WT and fails to extend to the furrow front as in WT (Figure A1.4). To ensure that the effect I observed on HSC70-3 localization was not due to misexpression of the protein in the mutant, I also assessed *Hsc70-3* mRNA and HSC70-3 protein levels in WT and *fs(1)ts319* embryos at the permissive and restrictive temperatures and found that abundance of mRNA and protein is not affected in the mutant (Figure A1.4). Together these observations suggest that ER morphology is disrupted in *fs(1)ts319* cellularizing embryos at the restrictive temperature.

### A1.2.6 *fs(1)ts319* embryos display ts defects de novo secretion during cellularization

Next, I examined *de novo* secretion in *fs(1)ts319* mutant embryos. *Neurotactin* (*Nrt*) is expressed zygotically during the syncytial stages, and Nrt protein accumulates almost exclusively in the plasma membrane in late cellularizing WT embryos (Lecuit and Wieschaus 2000). Surprisingly, apparent levels of Nrt protein are significantly reduced as detected by IF in *fs(1)ts319* late cellularizing embryos at the

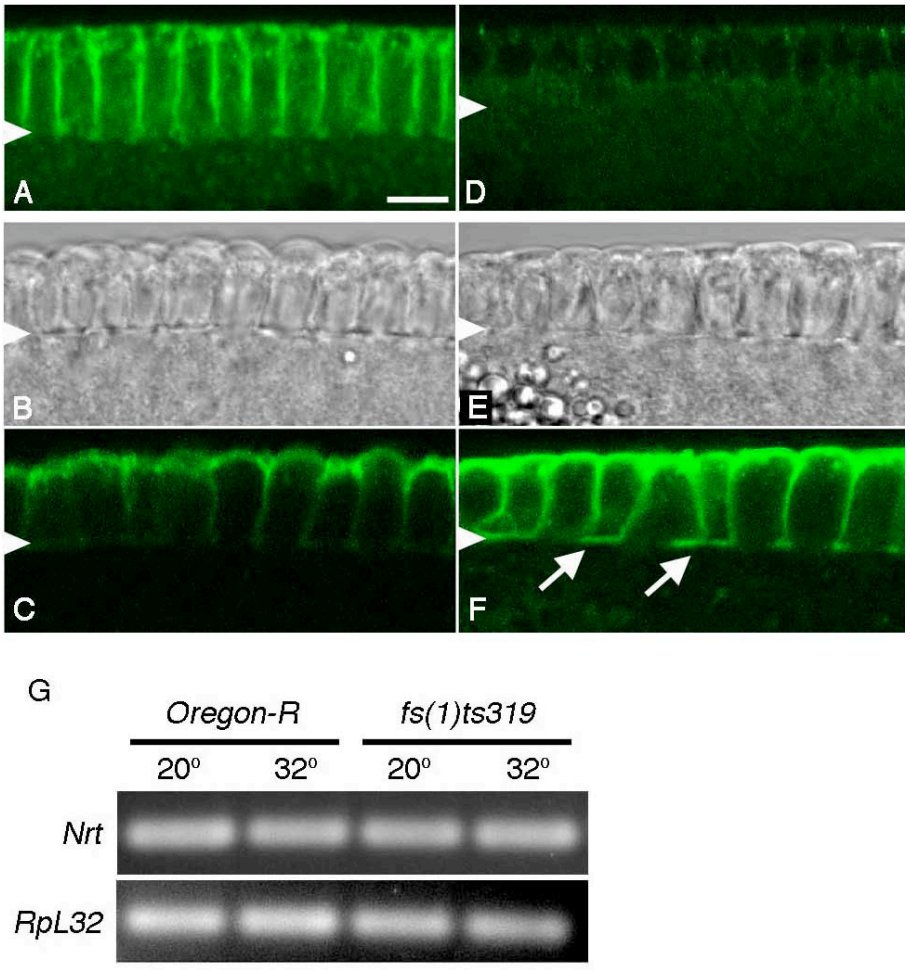


**Figure A1.5 De novo secretion of Neurotactin protein is disrupted in *fs(1)ts319* mutant embryos at the restrictive temperature**

IF analysis of WT (A) and *fs(1)ts319* (D) cellularizing embryos fixed at 32°C show a failure of Neurotactin protein to accumulate along the furrows in mutant embryos. WT (B-C) and *fs(1)ts319* (E-F) embryos stained with con-A (C and F) and imaged by DIC (B and E) show plasma membrane accumulates at furrows. Arrows indicate extent of con-A staining. Arrowheads indicate furrow front position. Scale bar represents 10 μm. (G) Quantification of *Nrt* and *RpL32* (control) mRNA levels by RT-PCR of total RNA extracted from WT and *fs(1)ts319* embryos subjected to the permissive (20°C) or restrictive (32°C) temperature during cellularization.

restrictive temperature (Figure A1.5). To assess if the *Nrt* gene is properly activated in *fs(1)ts319* embryos, I performed semi-quantitative reverse transcription polymerase chain reaction (RT-PCR) experiments. The results indicate that *Nrt* mRNA is present in *fs(1)ts319* embryos at levels comparable to WT (Figure A1.5). In addition, the onset of expression of a cytoplasmic zygotically expressed protein, Slow as molasses (Slam) (Lecuit *et al*. 2002), appears normal in *fs(1)ts319* embryos at the restrictive temperature, suggesting that the absence of NRT is not due to defects in the developmental timing of zygotic gene expression. These observations suggest that Nrt protein is not expressed at the same level in *fs(1)ts319* embryos as in WT embryos, and the absence of Nrt protein accumulation may be due to disruptions in cotranslational translocation of NRT into the ER. To further explore the apparent absence of NRT, I performed a quantitative immunoblot analysis of whole embryo extracts prepared from WT and *fs(1)ts319* embryos. I used antibodies against known secreted transmembrane proteins to determine if their steady-state levels are affected in mutant embryos. If the primary effect is in the cotranslational translocation of secreted proteins, I expected maternally loaded proteins localized to the plasma membrane (eg. Toll) to be expressed at normal levels in *fs(1)ts319* compared to WT embryos. Alternatively, plasma membrane proteins translated *de novo* during cellularization such as NRT would be in lower abundance in *fs(1)ts319* compared to WT embryos. My observations are consistent with these expectations and corroborate the IF in fixed embryos. I detected lower levels of NRT in *fs(1)ts319* compared to WT extracts and comparable levels of Toll in *fs(1)ts319* and WT extracts at the restrictive temperature (Figure A1.6). In addition, levels of E-Cadherin are also reduced in *fs(1)ts319* compared to WT extracts at the restrictive temperature (Figure A1.6). E-Cadherin, encoded by *shotgun* (*shg*), is a transmembrane protein that localizes to adherens junctions. It is maternally loaded, but zygotic expression is required during

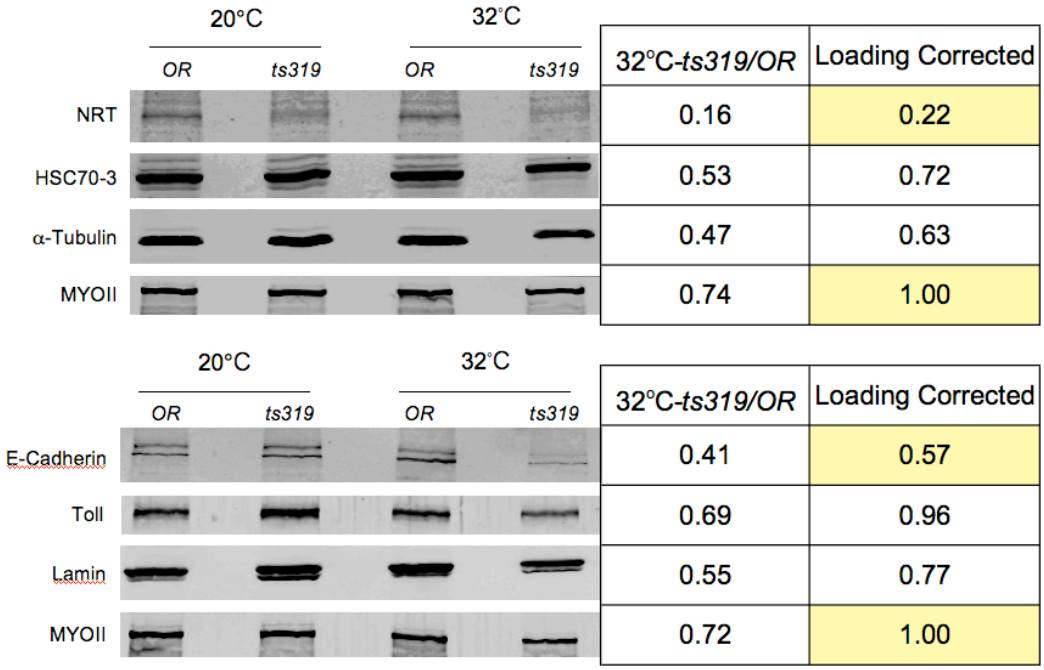


| | 32°C-*ts319/OR* | Loading Corrected |
|---|---|---|
| NRT | 0.16 | 0.22 |
| HSC70-3 | 0.53 | 0.72 |
| α-Tubulin | 0.47 | 0.63 |
| MYOII | 0.74 | 1.00 |

| | 32°C-*ts319/OR* | Loading Corrected |
|---|---|---|
| E-Cadherin | 0.41 | 0.57 |
| Toll | 0.69 | 0.96 |
| Lamin | 0.55 | 0.77 |
| MYOII | 0.72 | 1.00 |

**Figure A1.6 NRT and E-cadherin expression are affected in *fs(1)ts319* embryos at the restrictive temperature**

Quantitative protein blots of WT (*OR*) and *fs(1)ts319* extracts prepared from embryos at the permissive (20°C) and restrictive (32°C) temperatures as indicated at top. Protein probed for indicated to the left. Ratio of signal intensity indicated in first column and ratio corrected for loading errors by normalizing to MYOII signal indicated in second column.

cellularization (Uemura *et al*. 1996). Taken together, these observations suggest that the primary defect in *fs(1)ts319* is in the regulation of secreted protein synthesis or trafficking. It is known that *Nrt* is not required for cleavage furrow formation (Speicher *et al*. 1998), so it is likely that the cellularization phenotype in *fs(1)ts319* results from the misexpression of one or more other secreted proteins. Although I have not ruled out that the disruption of the microtubule cytoskeleton is the primary defect, it has been shown that depolymerization of microtubules during cellularization does not significantly disrupt ER morphology based on HSC70-3 localization and causes NRT to accumulate in punctate structures in the basal cytoplasm (Lecuit and Wieschaus 2000). Therefore, if the primary defect were in the microtubule cytoskeleton, I would expect NRT to be detectable but mislocalized and the ER morphology to be normal. However, it is certainly possible that the gene affected in *fs(1)ts319* has roles in multiple pathways.

### A1.2.7 Genetic complementation tests of cellularization-defective mutations

Genetic complementation tests were performed between four of the mutants and a Bloomington X-chromosome deficiency kit covering approximately 85% of the X chromosome. *fs(1)148* was previously mapped to the gene *small bristles*, which encodes the Drosophila homolog of a human mRNA export factor, NXF1/TAP (Korey *et al*. 2001), and was confirmed by non-complementation with a deficiency chromosome that removes the *sbr* gene (TableA1.3). In addition, I confirmed the presence of the T to A mutation at nucleotide 461 of the *sbr* gene in *fs(1)ts148* flies by sequence analysis, which is results in the amino acid change valine154 to glutamic acid (V154E) predicted to disrupt the RNA binding domain of SBR (Korey *et al*. 2001; Wilkie *et al*. 2001). It is likely that at least one or more mRNAs that are required to mediate the events of cellularization are blocked from being exported out the nucleus in $sbr^{ts148}$ mutants, resulting in the cellularization phenotype at the restrictive temperature.

| Mutant | Location | Non-complementing Df & Complementing Dp | Complementing Df & Non-complementing Dp |
|---|---|---|---|
| *fs(1)ts448* | 18E-F | *Df(1)HF396* | *Df(1)JA27, Df(1) Exel6253, Df(1)mal, Dp(1;Y)mal106* |
| *fs(1)ts567* | 10C1-5 | *Df(1)v-N48, Df(1)DA622, Dp(1;2)v+65b* | *Df(1)RA37, Df(1)GA112, Df(1)m13, Df(1)HA85* |
| *fs(1)ts148/ small bristles** | 9F4 | *Df(1)C52* | |
| *fs(1)ts242* | 4F4-8 | *Df(1)JC70, Df(1)HC244, Df(1)ovo44, Df(1)BA2-8* | *Df(1)rb14, Df(1)Exel6290, Df(1)Exel6235* |
| *fs(1)319* | 10A6 | *Df(1)v-N48, Df(1)RA37, Df(1)v-L3, Dp(1;2)v+63i, Dp(1;Y)y+v+#3* | *Df(1)v-L1, Df(1)KA7, Dp(1;2)v+65b* |

**Table A1.3 Temperature-sensitive mutations map to specific cytological loci on the X-chromosome**

Howard Wang was responsible for coordinating the genetic mapping of *fs(1)448, fs(1)567, and fs(1)242*, but the mapping was a group effort of many former and current students in the Sisson lab (including Howard Wang, Poornima Parameswaran, Jessica Cobarrubia, and Travis White). These mutants were mapped to regions on the X-chromosome using deficiency stocks and the zygotic lethality assay described in A3.5.2 (Table A1.3). We made some attempts to identify the *fs(1)ts242* mutation by sequencing candidate genes but were unable to identify a mutation (data not shown). Otherwise there have not been any other efforts to identify the genes affect in these three mutants.

### A1.2.8 Efforts to identify the gene disrupted in *fs(1)ts319*

*fs(1)ts319* was genetically mapped using the maternal sterility assay described in A3.5.2, and I was able to map the mutation to a region of about 30 kilobases in the cytological position 10A6 [approximate recombination map unit (m.u.) 33.5]. I later meiotically mapped the mutation using the cellularization assay to a region between *vermillion* (m.u. 33.0) and *forked* (m.u. 56.7), consistent with the original mapping data. The candidate gene region contains four genes that could possible be affected: *CG11122,* a novel protein with putative nucleic acid binding domain, *Rpt3,* a subunit of 19S regulatory particle of 26S proteosome, *Gtp-bp,* the signal recognition particle receptor α (SRPRα) subunit, and *Klp10A,* a minus-end microtubule depolymerizing motor. A lethal P element residing in the *Rpt3* gene complemented the maternal sterility of *fs(1)ts319,* suggesting that *Rpt3* is not affected in *fs(1)ts319*. I sequenced 77% of 28785 base pair region from genomic DNA and did not identify any missense or nonsense mutations in the protein coding regions of the four candidate genes (see A3.5.6 for a summary of sequence data). Conventional conditional mutations often do not affect the

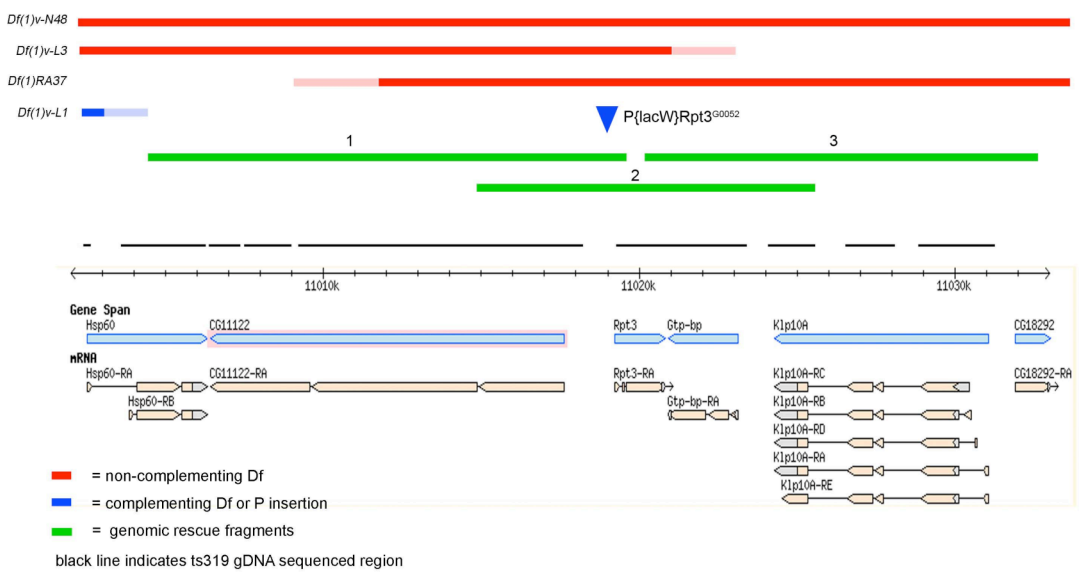


**Figure A1.7 Map for proposed *fs(1)ts319* gene region**

expression of a gene, but rather affect the function of the gene product at the restrictive condition. Despite this, there is a possibility that the mutated region in the *fs(1)ts319* resides outside of the protein coding sequence and affects the expression level of a gene in the candidate gene region at both the permissive and the restrictive temperatures, but the aberrant expression level only affects function of the gene product at the restrictive temperature. To test this idea, mRNA levels were measured using qRT-PCR with material from WT and *fs(1)ts319* cellularizing embryos at the restrictive temperatures. I did not detect a significant change in mRNA abundance for the four candidate genes in the mutant embryos suggesting that mRNA expression is not affected (Figure A1.8). In addition, protein levels could be measured by quantitative immunoblot analysis. Antibodies against KLP10A and GTP-BP have been described and could potentially be used for this analysis (Fredieu and Mahowald 1993; Rogers *et al*. 2004).

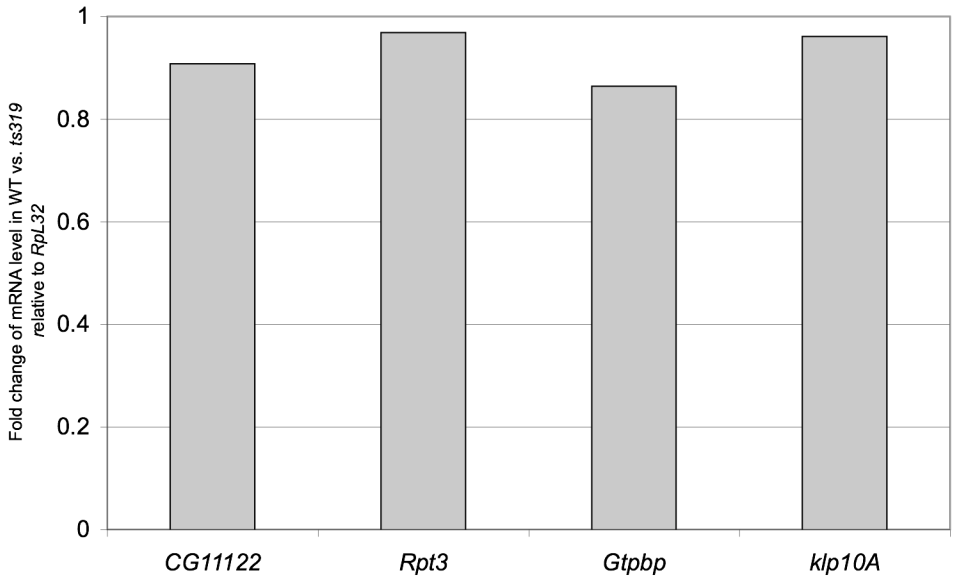


**Figure A1.8 qRT-PCR analysis of candidate gene expression in WT and *fs(1)ts319* embryos**

Histogram shows fold change of the indicated mRNAs relative to *RpL32* in WT vs. *fs(1)ts319* embryos cellularizing at the restrictive temperature.

Another approach to confirm the genetic position of the mutation is to attempt to rescue the mutant phenotype by introducing a WT copy of the gene region in the *fs(1)ts319* mutant. I generated germ-line transformants containing independent insertions of genomic rescue fragment 2 (*pinfr2*) using P element mediated transformation (Figure A1.7). These stocks can be used to test for rescue of the cellularization phenotype at the restrictive temperature.

## A1.3 DISCUSSION

In this study, I screened a collection of temperature-sensitive zygotic lethal and maternal sterile mutants to identify mutations that affect cellularization at the restrictive temperature. Five mutant stocks were found to display cellularization defects at the restrictive temperature. *fs(1)ts148* was previously shown to be an allele of *sbr*, the gene that encodes the mRNA export factor, NXF1/TAP (Korey *et al*. 2001; Wilkie *et al*. 2001). The identification of a cellularization phenotype led us to use $sbr^{ts148}$ in other studies as a tool to affect the accumulation of zygotic transcripts in the cytoplasm during the MBT (Figure 2.5). Embryos from *fs(1)ts448* and *fs(1)ts567* have relatively normal morphology during cellularization except that the furrowing rates are significantly perturbed (Table A1.1). This more moderate cellularization phenotype is likely due to complete loss-of-function of the gene. Embryos from hemizygous females (*fs(1)ts/Df*), which completely lack one copy of the gene, do not have a more severe furrowing phenotype (Table A1.1). The genes disrupted in these mutants could have interesting, specific roles in furrow formation. Embryos from *fs(1)ts242* and *fs(1)ts319* females display severe cellularization defects, which make the primary affect difficult to identify. Embryos from *fs(1)ts242/Df* do not display a more severe cellularization defect, yet embryos from *fs(1)ts319 /Df* had earlier defects even at the permissive temperature (Table A1.1). These observations suggest that *fs(1)ts242* is a complete loss-of-function mutant and that *fs(1)ts319* is a partial loss-of-function mutant, suggesting that the gene perturbed in *fs(1)ts319* is essential for other processes. I chose to focus on *fs(1)ts319* based on the cellularization phenotype and strong maternal sterility.

IF of fixed *fs(1)ts319* embryos revealed defects in the MT cytoskeleton, ER morphology, and most strikingly, secreted protein accumulation. The mutation was

genetically mapped to a region containing 4 candidate genes. Despite my efforts, I could not identify the affected gene in *fs(1)ts319*. Regardless, based on the observed phenotype affecting the secretion of secreted proteins, *Gtp-bp* is an interesting candidate. GTP-BP is a subunit of the receptor for Signal Recognition Particle (SRP). The SRP binds to the signal sequence of nascent peptides of integral membrane proteins destined for the ER and targets them to the SPR receptor (SR) (Hegde and Kang 2008). SR is composed of two subunits, alpha and beta, and *Drosophila Gtp-bp* encodes the alpha subunit. It is tempting to speculate how affecting the function of the SR could result in the phenotypes we observe in *fs(1)ts319* embryos. It has been shown in budding yeast that the SRP pathway is important for maintaining the reticular structure of the ER. In a screen for mutations that affect ER morphology, mutations in both the alpha and beta subunits of SR were found to have effects on ER morphology (Prinz *et al*. 2000). These observations in yeast could explain the ER morphology defect observed in *fs(1)ts319* embryos. As mentioned above, the disruption of MTs is likely a secondary effect and not the cause of the abnormal ER morphology. It is unclear if disruption of the ER could result in defects in MT morphology and remains a possibility.

Unfortunately, without the identification of the mutation present in *fs(1)ts319* or rescue data confirming the affected gene, we are left with an interesting phenotype and no molecular mechanism for its cause. I have great hopes that the next person who tackles this project will identify the affected gene, adding more to our understanding of the mechanisms that control cleavage furrow formation in the *Drosophila* embryo.

# Appendix 2: Miscellaneous experiments

## A2.1 Analysis of early mitotic waves in *dFMR1-* embryos

I have described in detail the cleavage furrow formation phenotype observed in *dfmr1-* embryos, but as mentioned in Chapter 2, I also found a modest defect in the duration and pattern of nuclear cycles 12 and 13. Here, I will describe the experiments I performed to assess these early divisions.

The early mitotic divisions in the *Drosophila* embryo are thought to generally occur synchronously with highly reproducible timing. In reality, the mitosis of nuclear cycles 10-13 occur metasynchronously, wherein entrance into and exit out of mitosis occurs in a wave-like pattern (Foe and Alberts 1983). This pattern of mitosis can be observed by examining embryos expressing GFP-tagged proteins that reveal nuclear or MT dyanamics, embryos that have been injected with fluorescently labeled proteins, or embryos that have been fixed and stained. The site from where the wave originates is variable, but the rate of the wave at any given cycle is highly reproducible. It is unclear what regulates these mitotic waves. In an effort to assess the early mitotic divisions, I injected fluorescently labeled tubulin into WT and *dfmr1-* embryos.

Shortly following injection of rhodamine tubulin (Rhod-TUB) into embryos during interphase of NC10, the labeled tubulin is incorporated into MTs. This incorporation is especially apparent during mitosis, when the mitotic spindles can be imaged along the surface of the embryo (Figure A2.1). I injected Rhod-TUB into WT and *dfmr1-* embryos and imaged them as they progressed through NC10-13 on a Leica SP2-LCS confocal microscope. I analyzed the movies by first measuring the time points from three locations at distinct locations for each embryo for each transition from interphase to mitosis (Figure A2.1). This analysis showed that interphase of NC12 and

13 is slightly longer in *dfmr1-* compared to WT embryos (Figure A2.2). Furthermore, when I quantified the rate of the mitotic waves, I found that that the rate in *dfmr1-* embryos is significantly slower that in WT (Figure A2.3). In addition to abnormal mitotic wave delays, I also observed occasional spindle defects, although these defects do not affect overall nuclear densities (Figure A2.4).

Together these observations are consistent with dFMRP having a role in controlling the mitotic waves of nuclear cycles 12 and 13. As I mentioned previously, it is unclear what controls these waves and if the regulation originates from nuclear or cytoplasmic factors. As described in Chapter 4, we have discovered that dFMRP controls the translational regulation of *CycB* during the MBT, and as I discussed in section 1.3.2, CycB mRNA and protein are thought to be spatially as well as temporally regulated in order to control cell cycle progression. Perhaps the translational regulation of *CycB* by dFMRP is also important for controlling the rates of the mitotic waves. Future work examining the specific mechanism of translational regulation of *CycB* by dFMRP will need to be done to address this outstanding question.

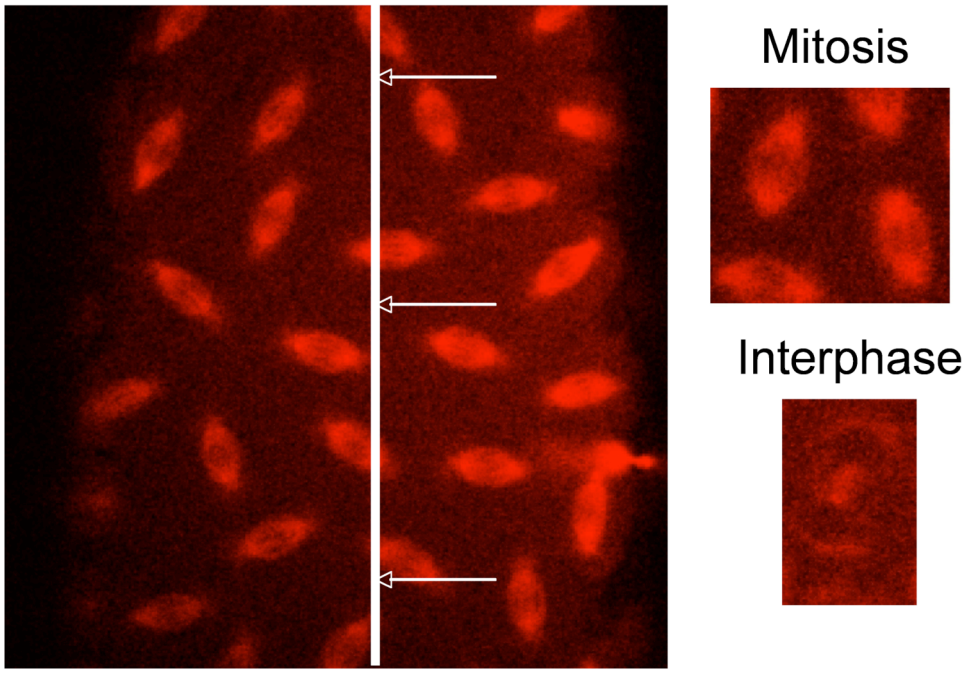


**Figure A2.1 Injected rhodamine tubulin incorporates into MTs in early embryos**

Still from a movie of a WT embryo injected with 10 mg/ml Rhod-TUB (Cytoskeleton, Inc.) during mitosis of NC10. Bleb on lower right side indicates site of injection. White line and three arrows indicate location of spindles scored for timing of transition of cycles. High magnification panels to right show examples of embryos in mitosis and interphase.

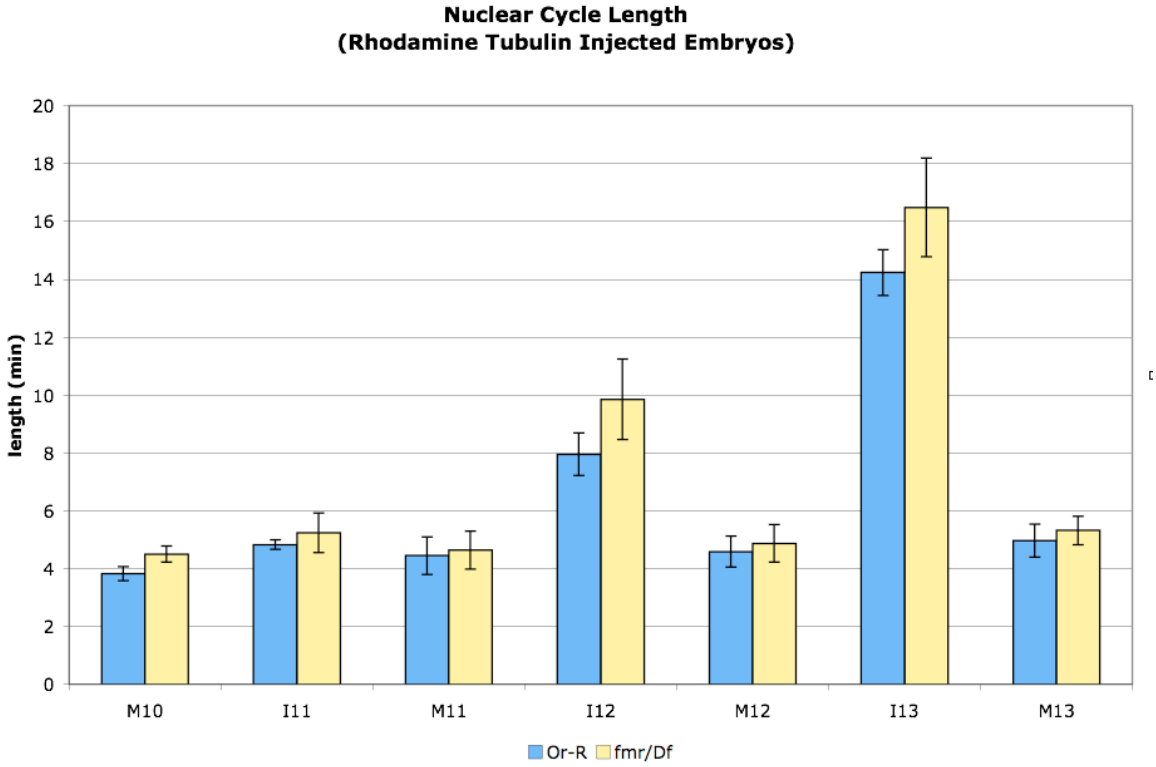


**Figure A2.2 Quantification of nuclear cycle length in WT and *dfmr1-* embryos**

Histogram shows the length in minutes of each mitosis and interphase of the cycles shown for WT (blue) and *dfmr1-* (yellow) embryos injected with Rhod-TUB during interphase of NC10. Embryos were injected and imaged in a temperature controlled perfusion incubator at 25°C. Number of movies quantified for each stage was as follows (M10=2, I11=4, M11=6, I12=6, M12=6, I13=6, M13=6). Bars indicate standard error.

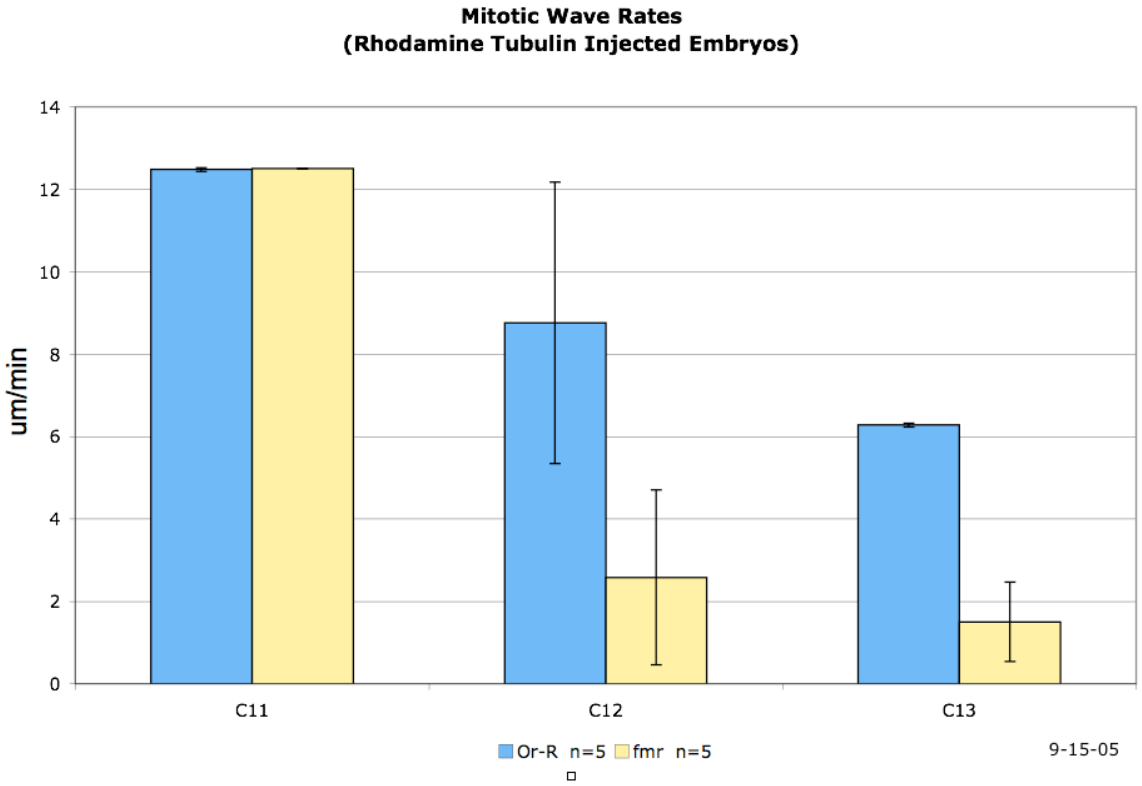


**Figure A2.3 Quantification of mitotic wave rates show defects in *dfmr1-* embryos**

Histogram shows rates of mitotic waves in WT (blue) and *dfmr1-* (yellow) embryos injected with Rhod-TUB. Rate was quantified by measuring the time points the nuclei entered the cycle from the three locations of the embryo as well as distance between the locations as described in the text. Embryos were injected and imaged in a temperature controlled perfusion incubator at 25°C. Five movies of each genotype were quantified. Bars indicate standard error.

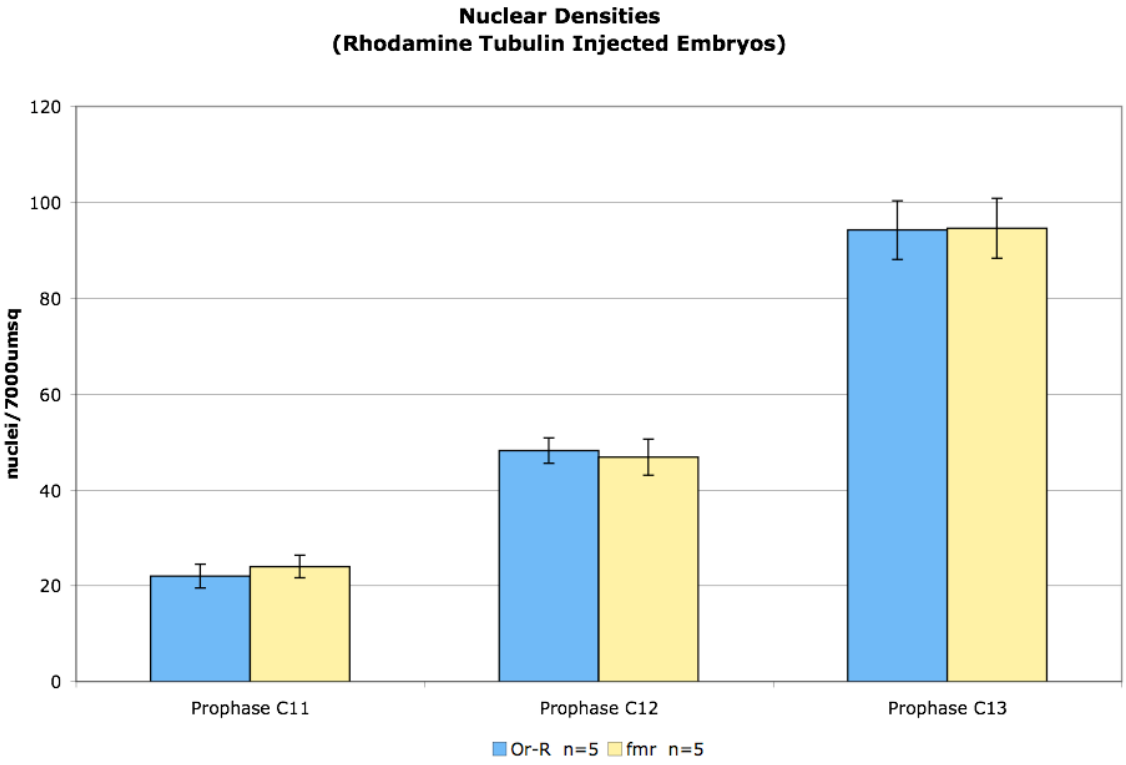


**Figure A2.4 Surface nuclear density of *dmfr1-* embryos is comparable to WT**

Histogram shows nuclear densities of WT (blue) and *dfmr1-* (yellow) embryos injected with Rhod-TUB during prophase of NC 11-13. The total number of nuclei within a 7000 $\mu m^2$ area were counted using the Leica confocal system software. Five embryos from each genotype were quantified. Bars indicate standard error.

## A2.2 STABLE ISOTOPE METABOLIC LABELING OF *dFMR1-* EMBRYOS

In collaboration with John Yates at Scripps, John Sisson initiated an additional proteomic screen to identify targets of dFMRP regulation using stable isotope metabolic labeling. This method has been successfully used in yeast and flies to label all proteins *in vivo* (Washburn *et al*. 2002; Krijgsveld *et al*. 2003). Proteins can be metabolically labeled with either $^{14}N$ or $^{15}N$ and the relative abundance of an individual protein can be determined by mass spectrometry. We decided to use this method to compare the proteomes of control and *dfmr1-* cleavage stage embryos, and I have established the protocol to be used in the Sisson lab.

To label the proteins in *Drosophila* embryos, adult flies were fed $^{14}N$- or $^{15}N$-labeled yeast. Embryos that were morphologically stage matched were collected, quickly frozen, and used to make extracts. These extracts were then sent to the Yates lab where the two extracts were combined and subjected to MudPIT mass spectrometry. I was able to complete one round of labeling and protein identification in collaboration with Lujian Liao, a post-doc in the Yates lab. At least two more rounds of labeling and mass spectrometry will be required to detect significant changes in the *dfmr1-* embryos. Here, I will describe the procedure for these experiments in detail, which I adapted from Washburn *et al*. 2002; Krijgsveld *et al*. 2003.

Prepare 1L cultures of *S. cerevisiae* Type II strain grown to high OD ~5.0 in Yeast $^{14}N$ or $^{15}N$ Minimal Media [1.7 g/L yeast nitrogen base w/o amino acids w/o ammonium sulfate (Difco), 20.0 g/L dextrose (Difco), 5.0 g/L ammonium sulfate ($^{14}N$) (Sigma) OR ammonium sulfate ($^{15}N$) (Cambridge Isotope Laboratories, Inc)] at 30°C for ~24-36 hours in 2.5L high yield flasks (Thomson Instruments CO) with AirOTop Seal - start from 5ml overnight cultures. This strategy was shown to label close to 98% of total

protein (John Yates, email correspondence). Pellet yeast in 500ml dry-spin bottles in SLA-3000 at 700rpm for 15min. Prepare agar mix for condos (Nalgene #2119-1000) and collection caps (35 x 10 mm Petri dish) [15 g/L granulated agar, 10% (w/v) sucrose, 0.03% (v/v) propionic acid, 0.2% (v/v), phosphoric acid, 0.1 mg/ml ampicillin] by pouring ~100 ml into each condo and ~3 ml into each collection cap and allowing to cool overnight. Cover half of agar with one layer of sterile cotton. Pipette ~30ml fly food mix [10% (w/v) sucrose, 0.03% (v/v), propionic acid, 0.2% (v/v) phosphoric acid, 0.1 mg/ml ampicillin] on cotton (add enough so cotton is almost saturated). Smear 1/3$^{rd}$ of pelleted yeast on agar.

Collect 0-24 hr WT and mutant embryos, remove agar from caps and place on agar in condo, and allow to develop at 25°C in humidified incubator. Labeling must be done in reciprocal, so I always set up two experiments in parallel as follows:

experiment 1 = $w^{1118}$ and *Df(3R)exel6265/TM3* embryos on unlabeled yeast

*fmr1*$^{3}$*/TM3* and *Df(3R)exel6265/TM3* embryos on $^{15}$N-labeled yeast

experiment 2 = *fmr1*$^{3}$*/TM3* and *Df(3R)exel6265/TM3* embryos on unlabeled yeast

$w^{1118}$ and *Df(3R)exel6265/TM3* embryos on $^{15}$N-labeled yeast

Transfer ~5 ml $^{15}$N-labeled or unlabeled adult flies to collection cages and repeat two additional times. During final round collect virgin females from *fmr1*$^{3}$*/TM3* and $w^{1118}$ and mate to *Df/TM3* in collection bottles, and repeat. Finally, transfer ~5 ml $^{15}$N-labeled or unlabeled adult flies to collection cages and hand sort mid-cellularizing embryos from 2-3 hr collections. The following procedure was adapted from Gong et al., Development 2004, Minden et al., Drosophila Protocols 2000, and email correspondence with Jon Minden (Carnegie Mellon University).

Prepare two 15 ml falcon tubes each with 10 ml ethanol (95%), one tube on ice and the other half way inserted into dry ice/EtOH bath. Dechorionate embryos in 50%

bleach, rinse with embryo wash buffer (EWB; 0.7% NaCl, 0.03% Triton X-100) and transfer to small petri dish or dissecting dish with EWB and sweep embryos into center of dish with gentle swirling. Examine embryos under dissecting stereomicroscope with transmitted-light illumination and form a pile of appropriate staged embryos by gently pushing embryos with stainless steel probe. Remove the desired embryos in a minimal volume of EWB with pasteur pipette and drop into the iced ethanol. As the embryos settle to the bottom, the EWB is diluted. Replace this ethanol every once in a while to keep the fraction of EWB low. Typically, transfer the embryos in less than 0.2 ml and change the ethanol every 1 ml of EWB added. Remove the settle embryos from the ice-cold ethanol and drop into the ethanol on dry ice, again using a minimal volume. The reason for only having the tube half way into the dry ice is to prevent any of the carry over water from freezing. Embryos can be stock-piled in the iced or the dry-iced ethanol. Once the embryos are frozen, do not let them thaw until ready to prepare them for gel electrophoresis. For long-term storage, transfer the embryos out of the falcon tube into an eppendorf tube, pre-cooled on dry ice. This can be store at -80°C or shipped on dry ice.

I made whole embryo lysates from each set of embryos by homogenizing embryos in 1.5 ml tubes with a plastic kontes pestle in 4X volumes of metabolic labeling extraction buffer [MLEB; 25mM HEPES pH 7.5 (with KOH), 100mM KCl, 500mM EDTA pH 8.0, 0.05% Triton X-100, protease inhibitor cocktail at 1:1000]. Concentration of each sample was quantified using Bradford assay, frozen in liquid N2 and stored at -80°C. Samples were then shipped to the Yates lab for mass spec analysis.

# Appendix 3: Materials and Methods

## A3.1 FLY HUSBANDRY

All fly stocks were grown on standard corn meal molasses and kept in incubators at 20°C, 25°C or 29°C as indicated. Genetic crosses were set up using standard methods. Fly food was prepared by John Loera, a laboratory research assistant at the University of Texas at Austin, using the following recipe: 76 g/L corn meal , 76 mL/L Karo syrup, 18 g/L brewer's yeast, 9 g/L agar, 1 g/L nipagin (mold inhibitor), 111 mL/L malt extract , 5 m/L propionic acid , and 5 mL/L 100% ethanol.

## A3.2 CHAPTER 2

### A3.2.1 Fly stocks and genetics

*Oregon-R* (WT) and $w^{1118}$; *Df(3R)Exel6265/TM6B Tb*, and *Df(3L)iro-2*, $Sb^{sbd-2}$/*TM3*, $Sb^{1}$ (Bloomington Stock Center), $tral^{2}$/*TM6B* and $tral^{3}$/*TM6B* (Exelixis collection), $w^{1118}$; $fmr1^{3}$/*TM6C*, *Tb*, *Sb*, and $w^{1118}$; *P(WTfmr1)*; $fmr1^{3}$/*TM6C*, *Tb*, *Sb* (T. Jongens, University of Pennsylvania), and *yw*, $sbr^{ts148}$ (W. Sullivan, University of California, and I. Davis, University of Edinburgh) were used. We believe there are additional mutations on the chromosome containing the $dfmr1^{3}$ allele. In our hands, homozygous $dfmr1^{3}$ females have a very severe maternal sterility defect, but $dfmr1^{3}$/*Df* have a more moderate maternal sterility defect.

### A3.2.2 Maternal and paternal fertility

Female and male fertility was assessed by measuring egg hatch percentages using the following procedure. ~12-15 virgin females were collected in a single day and

allowed to age 48 hours in yeasted vial. The absolute number of females was not important, but the same number must be used among genotypes being compared. The females were then mated to 4-5 males for 48 hr in yeasted vial. The adult flies were then transferred to an egg laying cluster (14 x10 ml plastic vials glued together with air holes drilled into bottom of tubes), with each cross in a single tube. The cluster was placed on grape juice agar plates [3% granulated agar (w/v), 5.5% sucrose (w/v), 25% grape juice, 1.25% glacial acetic acid (v/v), and 2.5% ethanol (v/v)] with a small amount of wet yeast for each tube and placed in a humidified chamber at 25°C. Embryos were collected for 12 hr and allowed to age for 24 hr. The numbers of hatched (empty) and unhatched egg shells were counted. I found that the collection and age times varied with experiment, and so I adjust as needed so WT control laid about 100-200 eggs with 95-100% hatch percentage. Hatch Percentage = # empty shells / total # eggs laid

### A3.2.3 Live embryo imaging

Embryos were collected from WT or specified mutant females mated to WT males at 25°C. Embryos were hand dechorionated, lined up on heptane glue (mixture of heptane and doublestick tape) on glass slides, and covered in Halocarbon 700 oil. Live embryos were imaged in a microincubator (PDMI-2; Harvard Apparatus) at 25°C every 15 sec using a Leica SP2-LCS confocal microscope with differential interference contrast (DIC) optics. Movies were compressed to 5 frames per second using either the Leica system software or QuicktimePro.

### A3.2.4 Fixed embryo analysis

Embryo fixations and indirect immunofluorescence was performed as described in Sisson *et al*. 2000. Embryos were dechorionated in 50% bleach and rinsed in embryo wash buffer (EB; 0.7% NaCl, 0.03% Triton X-100). The embryos were fixed in 19%

formaldehyde/paraformaldehyde/3% methanol in 1X PBS (1.4 M NaCl, 0.02 M KCl, 0.1 M $Na_2HPO_4$, 0.02 M $KH_2PO_4$ pH 7.4) over heptane for 25-30 min with gentle agitation. After fixation embryos were affixed to double stick tape and covered with 1X PBTA (1X PBS, 1% BSA, 0.05% Triton X-100, 0.02% $NaN_3$). Detection of ME31B required 1× PBTA with 0.5% Triton X-100. For temperature-shift experiments, WT and *sbr*$^{ts148}$ embryos were kept at 20°C or shifted to 32°C for 25 min in 0.7% NaCl/0.03% Triton X-100 on a slide warmer and fixed as described above. The vitelline membranes were removed by hand using a 27g needle on a syringe by gently nudging embryos with needles. Before incubating devitellinized embryos with primary antibody they were blocked in 1XPBTA for 1 hr at room temperature with agitation on Nutator (TCS Scientific). For immunofluorescence detection, embryos were incubated in primary antibody dilution overnight at 4°C on Nutator, washed 4-6 times in 1X PBTA at room temp, incubated in secondary antibody dilution for 2 hours at room temp on Nutator, washed 4-6 times in 1X PBTA at room temp on rocker, rinsed once in 1X PBS and mounted in Vectashield (Vector Labs) (~35ul Vectashield for 22x22mm coverslip).

### A3.2.5 Colocalization analysis

The colocalization between dFMRP and other proteins was quantified as follows. Fixed WT embryos of the exact same stage of cellularization were prepared for IF by using antibodies against dFMRP and either TRAL, ME31B, dAGO2, or LVA and imaged by scanning confocal microscopy. Optical sections were collected through the apical or basal cytoplasm, and a minimum of five identically staged embryos were analyzed for each IF experiment. Leica confocal system software was used to identify punctate protein localization within two separate 16 $\mu m^2$ fields of view along the length of each embryo. Puncta were defined as discrete localization that fit within electronically drawn 0.75 μm diameter circles with a mean fluorescence intensity of ≥175. The normal range for the

mean fluorescence intensity of a 0.75 μm diameter circular area within a 16 $\mu m^2$ field of view was 80-225. Generally, 20-30 punctate structures were observed within a given 16 $\mu m^2$ field of view for each of the proteins of interest. Any two distinct puncta within the same field of view that overlapped by 50% or more were considered to colocalize. Overlap below 50% was not considered colocalization. As a control to quantify a baseline colocalization for each double IF experiment, we electronically flipped the dFMRP IF images with respect to their matched image for TRAL, ME31B, dAGO2, or LVA and calculated the extent of colocalization between distinct puncta as before. Statistical analysis of colocalization compared with control colocalization data sets was performed using a two-tailed Student's *t* test.

### A3.2.6 General biochemistry and protein immunoblot analysis

Except as noted, extract preparation, protease inhibitor mixture, and standard Protein immunoblotting procedures were performed according to Sisson *et al*. 2000. Adult flies were collected on ice, homogenized in SDS sample buffer lacking dye, and boiled for 10 min. Clarified extracts were analyzed by standard immunoblot analysis. For quantitative immunoblots, S14 supernatants were prepared (see below) from WT or *dfmr1*- embryos and processed by using the manufacturer's protocol for the Odyssey Infrared Imaging System (LI-COR Biosciences). Antibodies described in above and mouse monoclonal anti-humanP68 (MAD1; F. Fuller-Pace, University of Dundee, Dundee, Scotland) were used for immunoblotting.

### A3.2.7 Sucrose Density Gradients

Cellularizing embryos were collected, dechorionated in 50% bleach, flash frozen, and stored at −80°C for a few days, then glass dounce homogenized in 5 volumes of Polysome Gradient Buffer [PGB; 15 mM Tris, pH 7.5/100 mM KCl/10 mM $MgCl_2$/2 mM

DTT/200 μg/ml cycloheximide/50 units/ml rRNasin (Promega) and protease inhibitors] and centrifuged at 3,000 × *g* for 10 min. The postnuclear supernatant was centrifuged at 14,000 × *g* for 10 min and the resulting supernatant (S14) was quantified for protein and nucleic acid. Gradients (12 ml) of equal layers of 5%, 20%, 35%, and 50% sucrose in PGB were allowed to equilibrate during horizontal storage at 4°C for ≈1.5 hr and then were loaded with 1.2 mg of S14, centrifuged at 285,000 × *g* (max) for 2.5 h in a SW40 rotor, and fractions were collected through a UV flow cell monitoring $A_{254}$. All of fractions 10–22 and 20% of fractions 1–9 were precipitated in 75 μg/ml insulin with 10% trichloroacetic acid and resuspended in SDS/PAGE sample buffer for protein immunoblot analysis.

### A3.2.8 Immunoprecipitations (IPs)

Postnuclear supernatants were made from frozen embryos homogenized in $TKT_{100}$ buffer (10 mM Tris·HCl, pH 8.0/100 mM KCl/0.05% Triton X-100 with 1 mM DTT/50 units/ml rRNasin/protease inhibitors) and centrifuged at 10,000 × *g* for 10 min. The S10A was diluted to 1 mg/ml, placed on ice for 30 min, and centrifuged as before to make a working S10B. Anti-dFMRP (6A15; AbCam) and anti-FLAG (M2; Sigma) antibodies were coupled to protein G Sepharose 4B (Sigma), and anti-TRAL polyclonal serum was coupled to Affi-Prep Protein A Gel for 1 hr at room temperature (Bio-Rad). The latter also was BSA-coated as a control. IPs were carried out for 1 h at 4°C with 25 μl of anti-dFMRP/beads or anti-FLAG/beads and 0.25 mg of S10B or 15 μl of anti-TRAL/beads or BSA/beads and 0.1 mg of S10B, washed extensively in $TKT_{100}$ buffer, eluted with SDS/PAGE sample buffer at 90°C for 2 min, and analyzed by immunoblot analysis.

### A3.2.9 Quantitative reverse transcription PCR (qRT-PCR)

RNA was isolated by using TRIzol-LS reagent (Invitrogen) from fresh cellularizing embryos (derived from WT or *dfmr1* $^{-}$ females), IPs, and corresponding S10B. RNA was treated with RQ1 DNase (Promega) according to the manufacturer's protocol, followed by the addition of EGTA and heat treatment (65°C for 10 min) or phenol-chloroform extraction and ethanol precipitation. IPd RNA samples were reprecipitated with NaCl and ethanol before reverse transcription. Treated RNA (1 μg from embryos or 73 ng from IPs and S10B) was reverse transcribed by using oligo(dT) and the SuperScript II RNase-H-Reverse Transcriptase protocol (Invitrogen). Real-time PCR was performed by using a 7900HT Sequence Detector and Power SYBR PCR Master Mix [Applied Biosystems (ABI)]. Levels of specific mRNAs were determined by relative quantification with a standard curve and normalized to *RpL32* mRNA. Specificity was confirmed by dissociation curve analysis and agarose gel electrophoresis. Statistical analysis was based on a minimum of triplicate samples.

### A3.2.10 Antibodies

The following antibodies were used: DSHB mouse monoclonal Abs dFMRP 5A11 (1:10), Tubulin (1:250) and Futsch 22C10 (1:50), rabbit polyclonal antibodies Trailer Hitch [1:500; M. Snee and P. Macdonald (University of Texas)], ME31B [1:500; A. Nakamura (RIKEN Genomic Sciences Center)], dAGO2-90 [1:50; G. Hannon (Cold Springs Harbor Laboratory)], Lava Lamp (1:5,000), Myosin II [1:100; C. Field (Harvard Medical School)], and Anillin 4-11 1:500 [C. Field (Harvard Medical School)]. Primary antibodies were detected with species-specific secondary affinity-purified Alexa Fluor® antibodies (Molecular Probes, Invitrogen). RNase-treatment was done with 10 mg/ml RNase A (Sigma) in 1X PBS for 4 h at 37°C prior to incubation with primary antibodies.

All other fixed embryos were not RNase-treated. Rhodamine-Phallodin was used at 1:100 to detect F-actin (Cytoskeleton).

## A3.3 CHAPTER 3

### A3.3.1 Fly stocks and genetics

The following stocks were obtained from the Bloomington Stock Center:

*$w^{1118}$; TM3, Sb/CxD*

*$y^{1}w$; $RpS13^{1}$/CyO*

*$w^{1118}$; Df(3R)Exel6191 /TM6B, $Tb^{1}$ - cct1*

*$w^{1118}$; Df(3R)Exel6270 /TM6B, $Tb^{1}$ - cct3*

*$w^{1118}$; Df(2L)Exel6034 /CyO - cct4*

*$w^{67c23}$ P{w[+mC]=lacW}Tcp-1zeta[G0057]/FM7c - cct6*

*$w^{1118}$; Df(3R)Exel6150/TM6B, $Tb^{1}$ - cct7*

*$w^{1118}$; Df(2R)Exel6052 /CyO - scra*

For the proteomic screen, to limit variation in genetic background between control and mutant embryos, single flies from *w; $dfmr1^{3}$/TM6C, Tb, Sb* and *$w^{1118}$; Df(3R)Exel6265/TM6B Tb, $Sb^{1}$* and *$w^{1118}$* were outcrossed to *$w^{1118}$; CxD/TM3* over three generations, and stocks were established from single flies.

### A3.3.2 Two dimensional difference gel electrophoresis and mass spectrometry (2D DIGE/MS)

Embryos were collected from *$w^{1118}$; $dfmr1^{3}$/Df(3R)Exel6265* (*dfmr1-*) and *$w^{1118}$; +/ Df(3R)Exel6265* (control), and midcellularizing embryos were hand sorted and frozen as described in (Gong *et al*. 2004). Mutant and control proteins were labeled and separated in 2D gels as described in (Gong *et al*. 2004; Viswanathan *et al*. 2006). In brief, equal

masses (100-150 ug) of total protein from control and mutant embryos were labeled with Cy3-NHS or Cy5-NHS, subjected to isoelectric focusing on 13 cm, pH 3-10 non-linear Immobiline strips according to the manufacturer's protocol (Amersham Biosciences), and separated through 10-15% SDS-PAGE gradient gels. For each experiment control and mutant proteins were reciprocally labeled in parallel: Cy3-NHS-labeled control/ Cy5-NHS-labeled mutant and Cy5-NHS-labeled control/ Cy3-NHS-labeled mutant. To control for loading error, 1 μg of BSA was added to each sample prior to labeling. Gels were imaged with imager integrated with robotic gel cutter. Gel images were analyzed using IPLab (Scanalytics) and QuickTime, and protein intensities were quantified using SExtractor (https://sourceforge.net/projects/sextractor) as described in (Viswanathan *et al*. 2006). Proteins of interest were excised from gels and mass spectrometry fingerprint analysis and protein identification was performed as described in (Gong *et al*. 2004).

### A3.3.3 Immunoprecipitations

WT and *dfmr1-* mid-cellularizing embryos were collected, dechorionated, and frozen. Because *dfmr1-* embryos are slightly developmentally delayed, *dfmr1-* embryos were allowed to age an additional 15 min (~2.25-3.25 hr for WT and ~2.5-3.5 hr for *dfmr1-*). A sample of each embryo collection was checked to ensure equivalent staging between the two genotypes. Anti-dFMRP IPs were performed using extracts made from the embryos (10,000 x *g* supernatants (S10) in $TKT_{100}$ buffer [10 mM Tris HCl pH 8.0, 100 mM KCl, 0.05% Triton X-100, 1 mM DTT, 50 units/ml rRNasin, protease inhibitors]) as described in 3.2.7. Anti-PNUT IPs were performed as follows. 250 μg WT and *dfmr1-* S10 was incubated with 0.75 μg Rabbit anti-PNUT antibody for 10-12 hrs at 4°C. A mock-IP was performed with WT extract and no antibody. 25 μl BSA-coated protein G Sepharose 4B (Sigma) was added to each mixture for 4 hrs at 4°C.

After supernatants were removed, beads were washed 5 times in $TKT_{100}$, eluted with SDS/PAGE sample buffer at 90°C for 2 min, and analyzed by immunoblot analysis.

### A3.3.4 qRT-PCR

Total RNA was extracted from embryos, immunoprecipitateed material and corresponding input S10 extracts using TRIzol-LS reagent (Invitrogen). 1 μg of total embryonic RNA or 100 ng of total immunoprecipitated or S10 RNA were digested with amplification grade DNAse I (Invitrogen) and heat inactivated according to manufacturer's protocol followed by reverse transcription using the High Capacity cDNA Reverse Transcription Kit (ABI) including RNase Inhibitors (Promega). Quantitative PCR was performed in 10μl reactions in 384-well plates with Power SYBR PCR Master Mix in a 7900HT Sequence Detector (ABI) using the following parameters:

1. 50° x 2min
2. 95° x 10min
3. 95° x 15sec
4. 60° x 1min (this temp will vary depending on primer set)
5. repeat steps 3 and 4 for 40 cycles
6. 95° x 15sec
7. 60° x 15sec
8. 95° x 15sec

PCR data was analyzed using SDS 2.3 software according to manufacturer's recommendations and relative levels of specific mRNAs were quantified as in A3.2.9.

When designing primers for these experiments I tried to stay within the following parameters: try to choose a primer pair that straddles an intron, limit amplification size to 60-175bp, limit GC content to 30-70%, the five nucleotides at the 3' end should have no more than two G and/or C bases, limit Tm to 57-60°C, check primer pair to ensure no

dimers will form, and blast primer to ensure there are no sites in the genome that have 100% identity to 18 consecutive bases.

### A3.3.5 Quantitative protein immunoblot analysis

Supernatants (S10) were prepared from WT or *dfmr1-* embryos as in A3.3.3, quantified using Bradford reagent (Biorad), and processed by using the manufacturer's protocol for the Odyssey Infrared Imaging System (LI-COR Biosciences). Blots were imaged using the Odyssey two-color infrared imaging system, and proteins were quantified using the system software (Institute for Cell and Molecular Biology Core Facility).

### A3.3.6 Gel filtration chromatography

WT and *dfmr1-* embryos were collected and extracts were prepared as described for IPs above. Between 1.0 mg and 1.3 mg of total protein from each genotype was separated by gel filtration chromatography on a Superose 6 column (GE Healthcare) at a rate of 0.2 ml/min with 1 ml fractions collected over the entire run. Fractions were precipitated using with 10% trichloroacetic acid, resuspended in SDS/PAGE sample buffer, and analyzed by immunoblot analysis. Molecular weight standards were separated through column prior to embryonic extracts.

### A3.3.7 Live embryo imaging

Embryos were collected from wild type or mutant females mated to wild type males at 25°C. Analysis of cellularization was done as described in A3.2.3 (Monzo *et al*. 2006). Embryos were imaged using a Zeiss AxioVert 200 microscope with a 40x EC Plan Neofluor objective equipped with differential interference contrast optics.

### A3.3.8 Fixed embryo analysis

Fixed analysis was performed as described in A3.2.4.

### A3.3.9 Antibodies

The following antibodies and stains were used in this study: anti-dFMRP (6A15; AbCam, Cambridge, MA), anti-alpha Tubulin (DM1A, Sigma), anti-PNUT [1:500; KEKK, C. Field (Field *et al*. 1996)], anti-PNUT (no dilution; 4C9H4, Developmental Studies Hybridoma Bank), anti-Anillin (1:500; C. Field), and anti-CCT1 (1:500; 91A, AbCam). Dilutions in parenthesis indicate those used for IF analysis on fixed embryos. Typically, a 100-fold dilution of the dilution for IF worked well for immunoblot analysis.

## A3.4 CHAPTER 4

The results in this chapter have not been published but are being prepared for submission for publication. Because of this, I am only including the methods for the experiments I performed. The methods of the experiments performed by Ophelia Papoulas will be published at a later date.

### A3.4.1 Fly stocks and genetics

The following stocks were obtained from the Bloomington Stock Center: *w; Df(3L)cat ri sbd e/TM3 Ser ri e* and $y^{1}$ $w^{67c23}$*; P{EPgy2}CG18811*$^{EY0749}$ and $w^{*}$*; CycB*$^{2}$*/CyO*. Ophelia Papoulas generated *w; capr*$^{2}$*/TM6B Hu* using standard imprecise P element excision techniques. Loss of *capr* was confirmed by PCR analysis and loss of CAPR was confirmed by immunoblot analysis.

### A3.4.2 Live embryo imaging

Initial analysis of cellularization was done as described in A3.2.3. For analysis of the cortical nuclear divisions, embryos were prepared as above and imaged using a Zeiss AxioVert 200 microscope with a 40X EC Plan Neofluar objective equipped with

differential interference contrast optics. Imaging was started just prior to nuclear cycle 10 shortly after pole buds were formed and imaged every 15 sec until the end of cellularization at room temperature (23.5-25.5°C). Duration of interphase and mitosis of each cortical division was determined by measuring lengths between nuclear envelope breakdown and reassembly. Penetrance of precocious mitosis 14 was determined by counting the total number of embryos imaged that either partially or completely cellularized during interphase of nuclear cycle 15. Nuclear densities at cortex were measured to confirm that mutant embryos begin cortical divisions relative to pole bud formation normally. In addition, mutant embryos that cellularize during nuclear cycle 15 have an increased nuclear density compared to wild type cellularizing embryos at nuclear cycle 14.

To test if reduction of zygotic *Cyclin B* can reduce the penetrance of the precocious mitosis 14 phenotype, embryos were collected from virgin $w^{1118}$; +/+; $capr^{2}$/*Df(3L)Cat, dfmr1*$^{3}$ females mated to $w^{1118}$; $CycB^{2}$/*CyO-GFP*; +/+ males and imaged as described above. Embryos were allowed to age at least 2 hr and imaged using a fluorescent microscope to determine if embryo received the *CycB-* or *CyO-GFP* chromosome.

### A3.4.3 Fixed embryo analysis

Fixed analysis was performed as described in A3.2.4. For visualization of spindle microtubules paclitaxel (Sigma) was added to a final concentration of 2.5 μM as described in Maldonado-Codina and Glover 1992.

### A3.4.4 qRT-PCR

Quantification of steady state mRNA levels was done as described in A3.3.4.

### A3.4.5 Antibodies

The following antibodies and stains were used for IF in this study: anti-dFMRP (1:10; 5A11, DSHB), anti-Caprin (1:500; 592), anti-alpha Tubulin (1:250; DM1A, Sigma), anti-phospho-Histone H3 (Ser10) (1:250; Cell Signaling Technology). DNA was visualized with TO-PRO-3 iodide (Invitrogen Molecular Probes).

## A3.5 APPENDIX 1

### A3.5.1 Fly stocks and genetics

All fly stocks were maintained at 20°C or 29°C as indicated. The collection of EMS-induced, X chromosome-linked, temperature-sensitive (ts) mutants was generated by Helen Francis-Lang and William Sullivan (Macdougall *et al*. 2001). The collection was screened for ts zygotic lethality and maternal sterility in collaboration with Drs. William Sullivan, Helmut Kramer and Bing Zhang. The following stocks were screened for ts cellularization defects:

*Oregon-R*, the X-chromosome deficiency kit, and other deficiency stocks were obtained from the Bloomington Stock Center. *Df(1)DA622/FM7* was a gift of N. Perrimon.

### A3.5.2 Maternal fertility and zygotic viability

Temperature-sensitive zygotic lethality was determined by comparing numbers of homozygous mutant flies reared at 20°C or 29°C. Homozygous mutant females were mated to hemizygous mutant males at 20°C. 48-72 hr collections of embryos were kept at either 20°C or shifted to 29°C and allowed to develop. Relative eclosure was calculated by dividing the total number of F1 adults eclosed from each cross by total number of WT F1 adults eclosed at 20°C. Maternal fertility was determined by counting

the numbers of embryos laid and hatched from homozygous mutant females mated to *FM7a* balancer males at 20°C and 29°C, as described in A3.2.2.

### A3.5.3 Complementation analysis

Genetic complementation tests for those mutations that displayed strong ts zygotic lethality were performed by crossing virgin females with the deficiency to ts males at 20°C in two replicate vials. After 48-72 hr collections at 20°C, adults were flipped into new vials. One replicate vial was kept at 20°C, and the other was shifted to 29°C. The total number of eclosed adults were counted from two collections and compared. We expected that crosses with non-complementing deficiencies would produce less adults in the cross reared at 29°C compared to the cross at 20°C.

To test for genetic complementation with *fs(1)ts319*, maternal fertility at the restrictive temperature was assayed. Virgin females from the deficiency stocks were crossed to *fs(1)ts319* males to obtain virgin *fs(1)ts319/Df* females at 20°C. These females were mated to *FM7a* males at 20°C for 5 days. Adults were flipped into new vials and shifted to 29°C and the 5 day collection of embryos was allowed to develop at 20°C. Adults at 29°C were flipped into new vial after 2 days (essentially to 'equilibrate females' to the restrictive temperature) and kept at 29°C. The numbers of adults hatched from 20° and 29° vials were compared. We expected that females heterozygous for *fs(1)ts319* and a non-complementing deficiency would produce less adults in the cross reared at 29°C compared to the cross at 20°C.

### A3.5.4 Live embryo imaging

Time-lapse recordings of all embryos were performed as follows. Embryos were hand prepared for imaging as described in A3.2.3. The development of the embryos was monitored at 20°C. At the onset of nuclear cycle 14, the temperature of the incubator

was increased to 32°C and time-lapse imaging began. Embryos were imaged with a 15 sec delay between frames until the onset of gastrulation. Movies were compressed to 5 frames per second in QuickTime Pro with Sorenson Video 3 Codec. Rates of nuclear elongation and furrow ingression were calculated from live time-lapse recordings. The distance from the cortex to the basal ends of representative nuclei and the corresponding furrow front at 25, 50, and 75% egg length were measured every 5 min using the Leica imaging software.

### A3.5.5 Fixed embryo analysis

Embryos were collected from homozygous mutant females and allowed to age at 20°C. Embryos were incubated at 32°C in small volume of embryo wash buffer (0.7% NaCl, 0.03% Triton X-100) for 25 min on a slide warmer and fixation and immunodetection of proteins was performed as described in A3.2.4. Detection of cell surface using concanavalin-A required embryos to be fixed in the absence of all detergent. Detection of Neurotactin required heat/methanol fixation. Dechorionated embryos were added to 10 ml of 150 mM NaCl, 0.05% Triton X-100 at 90°C in a test tube and were vortexed for 5 sec, decanted into 40 ml chilled 150 mM NaCl, 0.05% Triton X-100, and incubated on ice for 5 min. Embryos were then transferred to a 1.5 ml tube and devitellinized by adding equal parts hepatane and 100% methanol and shaking vigorously for about 30 sec. All of the liquid was aspirated off from the devitellinized embryos that were at the bottom of the tube. Fresh 10% methanol was added. Embryos were then rehydrated using changes of 75%, 50% and 25% methanol in 1X PBS.

### A3.5.6 Semi-quantitative RT-PCR and qRT-PCR

*Oregon-R* and *fs(1)ts319* cellularizing embryos were subjected to permissive or restrictive temperature during cellularization as described above except after

dechorionating, total RNA was extracted with TRIzol Reagent (Invitrogen) according to manufacturer's protocol. First strand cDNA synthesis was performed with 1 mg total RNA using SuperScript II Reverse Transcriptase and an oligo(dT) primer (Stratagene). 2 ul of RT reaction was used for PCR amplification using the following parameters: 26-28 cycles of 94°C x 20 sec, 55°C x 30 sec, 72°C for 20 sec. Cycle number was optimized to identify linear range of amplification for each gene. Primers were designed to span an intron. qRT-PCR was performed as described in A3.2.9.

**A3.2.7 Quantitative protein immunoblot analysis**

Whole embryo extracts were prepared from WT or *fs(1)ts319* embryos as in A3.3.3, quantified using Bradford reagent (Biorad), and processed using the manufacturer's protocol for the Odyssey Infrared Imaging System (LI-COR Biosciences). Blots were imaged using the Odyssey two-color infrared imaging system, and proteins were quantified using the system software (Institute for Cell and Molecular Biology Core Facility, The University of Texas at Austin).

**A3.5.8 gDNA rescue fragment**

Three genomic rescue fragments that overlap the candidate genes were designed by Howard Wang (Figure A1.7). Ophelia Papoulas subcloned rescue fragment 2 (infr2) containing *Rpt3* and *Gtp-bp* from a BAC clone (BACN02C07) into pCaSperR 4 vector using standard techniques. I used standard P-element mediated transformation techniques to generate germ-line clones: 0.5 mg/ml *pinfr2* and 0.15 mg/ml Transposase in 1X injection buffer (0.1 mM potassium phosphate pH 7.8, 5 mM KCl) was injected into posterior end of desiccated embryos. Insertions were mapped to chromosome using standard genetic techniques. The name of the rescue fragment (*infr2*) comes from our original name we gave the *fs(1)ts319* allele. Before mapping the mutation we named the

*fs(1)ts319* allele *inferno* because the disruptions observed during the live analysis was reminiscent of an inferno. The stocks have been maintained at 20°C.

**A3.5.9 Sequence analysis**

Genomic DNA (gDNA) was extracted from homozygous whole *fs(1)ts319* females using a protocol adapted from Ken Burtis, Stanford University. Fragments of candidate genes were amplified by PCR. PCR products were purified using the QIAquick PCR Purification Kit (Qiagen). Sequencing was performed by the Institute for Cellular and Molecular Biology DNA Core Facility at UT Austin. Sequence from 5' and 3' strand was analyzed in MacVector against sequence from the *D. melanogaster* sequence Release 5.1. Because we could not obtain the parental stock that was mutaginized, gDNA from other stocks in the collection was used as a control when needed. Because the ts stocks had been carried for many years here was a concern that the *fs(1)ts319* stock may not be homogenous for the affected chromosome, so I also sequenced gDNA from single *fs(1)ts319/Df(1)RA37* females that were tested for ts maternal sterility. Single-fly DNA preps was performed as described in (Gloor *et al.* 1993).

The following is a summary of the sequence results: 77% of 28785bp gene region sequenced (excludes sequence 5' of Hsp60 and 3' of Klp10A) and 47% of unsequenced gDNA is in introns of Hsp60 and Klp10A.

Missing sequence for ts319 gDNA

| Coordinates | Gene region annotation |
|---|---|
| 1-406 | intergenic 5' of Hsp60 |
| 764-1823 | Hsp60 intron |
| 4359-4395 | intergenic Hsp60-CG11122 |
| 5640-5704 | CG11122 exon |

| | |
|---|---|
| 7406-7460 | CG11122 exon |
| 15855-16001 | CG11122 exon |
| 1-1082 | intergenic CG11122-Rpt3 |
| 1171-1220 | intergenic CG11122-Rpt3 |
| 1220-1334 | Rpt3 5'UTR |
| 4213-6257 | intergenic Gtpbp-Klp10A |
| 6257-6336 | Klp10A 3'UTR |
| 7447-8572 | Klp10A intron |
| 9960-10858 | Klp10A intron |
| 11571 | Klp10A exon |
| 11620 | Klp10A exon |
| 13191-14000 | intergenic 3' of Klp10A |

Altered sequence in ts319 gDNA

| Coord | gene region | change | result of change |
|---|---|---|---|
| 11297 | CG11122 exon | T to G | CCA to CCC silent Proline |
| 2997 | Gtpbp 3'UTR | C to A | |
| 2999 | Gtpbp 3'UTR | A to G | |
| 3007 | Gtpbp 3'UTR | C to G | |
| 5211-5223 | intergenic Gtp-Klp | Extra A nucleotide | |
| 7328 | Klp10A exon | G to A | CAC to CAT silent Histidine |
| 7351 | Klp10A intron | G to A | |
| 11377 | Klp10A exon | T to C | CAA to CAG silent Glutamine |

### A3.5.10 Antibodies

Embryos were incubated in mouse monoclonal antibodies against Neurotactin (1:5, DSHB) and Tubulin (1:250, W. Sullivan), rabbit antibodies against Centrosomin (1:1000, T. Kaufmann), Myosin II (1:100, C. Field), Anillin 4-11 (1:500, C. Field), SLAM (1:1000, R. Lehmann), Lava Lamp (1:2500), mouse antibody against Tubulin (1:250, W. Sullivan), and rat antibodies against Rab11 (1:250, W. Sullivan) and MAC143 (BIP) (1:5, Babraham Institute) diluted as indicated in 1X PBTA at 4° overnight. Embryos were stained with 25 μg/ml concanavalin-A Alexa Fluor® 488 in 1X PBS for 20 min and washed in 1X PBS.

# Appendix 4: Primer sequences

## A4.1 CHAPTER 2

| primer name | Sequence 5' to 3' |
|---|---|
| RpL32 (rp49)+ | GCGCACACCAAGCAAGCACTTCATC |
| RpL32 (rp49)- | GACGCACTCTGTTGTCGATACC |
| tral+ | CAATGCCACGGACTCCAGTGC |
| tral- | CCACCTGTTGCGTCTGCTCTG |
| futsch+ | CAGTCGCCAGGTGT |
| futsch- | GCTCCTCGTTTCA |
| me31B+ | CGCCAAGGACTCTGTCGCAATC |
| me31B- | TCTGCCATTCGTGGGAAATCG |

## A4.2 CHAPTER 3

| primer name | Sequence 5' to 3' |
|---|---|
| CG8308+ | GAGGAGGTCGGTCTGGACAATG |
| CG8308- | TGTTGGGATGTGGGCTTAGAACTC |

| | |
|---|---|
| b’cop+ | CTGGAGGATGATGGTGTGGAGAG |
| b’cop- | TGCGGTCTAAGTGGGATACTGTCAC |
| blw+ | CGGTCGTGGTCAGCGTGAG |
| blw- | GCTTCTGGTTGATGATGGTGTCG |
| pros35+ | CGGATGAGCAAGGCAAAGATG |
| pros35- | TCGTCGTTCCTGGGCGTATC |
| Rpn11+ | TGTCCGACTACAATGAGCACTGTTC |
| Rpn11- | ATGCCGCTTGGGGTCCTG |
| RhoGDI+ | CTATCCGCCGAAGAAGGAGATTC |
| RhoGDI- | TGCTTGTCGTCATCCGTGAAGAC |
| Jafrac1+ | AAGCCCGCTCCCGCATTC |
| Jafrac1- | TGCCCTTGTAGTCGCTCAACTTG |
| Hsp23+ | GGTGCCCTTCTATGAGCCCTACTAC |
| Hsp23- | AAGCCATCCTTTCCGATTTTCG |
| fit+ | CCCGCATCCGCACTCTGTC |
| fit- | TCCAGTCGCTTATCCACCTTGTG |
| CG8351+ | GGCGACGATTTCCAACGATG |
| CG8351- | TCCACGAAGGGTTTCACCTGC |
| CG11596+ | AAGACGCCGAACGCCTACAAC |
| CG11596- | AGATTCACCCAAATGCCACCAG |
| Yp1+ | GCCGTATGGACAACTCCGTCAAC |
| Yp1- | TCTGCGACAGGTGGTAGACTTGC |
| CG5525+ | CAAAGCCGTTTCCGATGCTATC |
| CG5525- | TGGACACCTCGCCGTTGC |
| CG7433+ | CGAGGAAGTCGTGAAGGTCATCC |
| CG7433- | TCCAGGCTCAGCAAACCGTTC |
| GstD3+ | TCGCCGACATTGCCATTCTC |
| GstD3- | TGCCCAGTTTTCTTCCCATCC |
| RpLp0+ | TCACCCGACGAGTCCCTAATACAC |
| RpLp0- | GCCCACGATGAAGCACTTTGG |
| Sod+ | GTCAACGGGCAACGCTGG |
| Sod- | ATCGCTTAGACCTTGGCAATGC |
| SpdS+ | CGCTGAAGGATGACGGAATCG |
| SpdS- | GAACGGAGGTGACGGCATAGG |
| Tsf1+ | GCAGAGGGCTCAGGATGATGTC |
| Tsf1- | TTCAACAAGGCGGCAGCAG |
| vib+ | CAATCGCACTCCCCAGTTCG |
| vib- | TTCCACAGTCAATGGCAAAGTCAC |
| Aat-gly+ | TGGGTGGAGTGCGTAGGATGTG |
| Aat-gly- | GGTCTTTCCGAGAGCCTGCTTG |
| Cctg+ | CCGACATCATTGCCGTGAAAC |
| Cctg- | GTCAGTCTTACGCAGCCGACG |
| CG3590+ | TCGTGCTATGTGGGCGACAAC |
| CG3590- | GCTCTGGGCAAACTGGCTTAGAC |
| CG6045+ | TGTGCCAGGAGGGAGGATGTG |
| CG6045- | CGCAGGTATTCAGCAGAGTGAGG |

| | |
|---|---|
| CG32473+ | CTGCCACCACCGAGGATTACC |
| CG32473- | GAAGACCCATCTGCTCCGTCC |
| Hsc70Cb+ | GCTAATCTCGTCCGCCACTTTG |
| Hsc70Cb- | CGCCCTCTTGCTGACCATCC |
| Mms19+ | ATTCGCTGAGGGCACAGTGG |
| Mms19- | CGGCTCCAGAACGGAAGGC |
| tsr+ | AGAAATGCGGACCTGGAGAGTG |
| tsr- | GGACACCACGACATAAGGAACAGC |
| cct1+ | TCCTCATCAAGGGCACTAAGGC |
| cct1- | CACGCTTCACCACGCACAGAG |
| cct2+ | CATCATTTTCGGTGGCGGC |
| cct2- | AACCAGTTGGGCTGAATCGTAGC |
| cct5+ | GCTCAGAGTCATCCGAATCCGAG |
| cct5- | CGTGTCTTCTTGCTGCGTGTCAG |
| cct6+ | CAGGAGGAGCACTTGGGATACG |
| cct6- | CGGACAGCGGGTTCTTGC |
| cct8+ | TCAGGAGGAGTTGGGCTACTGC |
| cct8- | GGGCACGCTCAATGTCATCC |

## A4.3 CHAPTER 4

| | |
|---|---|
| cdc2+ | AGGGTCGCAACCGCCTGAC |
| cdc2- | CTCCATCAAAACATCCTCCAAACAG |
| cycB+ | CCGAGGACGAGCACCATACG |
| cycB- | GCAGCGACAGGAACAGTGAGG |
| frs+ | TCCCTGGACAGCAAGAAGTATTCC |
| frs- | CGCTTTTTGAGTTCGGTTTGG |
| stg+ | CCTATGCCCTGCCCCTGATG |
| stg- | CTGTTTCGCTGGAGATGCTCTTC |
| twn+ | TCCCACGCTGACCTCCAATC |
| twn- | GGTATGCTGACTTCTGTCGTTGCTC |
| sev+ | GTATGCGGCGAGGAACAACTTC |
| sev- | GCAAAGCAGGAGCAGGGAGTAAAG |

## A4.4 APPENDIX 1

| gene | primer set # | sequence 5' to 3' |
|---|---|---|
| Hsp60 | 1+ | CATTGGCTTTTGCTGTCAG |
| | 1- | TCCTTGACGGTGATAACGC |
| | 2+ | ATCCCGTCGAGATTCGTC |
| | 2- | CAGCTTCTCCTTCTCGTACTC |
| | 3+ | AGCACCCTCACCGATATG |

| | | |
|---|---|---|
| | 3- | GGTTGTGTTGGATTTGTGTG |
| | 4+ | ATGTAAGCGACTGCCACTG |
| | 4- | TCTCATTTGGGATGCCAG |
| | 5prime+ | TTACTTGAATGCGAGTCCC |
| CG11122 | 1+ | CAATAGTGTCCGATAACAGAGC |
| | 1- | GCAGGCGAAATACTTATCTG |
| | 2+ | GGACAAGTTTCACACCGAG |
| | 2- | GAGGTGATTCTGGAGGTTG |
| | 3+ | GTCGCCAACTCAGTGTTC |
| | 3- | CTTTTGGTTCCTGCTACG |
| | 4+ | GAACAGGCGGTCATCAAG |
| | 4- | TTGGTGCCGCAGTAGTAG |
| | 5+ | ACTGGAGCAGCAACAACC |
| | 5- | TGCTGCTTCTGTTTGCG |
| | 6+ | CAAGAACAAGGCGAAGG |
| | 6- | GCACTTGCTCCGTTTTG |
| | 7+ | GCAGCAAGAGGATTAGCG |
| | 7- | TTCCAGCGGAGGATACTG |
| | 8+ | TTCATCCACCGACGAGAC |
| | 8- | ACCAACTGGCGTAGGAAG |
| | 9+ | AAGTCGAGCAGGAAACCG |
| | 9- | GCAACAATGGCTGGAATAG |
| | 10+ | AAAGGGAGAGGGAGAAGG |
| | 10- | CGACGAGGTGTTGTTGTTC |
| | 11+ | ATCCTGTGCCCGTAAACC |
| | 11- | CGCAGGATGGAACTAACC |
| | 12+ | CTATCGAAGGGGAAAGGC |
| | 12- | CTCATCGTTCAGATTCGG |
| | 13+ | CAACGAGGACTTTGAGTTTG |
| | 13- | TCGGGATTGAGATTGAGAC |
| | 14+ | CAGGAGCAGGAGAGAATG |
| | 14- | ACTACCCAACGCAATGTC |
| | 15+ | GCGATGAAGGGCTATGAG |
| | 15- | GCTGGCGTGCTTAAATATC |
| | 16+ | TCAGAGGTGGAGTTGTAGCC |
| | 16- | GGCTTCCACCTTTGATTTC |
| | 17+ | CATCAGCACCATCATCAC |
| | 17- | CACTGGAGTTTTGCTCTTG |
| | 18+ | CGCCAGAAGTGCTAACTC |
| | 18- | GCCTATGGCTATGACTTGTC |
| | 19+ | ACAAGAAGCTCGTGAAGC |
| | 19- | TTACTGGCATCCCAAATG |

| | | |
|---|---|---|
| Rpt3 | 1+ | CTCGCAGAAAACGCAAAC |
| | 1- | TACAGCTCGAAGTGGGTCAG |
| | 2+ | AGCTCCATTTCGATGCTG |
| | 2- | GAAGAGTTTAGTGTGTTGGGG |
| | 5prime+ | CACCAGATGCTTTGAAACG |
| | 3prime- | GGCTATCCTTCCAATGCTC |
| Gtp-bp | 1+ | CGAGTAGAGTGCGTTGTTGTTG |
| | 1- | CGCCGTTTCTCCATGATGATC |
| | 2+ | CATCCAAATCACAGCCGTC |
| | 2- | GACACCGCAGAAGATTATCG |
| | 3+ | CGCATCGACATCATACGCGAT |
| | 3- | GATTCGGTGAAAAGAGTGG |
| | 5prime+ | ACAGGGAATCCTCTAACTGC |
| Klp10A | 1+ | AGGTGGAGTCAAAGAGGAAG |
| | 1- | GGCAATGTGTTATTAGGCAC |
| | 2+ | ACGACCACTGGATTACAGC |
| | 2- | TTGGAATGTGTGGTCACC |
| | 3+ | ATACACAGCCAAGCCGTTG |
| | 3- | ACAATCTGGAAAACGGCG |
| | 4+ | TCGAGGAGGTACTGAAGCTC |
| | 4- | GCCTTGTGTGTAACTTCTAGG |
| | 5+ | TTCCCCTTTGGGTCATAC |
| | 5- | GTGATTGTGGATGAACGG |
| | 6+ | CTTAGCCAATAGTAACCCTGC |
| | 6- | ACACTGACACACACATAGCG |
| | 7+ | GCGGAAAGCATTGATTGG |
| | 7- | ATGGCGTCCAGTTCTACCTC |
| | 3prime- | TTACTGGCTATGGGAATACG |
| sbr | + | TATCGCAGAACCAACACG |
| | - | CCATCACATTCTGACGAAAG |
| nrt | + | GGACGAACAGAAATCTCGC |
| | - | TGGCGTTCAAAAGTCCCAC |
| Hsc70-3 (bip) | + | CATTGATTTGGGCA |
| | - | TCAACTGATTCTTG |
| actin5c | + | GCCACTTGCGTTTA |
| | - | TTCAGGGTGAGGGAT |

# References


Adam, J. C., Pringle, J. R. and Peifer, M., 2000 Evidence for functional differentiation among Drosophila septins in cytokinesis and cellularization. Mol Biol Cell **11**: 3123-35.

Afshar, K., Stuart, B. and Wasserman, S. A., 2000 Functional analysis of the Drosophila diaphanous FH protein in early embryonic development. Development **127**: 1887-97.

Anderson, P. and Kedersha, N., 2006 RNA granules. J Cell Biol **172**: 803-8.

Arbeitman, M. N., Furlong, E. E., Imam, F., Johnson, E., Null, B. H., Baker, B. S., Krasnow, M. A., Scott, M. P., Davis, R. W. and White, K. P., 2002 Gene expression during the life cycle of Drosophila melanogaster. Science **297**: 2270-5.

Audhya, A., Hyndman, F., McLeod, I. X., Maddox, A. S., Yates, J. R., 3rd, Desai, A. and Oegema, K., 2005 A complex containing the Sm protein CAR-1 and the RNA helicase CGH-1 is required for embryonic cytokinesis in Caenorhabditis elegans. J Cell Biol **171**: 267-79.

Barbee, S. A., Estes, P. S., Cziko, A. M., Hillebrand, J., Luedeman, R. A., Coller, J. M., Johnson, N., Howlett, I. C., Geng, C., Ueda, R., Brand, A. H., Newbury, S. F., Wilhelm, J. E., Levine, R. B., Nakamura, A., Parker, R. and Ramaswami, M., 2006 Staufen- and FMRP-containing neuronal RNPs are structurally and functionally related to somatic P bodies. Neuron **52**: 997-1009.

Bashirullah, A., Halsell, S. R., Cooperstock, R. L., Kloc, M., Karaiskakis, A., Fisher, W. W., Fu, W., Hamilton, J. K., Etkin, L. D. and Lipshitz, H. D., 1999 Joint action of two RNA degradation pathways controls the timing of maternal transcript elimination at the midblastula transition in Drosophila melanogaster. Embo J **18**: 2610-20.

Bate, M. and Martinez Arias, A. (1993). The Development of Drosophila melanogaster. Plainview, N.Y., Cold Spring Harbor Laboratory Press.

Brown, V., Jin, P., Ceman, S., Darnell, J. C., O'Donnell, W. T., Tenenbaum, S. A., Jin, X., Feng, Y., Wilkinson, K. D., Keene, J. D., Darnell, R. B. and Warren, S. T.,

2001 Microarray identification of FMRP-associated brain mRNAs and altered mRNA translational profiles in fragile X syndrome. Cell **107**: 477-87.

Burgess, R. W., Deitcher, D. L. and Schwarz, T. L., 1997 The synaptic protein syntaxin1 is required for cellularization of Drosophila embryos. J Cell Biol **138**: 861-75.

Bushati, N., Stark, A., Brennecke, J. and Cohen, S. M., 2008 Temporal reciprocity of miRNAs and their targets during the maternal-to-zygotic transition in Drosophila. Curr Biol **18**: 501-6.

Castets, M., Schaeffer, C., Bechara, E., Schenck, A., Khandjian, E. W., Luche, S., Moine, H., Rabilloud, T., Mandel, J. L. and Bardoni, B., 2005 FMRP interferes with the Rac1 pathway and controls actin cytoskeleton dynamics in murine fibroblasts. Hum Mol Genet **14**: 835-44.

Caudy, A. A., Myers, M., Hannon, G. J. and Hammond, S. M., 2002 Fragile X-related protein and VIG associate with the RNA interference machinery. Genes Dev **16**: 2491-6.

Chihara, T., Luginbuhl, D. and Luo, L., 2007 Cytoplasmic and mitochondrial protein translation in axonal and dendritic terminal arborization. Nat Neurosci **10**: 828-37.

Coller, J. and Parker, R., 2005 General translational repression by activators of mRNA decapping. Cell **122**: 875-86.

Corbin, F., Bouillon, M., Fortin, A., Morin, S., Rousseau, F. and Khandjian, E. W., 1997 The fragile X mental retardation protein is associated with poly(A)+ mRNA in actively translating polyribosomes. Hum Mol Genet **6**: 1465-72.

Costa, A., Wang, Y., Dockendorff, T. C., Erdjument-Bromage, H., Tempst, P., Schedl, P. and Jongens, T. A., 2005 The Drosophila fragile X protein functions as a negative regulator in the orb autoregulatory pathway. Dev Cell **8**: 331-42.

Dahanukar, A., Walker, J. A. and Wharton, R. P., 1999 Smaug, a novel RNA-binding protein that operates a translational switch in Drosophila. Mol Cell **4**: 209-18.

Darnell, J. C., Fraser, C. E., Mostovetsky, O., Stefani, G., Jones, T. A., Eddy, S. R. and Darnell, R. B., 2005 Kissing complex RNAs mediate interaction between the Fragile-X mental retardation protein KH2 domain and brain polyribosomes. Genes Dev **19**: 903-18.

Darnell, J. C., Jensen, K. B., Jin, P., Brown, V., Warren, S. T. and Darnell, R. B., 2001 Fragile X mental retardation protein targets G quartet mRNAs important for neuronal function. Cell **107**: 489-99.

De Renzis, S., Elemento, O., Tavazoie, S. and Wieschaus, E. F., 2007 Unmasking activation of the zygotic genome using chromosomal deletions in the Drosophila embryo. PLoS Biol **5**: e117.

Dekker, C., Stirling, P. C., McCormack, E. A., Filmore, H., Paul, A., Brost, R. L., Costanzo, M., Boone, C., Leroux, M. R. and Willison, K. R., 2008 The interaction network of the chaperonin CCT. Embo J **27**: 1827-39.

Deshpande, G., Calhoun, G. and Schedl, P., 2005 Drosophila argonaute-2 is required early in embryogenesis for the assembly of centric/centromeric heterochromatin, nuclear division, nuclear migration, and germ-cell formation. Genes Dev **19**: 1680-5.

Deshpande, G., Calhoun, G. and Schedl, P., 2006 The drosophila fragile X protein dFMR1 is required during early embryogenesis for pole cell formation and rapid nuclear division cycles. Genetics **174**: 1287-98.

Dockendorff, T. C., Su, H. S., McBride, S. M., Yang, Z., Choi, C. H., Siwicki, K. K., Sehgal, A. and Jongens, T. A., 2002 Drosophila lacking dfmr1 activity show defects in circadian output and fail to maintain courtship interest. Neuron **34**: 973-84.

Edgar, B. A. and Datar, S. A., 1996 Zygotic degradation of two maternal Cdc25 mRNAs terminates Drosophila's early cell cycle program. Genes Dev **10**: 1966-77.

Edgar, B. A., Kiehle, C. P. and Schubiger, G., 1986 Cell cycle control by the nucleo-cytoplasmic ratio in early Drosophila development. Cell **44**: 365-72.

Edgar, B. A., Odell, G. M. and Schubiger, G., 1987 Cytoarchitecture and the patterning of fushi tarazu expression in the Drosophila blastoderm. Genes Dev **1**: 1226-37.

Edgar, B. A. and Schubiger, G., 1986 Parameters controlling transcriptional activation during early Drosophila development. Cell **44**: 871-7.

Edgar, B. A., Sprenger, F., Duronio, R. J., Leopold, P. and O'Farrell, P. H., 1994 Distinct molecular mechanism regulate cell cycle timing at successive stages of Drosophila embryogenesis. Genes Dev **8**: 440-52.

el Bekay, R., Romero-Zerbo, Y., Decara, J., Sanchez-Salido, L., Del Arco-Herrera, I., Rodriguez-de Fonseca, F. and de Diego-Otero, Y., 2007 Enhanced markers of oxidative stress, altered antioxidants and NADPH-oxidase activation in brains from Fragile X mental retardation 1-deficient mice, a pathological model for Fragile X syndrome. Eur J Neurosci **26**: 3169-80.

Feng, Y., Absher, D., Eberhart, D. E., Brown, V., Malter, H. E. and Warren, S. T., 1997 FMRP associates with polyribosomes as an mRNP, and the I304N mutation of severe fragile X syndrome abolishes this association. Mol Cell **1**: 109-18.

Field, C. M., al-Awar, O., Rosenblatt, J., Wong, M. L., Alberts, B. and Mitchison, T. J., 1996 A purified Drosophila septin complex forms filaments and exhibits GTPase activity. J Cell Biol **133**: 605-16.

Field, C. M., Coughlin, M., Doberstein, S., Marty, T. and Sullivan, W., 2005 Characterization of anillin mutants reveals essential roles in septin localization and plasma membrane integrity. Development **132**: 2849-60.

Foe, V. E. and Alberts, B. M., 1983 Studies of nuclear and cytoplasmic behaviour during the five mitotic cycles that precede gastrulation in Drosophila embryogenesis. J Cell Sci **61**: 31-70.

Fogarty, P., Kalpin, R. F. and Sullivan, W., 1994 The Drosophila maternal-effect mutation grapes causes a metaphase arrest at nuclear cycle 13. Development **120**: 2131-42.

Fredieu, J. R. and Mahowald, A. P., 1993 Characterization of a putative Drosophila GTP-binding protein. J Cell Sci **105 ( Pt 1)**: 81-91.

Gao, F. B., 2002 Understanding fragile X syndrome: insights from retarded flies. Neuron **34**: 859-62.

Gawlinski, P., Nikolay, R., Goursot, C., Lawo, S., Chaurasia, B., Herz, H. M., Kussler-Schneider, Y., Ruppert, T., Mayer, M. and Grosshans, J., 2007 The Drosophila mitotic inhibitor Fruhstart specifically binds to the hydrophobic patch of cyclins. EMBO Rep **8**: 490-6.

Gebauer, F. and Hentze, M. W., 2004 Molecular mechanisms of translational control. Nat Rev Mol Cell Biol **5**: 827-35.

Gingras, A. C., Raught, B. and Sonenberg, N., 1999 eIF4 initiation factors: effectors of mRNA recruitment to ribosomes and regulators of translation. Annu Rev Biochem **68**: 913-63.

Giraldez, A. J., Mishima, Y., Rihel, J., Grocock, R. J., Van Dongen, S., Inoue, K., Enright, A. J. and Schier, A. F., 2006 Zebrafish MiR-430 promotes deadenylation and clearance of maternal mRNAs. Science **312**: 75-9.

Girod, A., Storrie, B., Simpson, J. C., Johannes, L., Goud, B., Roberts, L. M., Lord, J. M., Nilsson, T. and Pepperkok, R., 1999 Evidence for a COP-I-independent transport route from the Golgi complex to the endoplasmic reticulum. Nat Cell Biol **1**: 423-30.

Gloor, G. B., Preston, C. R., Johnson-Schlitz, D. M., Nassif, N. A., Phillis, R. W., Benz, W. K., Robertson, H. M. and Engels, W. R., 1993 Type I repressors of P element mobility. Genetics **135**: 81-95.

Glotzer, M., 2001 Animal cell cytokinesis. Annu Rev Cell Dev Biol **17**: 351-86.

Gong, L., Puri, M., Unlu, M., Young, M., Robertson, K., Viswanathan, S., Krishnaswamy, A., Dowd, S. R. and Minden, J. S., 2004 Drosophila ventral furrow morphogenesis: a proteomic analysis. Development **131**: 643-56.

Grantham, J., Brackley, K. I. and Willison, K. R., 2006 Substantial CCT activity is required for cell cycle progression and cytoskeletal organization in mammalian cells. Exp Cell Res **312**: 2309-24.

Grill, B., Wilson, G. M., Zhang, K. X., Wang, B., Doyonnas, R., Quadroni, M. and Schrader, J. W., 2004 Activation/division of lymphocytes results in increased levels of cytoplasmic activation/proliferation-associated protein-1: prototype of a new family of proteins. J Immunol **172**: 2389-400.

Grosshans, J. and Wieschaus, E., 2000 A genetic link between morphogenesis and cell division during formation of the ventral furrow in Drosophila. Cell **101**: 523-31.

Hegde, R. S. and Kang, S. W., 2008 The concept of translocational regulation. J Cell Biol **182**: 225-32.

Hinton, V. J., Brown, W. T., Wisniewski, K. and Rudelli, R. D., 1991 Analysis of neocortex in three males with the fragile X syndrome. Am J Med Genet **41**: 289-94.

Huang, J. and Raff, J. W., 1999 The disappearance of cyclin B at the end of mitosis is regulated spatially in Drosophila cells. Embo J **18**: 2184-95.

Hutvagner, G. and Simard, M. J., 2008 Argonaute proteins: key players in RNA silencing. Nat Rev Mol Cell Biol **9**: 22-32.

Inlow, J. K. and Restifo, L. L., 2004 Molecular and comparative genetics of mental retardation. Genetics **166**: 835-81.

Ishizuka, A., Siomi, M. C. and Siomi, H., 2002 A Drosophila fragile X protein interacts with components of RNAi and ribosomal proteins. Genes Dev **16**: 2497-508.

Jakymiw, A., Lian, S., Eystathioy, T., Li, S., Satoh, M., Hamel, J. C., Fritzler, M. J. and Chan, E. K., 2005 Disruption of GW bodies impairs mammalian RNA interference. Nat Cell Biol **7**: 1267-74.

Jin, P., Zarnescu, D. C., Ceman, S., Nakamoto, M., Mowrey, J., Jongens, T. A., Nelson, D. L., Moses, K. and Warren, S. T., 2004 Biochemical and genetic interaction between the fragile X mental retardation protein and the microRNA pathway. Nat Neurosci **7**: 113-7.

Kanai, Y., Dohmae, N. and Hirokawa, N., 2004 Kinesin transports RNA: isolation and characterization of an RNA-transporting granule. Neuron **43**: 513-25.

Kennedy, M. J. and Ehlers, M. D., 2006 Organelles and trafficking machinery for postsynaptic plasticity. Annu Rev Neurosci **29**: 325-62.

Khandjian, E. W., Corbin, F., Woerly, S. and Rousseau, F., 1996 The fragile X mental retardation protein is associated with ribosomes. Nat Genet **12**: 91-3.

Korey, C. A., Wilkie, G., Davis, I. and Van Vactor, D., 2001 small bristles is required for the morphogenesis of multiple tissues during Drosophila development. Genetics **159**: 1659-70.

Krijgsveld, J., Ketting, R. F., Mahmoudi, T., Johansen, J., Artal-Sanz, M., Verrijzer, C. P., Plasterk, R. H. and Heck, A. J., 2003 Metabolic labeling of C. elegans and D. melanogaster for quantitative proteomics. Nat Biotechnol **21**: 927-31.

Laggerbauer, B., Ostareck, D., Keidel, E. M., Ostareck-Lederer, A. and Fischer, U., 2001 Evidence that fragile X mental retardation protein is a negative regulator of translation. Hum Mol Genet **10**: 329-38.

Leaman, D., Chen, P. Y., Fak, J., Yalcin, A., Pearce, M., Unnerstall, U., Marks, D. S., Sander, C., Tuschl, T. and Gaul, U., 2005 Antisense-mediated depletion reveals essential and specific functions of microRNAs in Drosophila development. Cell **121**: 1097-108.

Lecuit, T., Samanta, R. and Wieschaus, E., 2002 slam encodes a developmental regulator of polarized membrane growth during cleavage of the Drosophila embryo. Dev Cell **2**: 425-36.

Lecuit, T. and Wieschaus, E., 2000 Polarized insertion of new membrane from a cytoplasmic reservoir during cleavage of the Drosophila embryo. J Cell Biol **150**: 849-60.

Lee, A., Li, W., Xu, K., Bogert, B. A., Su, K. and Gao, F. B., 2003 Control of dendritic development by the Drosophila fragile X-related gene involves the small GTPase Rac1. Development **130**: 5543-52.

Liang, H. L., Nien, C. Y., Liu, H. Y., Metzstein, M. M., Kirov, N. and Rushlow, C., 2008 The zinc-finger protein Zelda is a key activator of the early zygotic genome in Drosophila. Nature **456**: 400-3.

Liao, L., Park, S. K., Xu, T., Vanderklish, P. and Yates, J. R., 3rd, 2008 Quantitative proteomic analysis of primary neurons reveals diverse changes in synaptic protein content in fmr1 knockout mice. Proc Natl Acad Sci U S A **105**: 15281-6.

Liou, A. K. and Willison, K. R., 1997 Elucidation of the subunit orientation in CCT (chaperonin containing TCP1) from the subunit composition of CCT micro-complexes. Embo J **16**: 4311-6.

Liu, J., Rivas, F. V., Wohlschlegel, J., Yates, J. R., 3rd, Parker, R. and Hannon, G. J., 2005 A role for the P-body component GW182 in microRNA function. Nat Cell Biol **7**: 1261-6.

Lu, R., Wang, H., Liang, Z., Ku, L., O'Donnell W, T., Li, W., Warren, S. T. and Feng, Y., 2004 The fragile X protein controls microtubule-associated protein 1B translation and microtubule stability in brain neuron development. Proc Natl Acad Sci U S A **101**: 15201-6.

MacDougall, N., Lad, Y., Wilkie, G. S., Francis-Lang, H., Sullivan, W. and Davis, I., 2001 Merlin, the Drosophila homologue of neurofibromatosis-2, is specifically required in posterior follicle cells for axis formation in the oocyte. Development **128**: 665-73.

Mata, J., Curado, S., Ephrussi, A. and Rorth, P., 2000 Tribbles coordinates mitosis and morphogenesis in Drosophila by regulating string/CDC25 proteolysis. Cell **101**: 511-22.

Mazroui, R., Huot, M. E., Tremblay, S., Filion, C., Labelle, Y. and Khandjian, E. W., 2002 Trapping of messenger RNA by Fragile X Mental Retardation protein into cytoplasmic granules induces translation repression. Hum Mol Genet **11**: 3007-17.

Mazumdar, A. and Mazumdar, M., 2002 How one becomes many: blastoderm cellularization in Drosophila melanogaster. Bioessays **24**: 1012-22.

Merrill, P. T., Sweeton, D. and Wieschaus, E., 1988 Requirements for autosomal gene activity during precellular stages of Drosophila melanogaster. Development **104**: 495-509.

Meyer, W. J., Schreiber, S., Guo, Y., Volkmann, T., Welte, M. A. and Muller, H. A., 2006 Overlapping functions of argonaute proteins in patterning and morphogenesis of Drosophila embryos. PLoS Genet **2**: e134.

Miyashiro, K. Y., Beckel-Mitchener, A., Purk, T. P., Becker, K. G., Barret, T., Liu, L., Carbonetto, S., Weiler, I. J., Greenough, W. T. and Eberwine, J., 2003 RNA cargoes associating with FMRP reveal deficits in cellular functioning in Fmr1 null mice. Neuron **37**: 417-31.

Monzo, K., Papoulas, O., Cantin, G. T., Wang, Y., Yates, J. R., 3rd and Sisson, J. C., 2006 Fragile X mental retardation protein controls trailer hitch expression and cleavage furrow formation in Drosophila embryos. Proc Natl Acad Sci U S A **103**: 18160-5.

Moore, C. D., Thacker, E. E., Larimore, J., Gaston, D., Underwood, A., Kearns, B., Patterson, S. I., Jackson, T., Chapleau, C., Pozzo-Miller, L. and Theibert, A., 2007 The neuronal Arf GAP centaurin alpha1 modulates dendritic differentiation. J Cell Sci **120**: 2683-93.

Nakamura, A., Amikura, R., Hanyu, K. and Kobayashi, S., 2001 Me31B silences translation of oocyte-localizing RNAs through the formation of cytoplasmic RNP complex during Drosophila oogenesis. Development **128**: 3233-42.

Nelson, M. R., Leidal, A. M. and Smibert, C. A., 2004 Drosophila Cup is an eIF4E-binding protein that functions in Smaug-mediated translational repression. Embo J **23**: 150-9.

Newport, J. and Kirschner, M., 1982 A major developmental transition in early Xenopus embryos: I. characterization and timing of cellular changes at the midblastula stage. Cell **30**: 675-86.

Newport, J. and Kirschner, M., 1982 A major developmental transition in early Xenopus embryos: II. Control of the onset of transcription. Cell **30**: 687-96.

O'Donnell, W. T. and Warren, S. T., 2002 A decade of molecular studies of fragile X syndrome. Annu Rev Neurosci **25**: 315-38.

Papoulas, O., Hays, T. S. and Sisson, J. C., 2005 The golgin Lava lamp mediates dynein-based Golgi movements during Drosophila cellularization. Nat Cell Biol **7**: 612-8.

Pelissier, A., Chauvin, J. P. and Lecuit, T., 2003 Trafficking through Rab11 endosomes is required for cellularization during Drosophila embryogenesis. Curr Biol **13**: 1848-57.

Penagarikano, O., Mulle, J. G. and Warren, S. T., 2007 The pathophysiology of fragile x syndrome. Annu Rev Genomics Hum Genet **8**: 109-29.

Pilot, F., Philippe, J. M., Lemmers, C. and Lecuit, T., 2006 Spatial control of actin organization at adherens junctions by a synaptotagmin-like protein Btsz. Nature **442**: 580-4.

Price, D. M., Jin, Z., Rabinovitch, S. and Campbell, S. D., 2002 Ectopic expression of the Drosophila Cdk1 inhibitory kinases, Wee1 and Myt1, interferes with the second mitotic wave and disrupts pattern formation during eye development. Genetics **161**: 721-31.

Prinz, W. A., Grzyb, L., Veenhuis, M., Kahana, J. A., Silver, P. A. and Rapoport, T. A., 2000 Mutants affecting the structure of the cortical endoplasmic reticulum in Saccharomyces cerevisiae. J Cell Biol **150**: 461-74.

Pritchard, D. K. and Schubiger, G., 1996 Activation of transcription in Drosophila embryos is a gradual process mediated by the nucleocytoplasmic ratio. Genes Dev **10**: 1131-42.

Raff, J. W., Jeffers, K. and Huang, J. Y., 2002 The roles of Fzy/Cdc20 and Fzr/Cdh1 in regulating the destruction of cyclin B in space and time. J Cell Biol **157**: 1139-49.

Reeve, S. P., Bassetto, L., Genova, G. K., Kleyner, Y., Leyssen, M., Jackson, F. R. and Hassan, B. A., 2005 The Drosophila fragile X mental retardation protein controls actin dynamics by directly regulating profilin in the brain. Curr Biol **15**: 1156-63.

Riggs, B., Rothwell, W., Mische, S., Hickson, G. R., Matheson, J., Hays, T. S., Gould, G. W. and Sullivan, W., 2003 Actin cytoskeleton remodeling during early Drosophila furrow formation requires recycling endosomal components Nuclear-fallout and Rab11. J Cell Biol **163**: 143-54.

Rogers, G. C., Rogers, S. L., Schwimmer, T. A., Ems-McClung, S. C., Walczak, C. E., Vale, R. D., Scholey, J. M. and Sharp, D. J., 2004 Two mitotic kinesins cooperate to drive sister chromatid separation during anaphase. Nature **427**: 364-70.

Rothwell, W. F., Fogarty, P., Field, C. M. and Sullivan, W., 1998 Nuclear-fallout, a Drosophila protein that cycles from the cytoplasm to the centrosomes, regulates cortical microfilament organization. Development **125**: 1295-303.

Royou, A., Field, C., Sisson, J. C., Sullivan, W. and Karess, R., 2004 Reassessing the role and dynamics of nonmuscle myosin II during furrow formation in early Drosophila embryos. Mol Biol Cell **15**: 838-50.

Royou, A., Macias, H. and Sullivan, W., 2005 The Drosophila Grp/Chk1 DNA damage checkpoint controls entry into anaphase. Curr Biol **15**: 334-9.

Schaeffer, C., Bardoni, B., Mandel, J. L., Ehresmann, B., Ehresmann, C. and Moine, H., 2001 The fragile X mental retardation protein binds specifically to its mRNA via a purine quartet motif. Embo J **20**: 4803-13.

Schejter, E. D., Rose, L. S., Postner, M. A. and Wieschaus, E., 1992 Role of the zygotic genome in the restructuring of the actin cytoskeleton at the cycle-14 transition during Drosophila embryogenesis. Cold Spring Harb Symp Quant Biol **57**: 653-9.

Schupbach, T. and Wieschaus, E., 1989 Female sterile mutations on the second chromosome of Drosophila melanogaster. I. Maternal effect mutations. Genetics **121**: 101-17.

Semotok, J. L., Cooperstock, R. L., Pinder, B. D., Vari, H. K., Lipshitz, H. D. and Smibert, C. A., 2005 Smaug recruits the CCR4/POP2/NOT deadenylase complex to trigger maternal transcript localization in the early Drosophila embryo. Curr Biol **15**: 284-94.

Sen, G. L. and Blau, H. M., 2005 Argonaute 2/RISC resides in sites of mammalian mRNA decay known as cytoplasmic bodies. Nat Cell Biol **7**: 633-6.

Sheng, M., 2001 Molecular organization of the postsynaptic specialization. Proc Natl Acad Sci U S A **98**: 7058-61.

Sibon, O. C., Laurencon, A., Hawley, R. and Theurkauf, W. E., 1999 The Drosophila ATM homologue Mei-41 has an essential checkpoint function at the midblastula transition. Curr Biol **9**: 302-12.

Sibon, O. C., Stevenson, V. A. and Theurkauf, W. E., 1997 DNA-replication checkpoint control at the Drosophila midblastula transition. Nature **388**: 93-7.

Siomi, H., Siomi, M. C., Nussbaum, R. L. and Dreyfuss, G., 1993 The protein product of the fragile X gene, FMR1, has characteristics of an RNA-binding protein. Cell **74**: 291-8.

Siomi, M. C., Zhang, Y., Siomi, H. and Dreyfuss, G., 1996 Specific sequences in the fragile X syndrome protein FMR1 and the FXR proteins mediate their binding to 60S ribosomal subunits and the interactions among them. Mol Cell Biol **16**: 3825-32.

Sisson, J. C., Field, C., Ventura, R., Royou, A. and Sullivan, W., 2000 Lava lamp, a novel peripheral golgi protein, is required for Drosophila melanogaster cellularization. J Cell Biol **151**: 905-18.

Sokac, A. M. and Wieschaus, E., 2008 Zygotically controlled F-actin establishes cortical compartments to stabilize furrows during Drosophila cellularization. J Cell Sci **121**: 1815-24.

Solomon, S., Xu, Y., Wang, B., David, M. D., Schubert, P., Kennedy, D. and Schrader, J. W., 2007 Distinct structural features of caprin-1 mediate its interaction with G3BP-1 and its induction of phosphorylation of eukaryotic translation initiation factor 2alpha, entry to cytoplasmic stress granules, and selective interaction with a subset of mRNAs. Mol Cell Biol **27**: 2324-42.

Speicher, S., Garcia-Alonso, L., Carmena, A., Martin-Bermudo, M. D., de la Escalera, S. and Jimenez, F., 1998 Neurotactin functions in concert with other identified CAMs in growth cone guidance in Drosophila. Neuron **20**: 221-33.

Stiffler, L. A., Ji, J. Y., Trautmann, S., Trusty, C. and Schubiger, G., 1999 Cyclin A and B functions in the early Drosophila embryo. Development **126**: 5505-13.

Stukenberg, P. T., Lustig, K. D., McGarry, T. J., King, R. W., Kuang, J. and Kirschner, M. W., 1997 Systematic identification of mitotic phosphoproteins. Curr Biol **7**: 338-48.

Su, T. T., Sprenger, F., DiGregorio, P. J., Campbell, S. D. and O'Farrell, P. H., 1998 Exit from mitosis in Drosophila syncytial embryos requires proteolysis and cyclin degradation, and is associated with localized dephosphorylation. Genes Dev **12**: 1495-503.

Sullivan, W., Fogarty, P. and Theurkauf, W., 1993 Mutations affecting the cytoskeletal organization of syncytial Drosophila embryos. Development **118**: 1245-54.

Swanson, M. M. and Poodry, C., 1981 The shibirits mutant of Drosophila: A probe for the study of embryoinc development. Developmental Biology **84**: 465-470.

Tada, T., Simonetta, A., Batterton, M., Kinoshita, M., Edbauer, D. and Sheng, M., 2007 Role of Septin cytoskeleton in spine morphogenesis and dendrite development in neurons. Curr Biol **17**: 1752-8.

Tadros, W., Goldman, A. L., Babak, T., Menzies, F., Vardy, L., Orr-Weaver, T., Hughes, T. R., Westwood, J. T., Smibert, C. A. and Lipshitz, H. D., 2007 SMAUG is a major regulator of maternal mRNA destabilization in Drosophila and its translation is activated by the PAN GU kinase. Dev Cell **12**: 143-55.

Tadros, W. and Lipshitz, H. D., 2005 Setting the stage for development: mRNA translation and stability during oocyte maturation and egg activation in Drosophila. Dev Dyn **232**: 593-608.

Thomas, J. H. and Wieschaus, E., 2004 src64 and tec29 are required for microfilament contraction during Drosophila cellularization. Development **131**: 863-71.

Todd, P. K., Mack, K. J. and Malter, J. S., 2003 The fragile X mental retardation protein is required for type-I metabotropic glutamate receptor-dependent translation of PSD-95. Proc Natl Acad Sci U S A **100**: 14374-8.

Uemura, T., Oda, H., Kraut, R., Hayashi, S., Kotaoka, Y. and Takeichi, M., 1996 Zygotic Drosophila E-cadherin expression is required for processes of dynamic epithelial cell rearrangement in the Drosophila embryo. Genes Dev **10**: 659-71.

Viswanathan, S., Unlu, M. and Minden, J. S., 2006 Two-dimensional difference gel electrophoresis. Nat Protoc **1**: 1351-8.

Wan, L., Dockendorff, T. C., Jongens, T. A. and Dreyfuss, G., 2000 Characterization of dFMR1, a Drosophila melanogaster homolog of the fragile X mental retardation protein. Mol Cell Biol **20**: 8536-47.

Wang, B., David, M. D. and Schrader, J. W., 2005 Absence of caprin-1 results in defects in cellular proliferation. J Immunol **175**: 4274-82.

Washburn, M. P., Ulaszek, R., Deciu, C., Schieltz, D. M. and Yates, J. R., 3rd, 2002 Analysis of quantitative proteomic data generated via multidimensional protein identification technology. Anal Chem **74**: 1650-7.

Wieschaus, E. and Sweeton, D., 1988 Requirements for X-linked zygotic gene activity during cellularization of early Drosophila embryos. Development **104**: 483-93.

Wilhelm, J. E., Buszczak, M. and Sayles, S., 2005 Efficient protein trafficking requires trailer hitch, a component of a ribonucleoprotein complex localized to the ER in Drosophila. Dev Cell **9**: 675-85.

Wilkie, G. S., Zimyanin, V., Kirby, R., Korey, C., Francis-Lang, H., Van Vactor, D. and Davis, I., 2001 Small bristles, the Drosophila ortholog of NXF-1, is essential for mRNA export throughout development. Rna **7**: 1781-92.

Xie, Y., Vessey, J. P., Konecna, A., Dahm, R., Macchi, P. and Kiebler, M. A., 2007 The GTP-binding protein Septin 7 is critical for dendrite branching and dendritic-spine morphology. Curr Biol **17**: 1746-51.

Xu, K., Bogert, B. A., Li, W., Su, K., Lee, A. and Gao, F. B., 2004 The fragile X-related gene affects the crawling behavior of Drosophila larvae by regulating the mRNA level of the DEG/ENaC protein pickpocket1. Curr Biol **14**: 1025-34.

Yam, A. Y., Xia, Y., Lin, H. T., Burlingame, A., Gerstein, M. and Frydman, J., 2008 Defining the TRiC/CCT interactome links chaperonin function to stabilization of newly made proteins with complex topologies. Nat Struct Mol Biol **15**: 1255-62.

Zalfa, F., Achsel, T. and Bagni, C., 2006 mRNPs, polysomes or granules: FMRP in neuronal protein synthesis. Curr Opin Neurobiol **16**: 265-9.

Zhang, Y. Q., Bailey, A. M., Matthies, H. J., Renden, R. B., Smith, M. A., Speese, S. D., Rubin, G. M. and Broadie, K., 2001 Drosophila fragile X-related gene regulates the MAP1B homolog Futsch to control synaptic structure and function. Cell **107**: 591-603.

Zhang, Y. Q., Friedman, D. B., Wang, Z., Woodruff, E., 3rd, Pan, L., O'Donnell, J. and Broadie, K., 2005 Protein expression profiling of the drosophila fragile X mutant brain reveals up-regulation of monoamine synthesis. Mol Cell Proteomics **4**: 278-90.

Zhang, Y. Q., Matthies, H. J., Mancuso, J., Andrews, H. K., Woodruff, E., 3rd, Friedman, D. and Broadie, K., 2004 The Drosophila fragile X-related gene regulates axoneme differentiation during spermatogenesis. Dev Biol **270**: 290-307.

# Vita

Kate Monzo was born on October 22, 1976 in Evanston, IL to Aine Ruane and Daniel Monzo. Shortly after graduating from Evanston Township High School, Kate moved to Austin, TX where she worked as a veterinary technician at Arbor Animal Clinic while attending Austin Community College part time. She eventually became a full-time student at the University of Texas at Austin in January of 2002, joined the Sisson lab as an undergraduate research assistant in January of 2003, and earned a B.S. in Biology in December of 2003. In August 2004, Kate continued doing research in the Sisson lab as a graduate student in the Cell and Molecular Biology program at the University of Texas at Austin studying the role of Fragile X mental retardation protein during early development. She was given several fellowships and awards as an undergraduate and graduate student including the A. D. Hutchinson Student Endowment Fellowship from the University of Texas Graduate School. Her current scientific publications and works in preparation include:

Monzo K, Dowd SR, Minden JS, and Sisson JC. The chaperonin containing TCP-1 (CCT) complex is a target of Fragile X mental retardation protein-dependent regulation in *Drosophila* cleavage stage embryos. Manuscript in preparation.

Papoulas O*, Monzo K*, Cantin GT, Ruse C, Yates JR, and Sisson JC. Synaptic plasticity regulators control the cell cycle machinery at the midblastula transition. *equal contributing authors. Manuscript in preparation.

Dagani GT, Monzo K, Fakhoury JR, Chen CC, Sisson JC, Zhang X. Microfluidic self-assembly of live *Drosophila* embryos for versatile high-throughput analysis of embryonic morphogenesis. *Biomedical Microdevices*. **9**:681-94, 2007.

Monzo K, Papoulas O, Cantin GT, Wang Y, Yates JR, Sisson JC. Fragile X mental retardation protein controls trailer hitch expression and cleavage furrow formation in *Drosophila* embryos. *The Proceedings of the National Academy of Sciences*. **103**: 18160-18165, 2006.

Permanent address: 903 E 53rd ST, Austin, TX 78751-2213

This dissertation was typed by Kate Monzo.